PUNCHING BEHAVIOR OF HYBRID FIBER
REINFORCED CONCRETE PANELS

**A Thesis Submitted to
the Graduate School
İzmir Institute of Technology
In Partial Fulfillment of the Requirements for the Degree of**

MASTER OF SCIENCE

in Civil Engineering

**by
Jamalullah NASERI**

December 2020

İZMİR

ACKNOWLEDGEMENTS

I would like to express my deepest appreciation to my supervisor Assist. Prof. Dr. Selçuk Saatcı for giving me the chance to join this precious project, his keen guidance and making me capable of conducting independent research. Without his continuous support and patience, it would be an enormous task. I also owe to Assoc. Prof. Dr. Tahir Kemal Erdem for helping and guiding me in the concrete mix design and casting process. Also, I would like to thank Assoc. Prof. Dr Cemalettin Dönmez, who inspired my interest in reinforced concrete. Moreover, I am grateful to thank all my professors and teachers from university and school who have played a crucial role in my life. In addition, appreciation extended to the thesis committee, Assoc. Prof. Dr. Ninel Alver and Assist. Prof. Dr. Korhan Deniz Dalgiç for reviewing and offering helpful comments and suggestions.

I am grateful to Cemal Kılıç, Structural Mechanics Laboratory Technician, for his help and guidance which was essential in facilitating and carrying out the experimental work. I would also thank my colleagues and friends in the university and outside the university for their support and encouragement.

I owe a lot to my family specially my parents, who at every point of life, have been selfless in bringing me up and supporting me, words cannot express how grateful I am for having them in my life. Their constant love, prays and faith in whatever path I have chosen, has helped to bring out the best in me.

ABSTRACT

PUNCHING BEHAVIOR OF HYBRID FIBER REINFORCED CONCRETE PANELS

Hybrid fiber reinforced concrete (HyFRC) is a more recent type of fiber reinforced concrete (FRC), which includes two or more different fibers types. HyFRC may result in a multifunctional material due to synergetic effects of the various type of fibers added in the mixture.

In this study, punching behavior of HyFRC thin panels using three different types of steel fibers and polyvinyl alcohol (PVA) fibers were experimentally investigated. In total 13 panel specimens were cast with dimensions of 1700 x 1700 mm^2 and thickness of 50 mm. The specimens were simply supported along the edges and loaded through a 150 mm circular steel plate at the center by a displacement-controlled hydraulic actuator. A load cell and fifteen displacement transducers were used to measure the applied load and vertical deflection of the specimens, respectively.

All specimens that contained only steel fibers failed under punching. In hybrid fiber reinforced specimens with steel and PVA fibers, either a flexural failure or a punching failure followed by significant flexural deformations were observed. Test results confirm that fiber reinforced concrete has a very significant effect on thin panel's punching strength and displacement capacity. It was seen that hybridization of two different types of fiber, steel and PVA fibers, brings advantages in terms of punching load capacity, deformation characteristics and failure mode.

Keywords: Fiber Reinforced Concrete, Hybrid Fiber Reinforced Concrete, Punching, Thin Panels

ÖZET

HİBRİT FİBERLİ BETON PANELLERİN ZIMBALAMA DAVRANISI

Hibrit lif takviyeli beton (HLTB), iki veya daha fazla farklı lif türünü bir arada içeren yeni bir lif takviyeli beton türüdür. HLTB'de karışıma eklenen çeşitli tipteki liflerin sinerjik etkilerinden dolayı çok işlevli bir malzeme elde edilebilir.

Bu çalışmada, üç farklı çelik lif tipi ve polivinil alkol (PVA) lif kullanılarak HLTB ince panellerin zımbalama davranışı deneysel olarak araştırılmıştır. Toplamda 1700 x 1700 mm^2 boyutlarında ve 50 mm kalınlığında 13 adet panel numune dökülmüştür. Numuneler kenarlar boyunca basit mesnetli olup orta noktadan 150 mm dairesel çelik plakayla yer değiştirme kontrollü bir hidrolik veren ile yüklenmiştir. Deneylerde uygulanan yükü ölçmek için bir yük hücresi, düşey yerdeğiştirmeleri ölçmek için 15 adet yer değiştirme ölçer kullanılmıştır.

Sadece çelik lif içeren tüm numuneler zımbalama göçmesine uğramışlardır. Çelik ve PVA lifli hibrit lif takviyeli numunelerde eğilme göçmesi veya yüksek eğilme yer değiştirmeleri sonrasında zımbalama göçmesi gözlemlenmiştir. Deney sonuçları lif takviyeli betonun ince panellerin zımbalama dayanımı ve yer değiştirme kapasitesi üzerinde çok önemli bir etkiye sahip olduğunu doğrulamaktadır. Çelik ve PVA lifler gibi iki farklı tipte lifin hibritleştirilmesinin zımbalama yükü kapasitesi, yer değiştirme özellikleri ve göçme modu açısından avantajları olduğu görülmüştür.

Anahtar Kelimeler: lif takviyeli beton, Hibrit lif takviyeli beton, zımbalama, ince paneller

TABLE OF CONTENTS

LIST OF FIGURES

LIST OF TABLES

CHAPTER 1

INTRODUCTION

Reinforced concrete flat-slabs, developed earlier in the 20th century, was a historical development in concrete industry. However, brittle punching failure has always been a subject of concern for this slab type. To transfer the localized forces from the slab to the column, large mushroom-shaped column capitals were used (Fürst & Marti, 1997, Gasparini & M.ASCE, 1905-1909). Flat slabs without capitals became popular in 1950s (Muttoni, 2008).

Reinforced concrete flat slabs or slab-column connection systems consist of slabs with uniform thickness supported directly by columns without beams, capitals or drop panels. Flat slabs are widely used in average height office buildings, residential structures, and car parks. Flat slabs are mostly recommended and preferred due to their economical, practical, and architectural advantages, which can be summarized as follows.

- Easy formwork and reinforcement placement which reduce the construction period and cost
- Minimizing the ceiling height which reduces overall height of the structure and foundation load that further reduce the related material cost
- In the absence of the beams, column capitals and drop panels, flat plates offer flexibility in room layout

Despite its advantages, punching shear failure is one of the vital risks in flat plates that leads to sudden and brittle failure, in which little or sometimes no warning occurs prior to failure (Maya et al, 2012). In addition, reinforced concrete plate failure might be caused by corrosion of steel reinforcement which could be due to poor design and workmanship, inadequate concrete cover, and existence of numerous hostile agents which pierce through the cracks. Since stiffness of elements reduce due to cracking, this can cause a flexure, shear, or torsion failure. Therefore, normal concrete may not be suitable for such applications (Ramin, 2014).

Over the past century, many researches were performed in order to improve the punching behavior of plat slabs. These include increasing the thickness of the slabs or using column capitals and drop panels. Furthermore, using various type of steel reinforcement such as flexural reinforcement, closed stirrups, bent-bars, shear studs, and

prestressed tendons were also investigated to improve the punching shear capacity (Menétrey, 2002).

Increasing slab thickness is usually not an affordable choice since it increases the weight and cost of the structure. Similarly, column capitals and drop panels are not favorable due to complexity of formwork and architectural disadvantages. In addition, placement of shear reinforcement is not practical, especially for thin slabs.

Recently, researchers were interested in improving the strength of construction materials such as concrete with having in mind the impact on the economy and environment. Studies show that addition of randomly distributed fibers in concrete mix, fiber reinforced concrete (FRC), lead to improvement in concrete's load capacity and durability. Furthermore, by improving the concrete strength and ductility, fiber reinforced concrete could avoid punching shear failure and improve ductility and energy-absorption properties of flat slabs. Additionally, FRC transforms a brittle failure mode into a more ductile one since the fiber continue to carry tensile stresses across crack surfaces after cracking.

Over the past years, experimental studies were carried out to show the possibility of replacing the conventional reinforcement rebars with fiber reinforced concrete (Destrée & Mandl, 2008, Hedebratt & Silfwerbrand, 2014, Michels et al, 2012, Singh, 2015, Tan & Venkateshwaran, 2019). It was believed that steel fiber reinforced concrete (SFRC) can easily be used to replace traditional reinforced concrete, particularly in slabs which can allocate the moments (of comparatively lower magnitude) very easily than beams because of their higher redundancy. Members cast using SFRC were able to retain their flexural ability and post-cracking behavior across a wider range of strain values compared to those cast with reinforced and plain concrete. Additionally, having simple formwork, it allows quick and cost-effective flat plate structures due to a reduced in manpower and construction period (Singh, 2015) .

1.1 Research Objective and Scope

As aforementioned, one of the methods proposed to improve the punching capacity of flat slabs was increasing the concrete capacity by adding fibers to concrete mixture. Hybrid fiber reinforced concrete (HyFRC) is relatively a new type of the FRC that contains two or more type of fibers. Fibers could be added to concrete mixture with

various shapes, aspect ratio and materials. Using hybrid fiber composite, moreover, the mutual effect of hybrid fiber composites exceeds the total individual performances between the fibers because of the synergetic effects of the various added fibers. There is limited information about the behavior of the HyFRC used in flat slabs. Therefore, the investigation presented here is aimed to provide insight into the gap in this area.

This study was performed to investigate the effectiveness of using steel and hybrid fiber reinforced concrete with steel and PVA fibers on the punching behavior of thin flat slabs.

1.2 Thesis Layout

This study consists of five chapters as follows.

Chapter 1 provides a brief introduction to the punching behavior of flat slab system, the scope, and the object of the study

Chapter 2 gives a detailed review of the previous studies on the punching behavior of steel fiber reinforced concrete and hybrid fiber reinforced concrete flat slabs.

Chapter 3 describes the experimental program and work performed, including details of slab specimens, test setup, used equipment and material properties.

Chapter 4 provides test results regarding load-deflection behavior and crack patterns. Moreover, effects of key variables, for instance steel fiber types and volume content, PVA fiber and steel reinforcement are discussed in detail in this chapter.

Chapter 5 provides the main conclusions reached in this study.

CHAPTER 2

LITERATURE REVIEW

Reinforced concrete flat slab systems are one of the main types of reinforced concrete construction. Therefore, research on the behavior and strength of flat slabs is quite extensive in the literature. Various methodologies were developed on the analysis and design of flat slab systems over decades. Fiber reinforced concrete (FRC) is a relatively new material, proved to be effective in providing punching strength in flat slab systems. In this chapter, a literature review is provided on flat slabs with FRC and recent significant studies are discussed.

Gouveia et al (2018) evaluated the punching shear capacity of SFRC flat slabs in their experimental and analytical study. Total of five slab specimens which had 160 mm thickness, fiber volume fraction of 0, 1.0 and 1.5 % and bending reinforcement ratio of 0.75 and 1.5% were tested. Properties of the slab specimens are given in Table 2.1. A simply supported system was used and specimens were loaded centrally through a steel plate of 200 x 200 x 50 mm. The load was applied by a hydraulic jack from the bottom of the slab with a constant rate of 285 N/s force. The study used 11 displacement transducers, 8 strain gauges and 8 load cells to determine the vertical displacement, strains of steel bar, and vertical load, respectively. Test setup is presented in Figure 2.1

Table 2.1 Slab Specimens properties (Gouveia et al (2018)

Specimens	ρ_f (%)	ρ_l (%)	d (mm)	f_y (MPa)
F0_R0.75	0	0.75	136	534
F0_R1.5	0	1.5	128	529
F1_R0.75	1.0	0.75	135	534
F1_R1.5	1.0	1.5	128	529
F1.5_R1.5	1.5	1.5	128	529

❖ p_f is the ratio of fiber reinforcement; p_l is the ratio of flexural reinforcement; d effective depth; f_y yield strength of the steel bars.
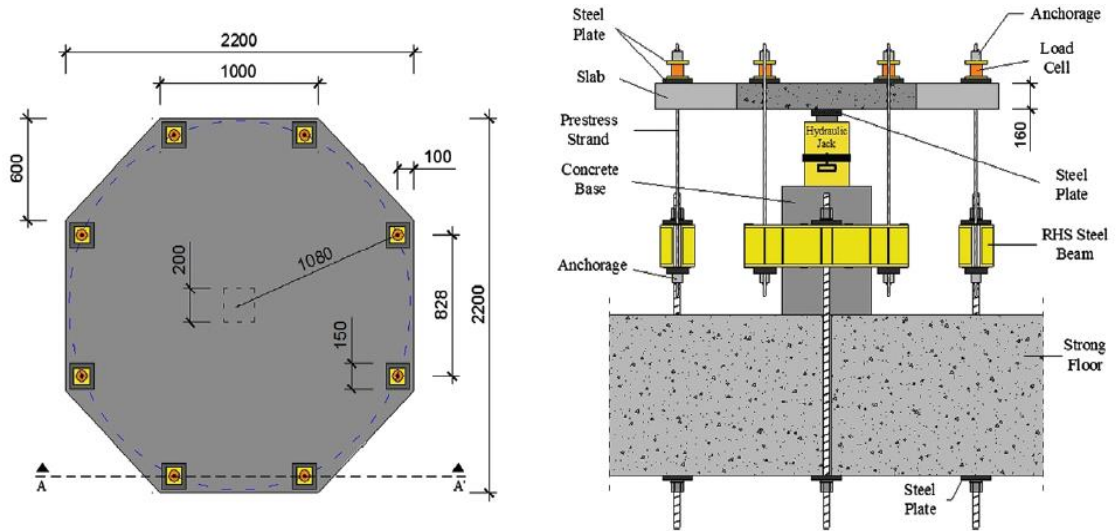
Figure 2.1 Geometry of specimen: top view and section A–A' (All dimensions in mm)
(Gouveia et al, 2018)

Results of the study showed that the addition of fibers enhance the punching strength and ductility of flat slabs. Maximum increase in load capacity due to the addition of fibers up to 1% was around 54% compared to the slab without fibers. Moreover, in some instances, the presence of fibers changed the failure mechanism from punching to flexural-punching failure. Also, the deflection capacity was increased in the slabs containing fibers. Authors also analyzed their test results using Critical Shear Crack Theory (CSCT (Muttoni, 2008)) and claimed that the experimental and theoretical results showed a good agreement. In particular, the experimental values were very close to the estimated punching load capacity as presented in Table 2.2.

Table 2.2 Theoretical and experimental results (Gouveia et al, 2018)

| Specimens | ρ_f (%) | ρ_l (%) | V_{exp} (kN) | $\psi_{R,exp}$ | $V_{calc,CSCT}$ | | | | $\psi_{R,CSCT}$ | V_{exp}/V_R |
					$V_{R,c}$ (kN)	$V_{R,f}$ (kN)	V_R (kN)	V_{flex} (kN)		
F0_R0.75	0	0.75	385	0.0149	416	0	416	506	0.0174	0.93
F0_R1.5	0	1.50	508	0.0127	493	0	493	862	0.0112	1.03
F1_R0.75	1.0	0.75	595	0.0442	307	225	532	614	0.0254	1.12
F1_R1.5	1.0	1.50	674	0.0192	408	174	582	970	0.0135	1.16
F1.5_R1.5	1.5	1.50	708	0.0235	375	279	654	996	0.0163	1.08
									Average (SFRC slabs)	1.12
									COV (SFRC slabs)	0.03

❖ CSCT = critical shear crack theory; SFRC = steel fiber reinforced concrete

Another study performed by Gouveia et al (2019), investigated the behavior and load capacity of SFRC slab-column connection. The specimens were cast in a manner that steel fiber reinforced concrete was poured around the column region with a square area (approximately the column size plus three times the effective depth on all sides) and the remaining of the slab was cast with normal concrete without fibers as presented in Figure 2.2. The test consisted of six slab specimens of 150 mm thickness with main variables as steel fibers volumetric ratio (0.0, 0.5, 0.75, and 1.0%) and longitudinal bar ratio (1 and 5%). Flexural tests were performed on notched beams as well in order to determine the flexural behavior. The load was applied centrally by a hydraulic jack from the bottom of the specimens through a steel plate of size 250 x 250 mm with a constant rate of 285 N/s.

| a) SFRC in central region | b) outside region with normal concrete |

Figure 2.2 Regions of different concretes inside the specimens

(Gouveia et al, 2019)

Results of the tests revealed that addition of steel fibers near the column region improved the load and deformation capacities of the slabs (Figure 2.3). The load capacity increased by 36%, as the fiber volume fraction increased from zero to 1%. Also, SFRC caused changes in failure modes from brittle punching failure to flexural-punching or even flexural failure. It was also found that for improving the load and deformation capacity of flat slab, casting SFRC for an area up to three times the effective depth from column edge is sufficient.

6
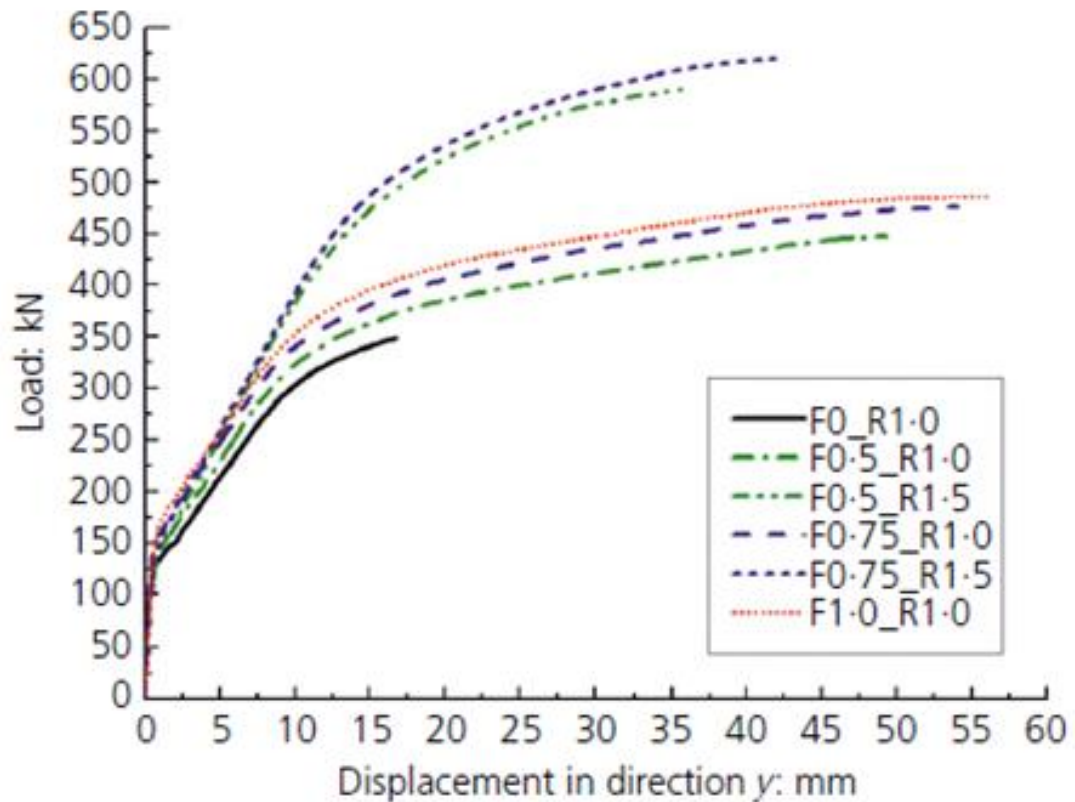
Figure 2.3 Load–displacement test results

(Gouveia et al, 2019)

Saatcı et al (2018) evaluated the effect of steel fibers on the punching behavior of reinforced concrete slabs. Eight slab specimens were cast in two groups of flexural reinforcement ratio as 0.4 % (D1 series) and 0.2% (D2 series) in two orthogonal directions (Figure 2.4). Both groups had four specimens with varying steel fiber volume content (0.0, 0.5, 1.0, and 1.5%). Simply supported conditions were provided and specimens were loaded by hydraulic jack placed at the bottom of the slabs. The load was applied at the center of the specimen through a circular steel plate of 200 mm diameter.

From the results, it was concluded that the punching shear capacity of both series were increased as the steel fiber ratio increased. The load capacity was increased up to two times compared to reference specimen. The steel fiber ratio had more influence on displacement capacity of the slabs with high reinforcement ratio than the slabs with low reinforcement ratio (Figure 2.5). It was found that flexural reinforcement yielded before punching in slabs with low reinforcement ratio, so the yielding of the bending reinforcement was controlling the displacement capacity in these specimens.
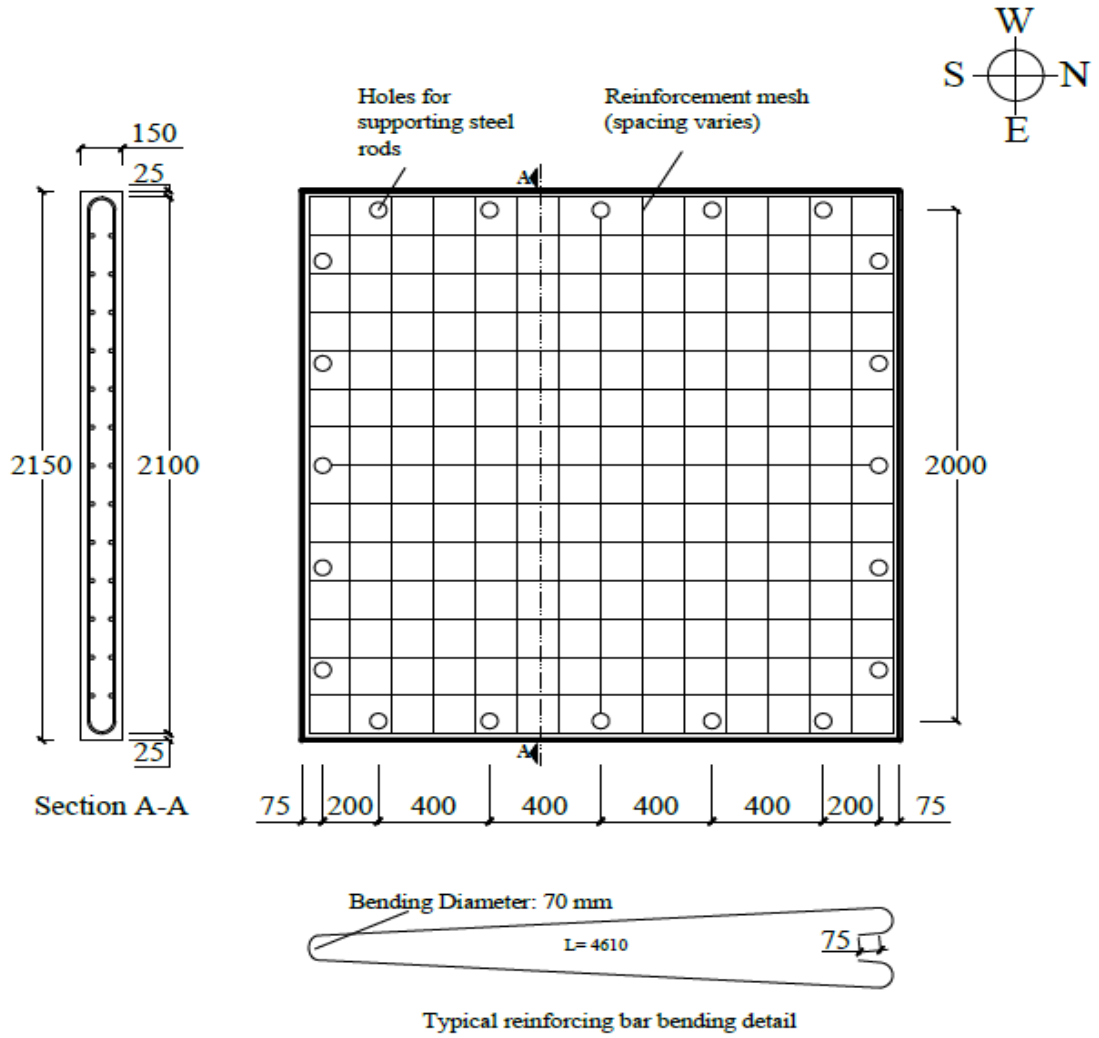
Figure 2.4 Test specimens (all dimensions in mm)

(Saatcı et al, 2018)
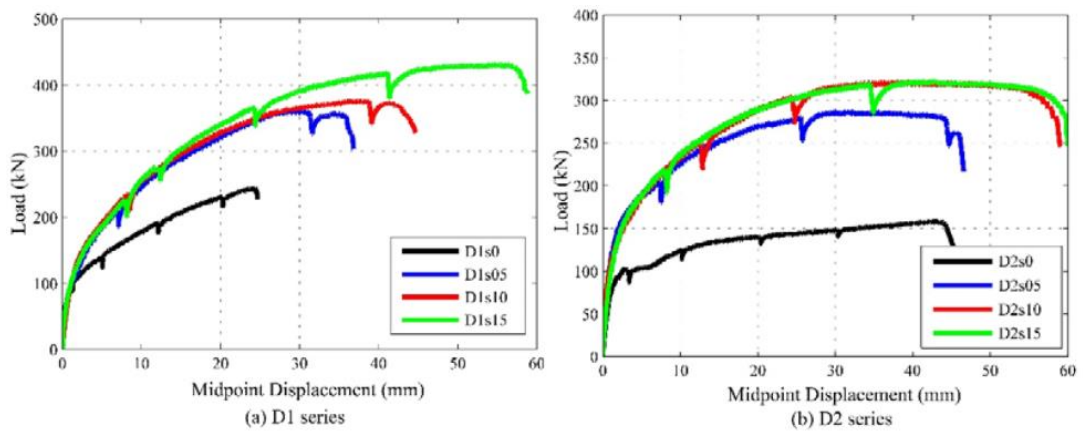
Figure 2.5 Load-displacement curves for slabs

(Saatcı et al, 2018)

Tan and Venkateshwaran (2019) performed an experimental study to investigate the punching capacity of SFRC slabs without traditional reinforcement. Twelve square slabs of 700 x 700 mm were tested. Main parameters were fiber hook geometry, concrete compressive strength, slab thickness and fiber reinforcing index ($V_f L_f/D_f$); where V_f is volume fraction, L_f is length and D_f is the diameter of the steel fibers. Details of the slab specimens are presented in Table 2.3.

Table 2.3 Details of tested SFRC specimens (Tan & Venkateshwaran, 2019)

Set	Specimen label	Concrete class	f_c', MPa (ksi)	Fiber type	Fiber content, %	Slab thickness, mm (in.)	P_{test}, kN (kip)	P_{pred}, kN (kip) Yield line theory	P_{pred}, kN (kip) Proposed model
I	M42		36.0 (5.2)	4-D	0.25		53.0 (11.9)	50.3 (11.3)	59.4 (13.4)
	M44		36.0 (5.2)		0.5		67.0 (15.1)	66.3 (14.9)	76.4 (17.2)
	M46		31.4 (4.6)		0.75		80.0 (18.0)	80.0 (18.0)	90.8 (20.4)
	M48		36.1 (5.2)		1	150 (5.9)	84.0 (18.9)	97.3 (21.9)	109.8 (24.7)
II	M52	C30/37	37.4 (5.4)	5-D	0.25		85.0 (19.1)	58.9 (13.3)	60.0 (13.5)
	M54		36.5 (5.3)		0.5		69.1 (15.5)	74.4 (16.7)	76.6 (17.2)
	M56		40.8 (5.9)		0.75		74.2 (16.7)	91.6 (20.6)	95.5 (21.5)
	M58		42.2 (6.1)		1		90.1 (20.3)	107.5 (24.2)	112.7 (25.4)
III	M54A		34.9 (5.1)			90 (3.5)	37.3 (8.4)	44.6 (10.0)	57.8 (13.0)
	M54B		34.9 (5.1)		0.5	150 (5.9)	127.6 (28.7)	107.2 (24.1)	93.9 (21.1)
IV	L54	C16/20	21.1 (3.1)			120 (4.7)	54.6 (12.3)	67.2 (15.1)	68.4 (15.4)
	H54	C50/60	51.8 (7.5)				88.5 (19.9)	79.3 (17.8)	83.2 (18.7)

❖ L=low , M= medium, and H= high, strength concrete. All fibers had 60 mm length and 0.9 mm diameter. 4-D and 5-D show end-hooks number of steel fibers (N) = 1.5 and 2, accordingly. The changes of slab thickness represented by A and B.

A simply supported system was used with a clear span of 600 mm (Figure 2.6) and specimens were loaded monotonically at a displacement rate of 0.1 mm/min. This rate was gradually increased to 0.3 mm/min after reaching the ultimate load in order to obtain the descending portion of the load-deflection curve.

Based on the test results, all slabs specimens failed in flexure, as seen from formation of yield lines at the bottom of the specimens (Figure 2.7). According to the authors, the occurrence of flexural failure was attributed to the lower energy needed to propagate an existing flexural crack than for the development of a new tangential crack around the column edge.
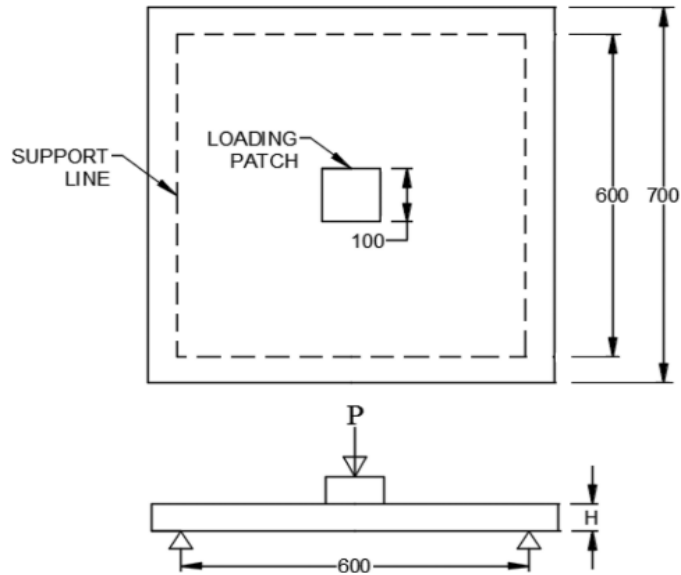
Figure 2.6 Central point load tests on SFRC slabs (Note: All dimensions are in mm)

(Tan & Venkateshwaran, 2019)

The load-deflection curves given in Figure 2.8 showed plastic behavior between the deflection of approximately 3 mm to 5 mm and 8 mm to 10 mm in most specimens. Also, it was observed that the thickness of the slab had the highest effect on the ultimate load capacity, followed by the index of the fiber reinforcing and compressive strength of concrete. Influence of the fiber hook geometry was marginal on the ultimate load. Furthermore, tests results were compared with a proposed punching shear model and yield line theory. It was found that the yield line theory showed better prediction then the proposed punching shear model. Results are presented in Table 2.3.

(a) M44   (b) M48   (c) M54
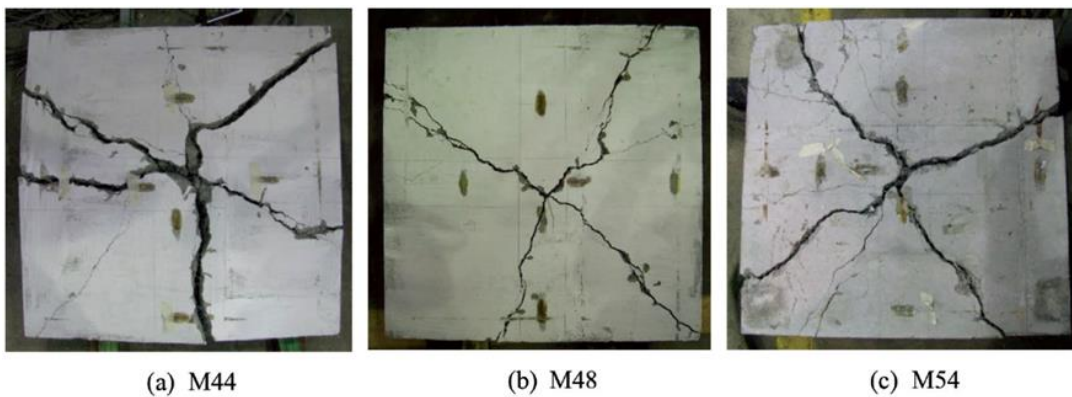
Figure 2.7 Crack patterns on underside of SFRC slabs

(Tan & Venkateshwaran, 2019)

(a) Influence of concrete compressive strength

(b) Influence of fiber content (SFRC with 4D fibers)

(c) Influence of fiber content (SFRC with 5D fibers)

(d) Influence of slab thickness

(e) Influence of end anchorage (Fiber content = 20 kg/m³ (V_f = 0.25%))

(f) Influence of end anchorage (Fiber content = 40 kg/m³ (V_f =0.5%))

(g) Influence of end anchorage (Fiber content = 60 kg/m³ (V_f = 0.75%))

(h) Influence of end anchorage (Fiber content = 80 kg/m³ (V_f = 1%))

Figure 2.8 Load-deflection curves of SFRC slabs

(Tan & Venkateshwaran, 2019)

11

Punching behavior of SFRC thin slabs and panels has also been a subject of research. Narayanan and Darwish (1987), studied the behavior and strength characteristics of steel fiber reinforced concrete slabs exposed to punching shear. In their study twelve slab specimens, with dimensions of 780 x 780 x 60 mm, were cast with main parameters as the steel fiber volume content, bending reinforcement ratio and concrete compressive strength. Details of specimens are shown in Table 2.4. All specimens were centrally loaded on column stubs (100 x 100 x 100 mm) by a hydraulic jack provided with deflection control. Results displayed that all slabs failed in shear, except for the one with lower flexure reinforcement ratio (1.79%). A gradual and ductile punching failure were occurred in all slab specimens with fiber volume content greater than 0.5 %. The post-ultimate ductility and residual strength increased substantially especially in slabs with higher values of fiber factor. Also, these slabs sustained broad cracking prior to total collapse. The result showed that critical punching shear perimeter around the column decrease with increasing fiber volume content.

Table 2.4 Tested specimens' details and results (Narayanan & Darwish, 1987)

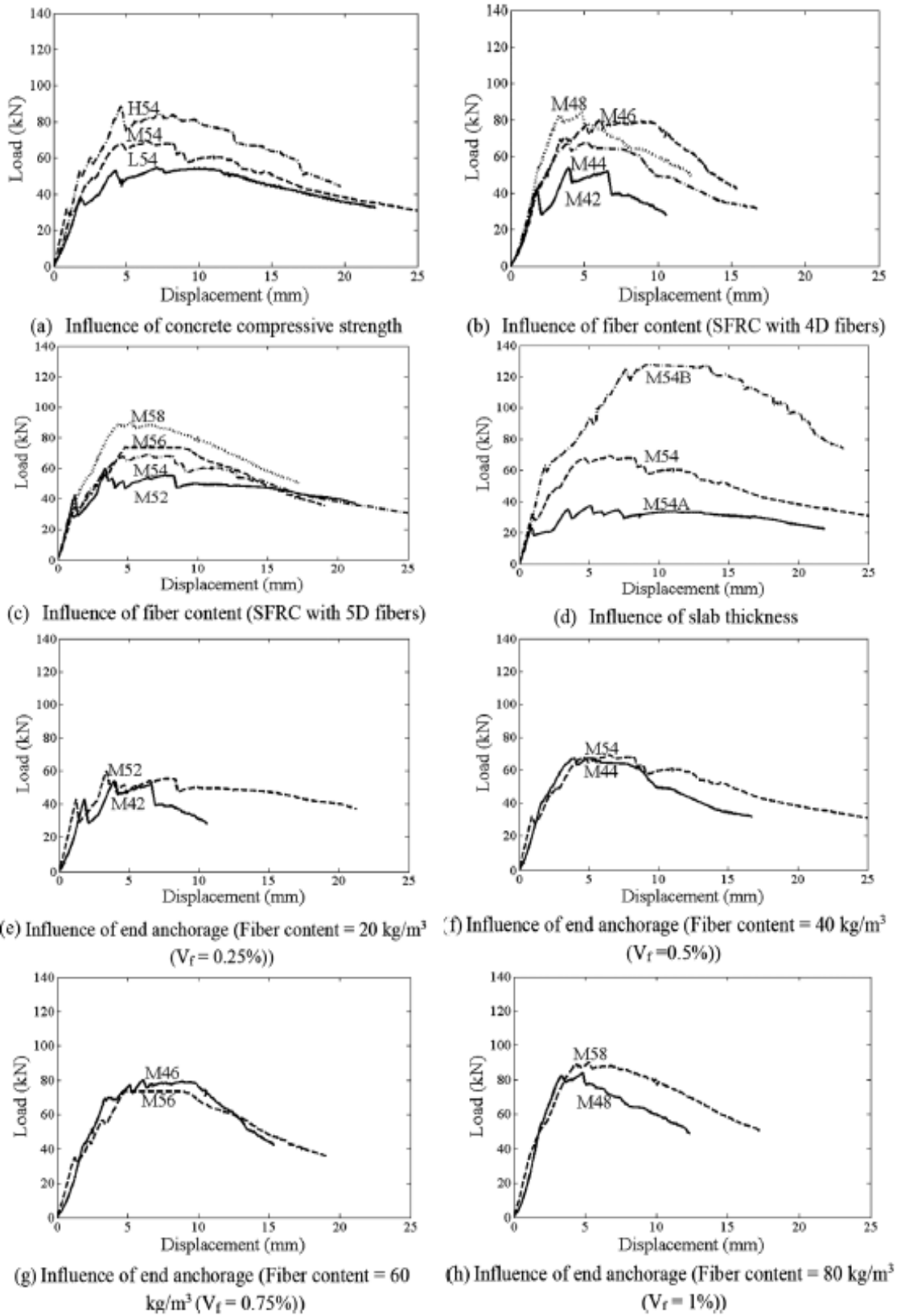| Series | Slab No. | Mix | Tensile Reinforcement | | | | Fibres | | f_{cuf} (N/mm^2) | f_{spf} (N/mm^2) | b_{pf} (mm) | V_{uo} (kN) | v_{uo} (N/mm^2) | v_{up} * (N/mm^2) | v_{uo}/v_{up} |
			No.	Dia. (mm)	Spacing (mm)	ϱ (%)	ϱ_f (%)	F							
1	S1	A	9	10	95	2·01	—	—	54·1	3·41	966	86·5	1·99	1·60	1·24
	S2	A	9	10	95	2·01	0·25	0·19	65·1	4·17	865	93·4	2·40	2·30	1·04
	S3	A	9	10	95	2·01	0·50	0·37	55·9	3·92	769	102·0	2·94	2·65	1·11
	S4	A	9	10	95	2·01	0·75	0·56	57·5	4·22	668	107·5	3·57	3·20	1·11
	S5	A	9	10	95	2·01	1·00	0·75	66·2	4·89	567	113·6	4·45	3·88	1·15
	S6	A	9	10	95	2·01	1·25	0·94	66·3	5·12	467	122·2	5·81	4·41	1·32
2	S7	A	8	10	109	1·79	1·00	0·75	58·7	4·50	567	92·6	3·63	3·70	0·98
	S8	A	10	10	84	2·24	1·00	0·75	56·6	4·39	567	111·1	4·35	3·76	1·15
	S9	A	11	10	76	2·46	1·00	0·75	54·4	4·28	567	111·3	4·36	3·77	1·15
	S10	A	12	10	69	2·69	1·00	0·75	59·5	4·54	567	113·3	4·44	3·91	1·13
3	S11	B	9	10	95	2·01	1·00	0·75	37·2	3·38	567	82·1	3·22	3·37	0·96
	S12	B	9	10	95	2·01	1·00	0·75	40·5	3·55	567	84·9	3·33	3·43	0·97

Harajli et al (1995), studied the effects of steel fiber reinforcement on the punching shear strength of flat slabs. The test consisted of 12 slabs specimens of dimension 650 x 650 mm and divided into two groups. Key variables were fiber type, volume content and aspect ratio as shown in Table 2.5. All specimens had 1.12% of flexural reinforcement ratio.

Load-deflection plots of slab specimens are given in Figure 2.9 & 2.10 . The results revealed that the ultimate load of flat slabs generally increase by increasing volume content of steel fiber. Hooked-end steel fibers of 1 and 2% by volume content, increased

the peak load capacity approximately 22 % and 36%, respectively, compared to reference slab without steel fiber. For the variety used in this study, the aspect ratio of fibers did not have much effect on the punching shear capacity. Addition of the fibers enlarged the failed area on the tension surface of the slab. Thus, the failure surface was pulled away from the edge of the column, increasing punching shear resistance.

Table 2.5 Test variables summary (Harajli et al, 1995)

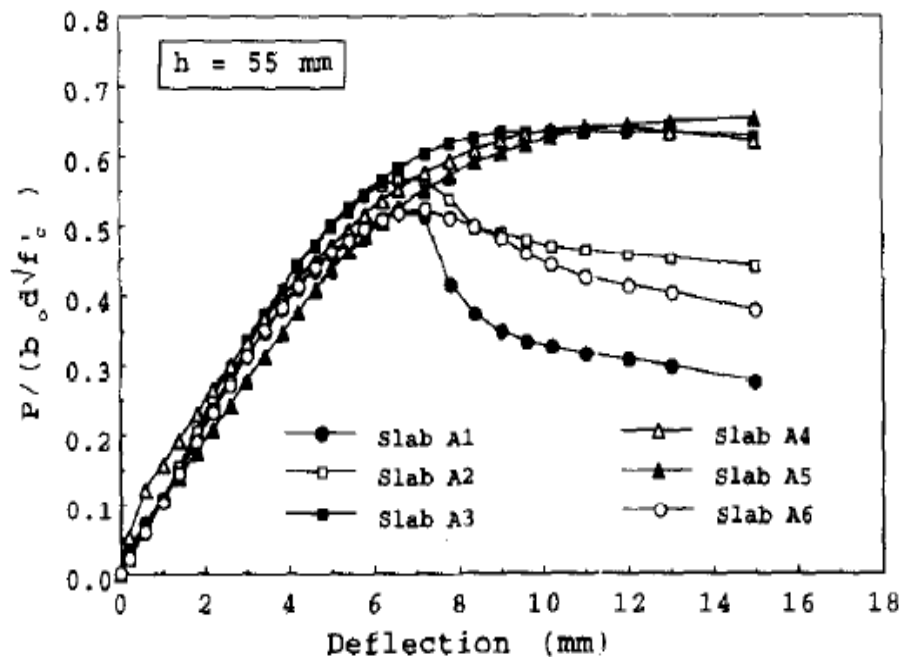| Series	Slab	Fiber reinforcement			Concrete compressive strength (MPa)	No. of slabs tested
		Fiber type	Fiber volume fraction (%)	Fiber aspect ratio		
A	A1	—	0·0	—	29·6	2
h = 55 mm	A2	Steel	0·45	100	30·0	2
d = 39 mm	A3	Steel	0·8	100	31·4	2
Ordinary	A4	Steel	1·0	60	24·6	2
reinf. = 5 (10 mm)	A5	Steel	2·0	60	20·0	2
deformed bars	A6	Polypr.	1·0	0·5 in long	32·2	2
B	B1	—	0·0	—	31·4	2
h = 75 mm	B2	Steel	0·45	100	31·4	2
d = 55 mm	B3	Steel	0·8	100	31·8	2
Ordinary	B4	Steel	1·0	60	29·1	2
reinf. = 7(10 mm)	B5	Steel	2·0	60	29·2	2
deformed bars	B6	Polypr.	1·0	0·5 in long	34·1	2

Figure 2.9 Normalized Load deflection curve of group A
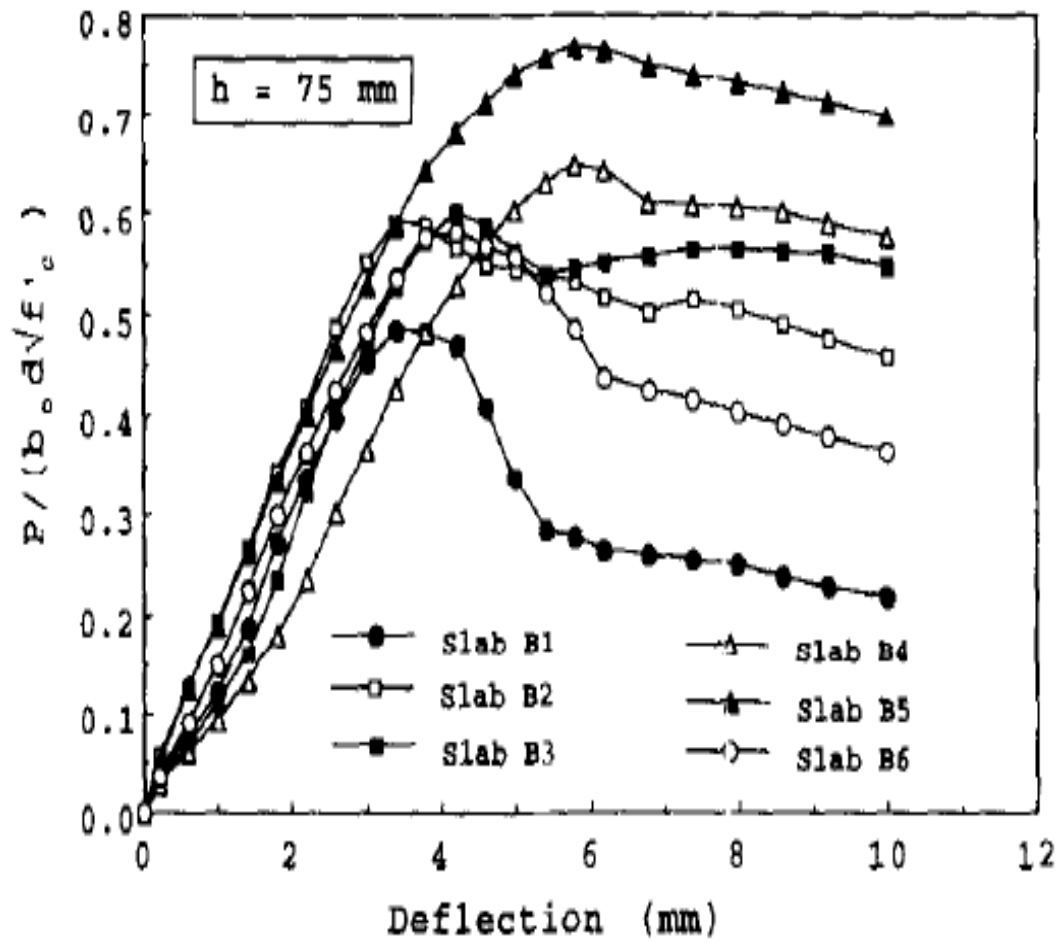
(Harajli et al, 1995)

Figure 2.10 Normalized load deflection curve of group B

(Harajli et al, 1995)

Tan and Paramasivam (1994) tested 14 simply supported square slabs to evaluate the punching shear behavior of SFRC slabs. Main parameters were span to depth ratio (a/d), steel fiber content by volume (p_f), slab thickness (h), strength of concrete (f'_c), and size of load- bearing plate (r). More details of the specimens are shown in Table 2.6.

Test results showed that increase in steel fiber content, slab thickness, steel fiber concrete compressive strength, or the loaded area in general results an increase in cracking load, yield load, peak load, and ductility of steel fiber reinforced concrete slabs. Punching shear failure occurred after yielding of steel bars, accompanied by cracks in the radial direction and partially in the tangential direction. In addition, load-deformation curves of SFRC slabs displayed four different states: initial elastic uncracked, crack growing, post yielding and post ultimate region.

14

Table 2.6 Details of Test Specimens (Tan & Paramasivam, 1994).

Series (1)	Slab number (2)	a/d (3)	ρ_f (%) (4)	h (mm) (5)	f_{cu}[a] (MPa) (6)	r (mm) (7)
1	SFRC1-1	27.2	0.31	35	50	100
1	SFRC1-2	40.9	0.31	35	50	100
1	SFRC1-3	54.5	0.31	35	50	100
2	SFRC2-1	40.9	0.50	35	50	100
2	SFRC2-2	40.9	1.00	35	50	100
2	SFRC2-3	40.9	1.50	35	50	100
2	SFRC2-4	40.9	2.00	35	50	100
3	SFRC3-1	65.2	0.31	22	50	100
3	SFRC3-2	25.1	0.31	57	50	100
3	SFRC3-3	20.5	0.31	70	50	100
4	SFRC4-1	40.9	0.31	35	35	100
4	SFRC4-2	40.9	0.31	35	65	100
5	SFRC5-1	40.9	0.31	35	50	200
5	SFRC5-2	40.9	0.31	35	50	150

Note: $d/h = 0.625$; $\rho_s = 0.87$ for all slabs.
[a] f_{cu} = design cube compressive strength.

A.Yaseen (2006) tested fourteen 800 x 800 x 60 mm simply supported high strength steel fiber reinforced concrete slabs to investigate the effect of steel fibers on the punching capacity of high strength reinforced concrete slabs. Key variables were compressive strength of concrete (35 to 65 MPa), size of column (75, 100 and 150 mm), steel fibers volume fraction (0.0, 0.25, 0.5, 0.75 and 1.0 %) and steel fiber aspect ratio (50, 67, 83, 100 and 133). Flexure reinforcement had the same ratio of 1.5 % in each direction. Load was applied centrally on the column stub in two increments, 0.5 ton until the first crack and then increased to 1 ton until the punching shear failure observed.

All slabs failed in punching (Figure 2.11). Steel fiber not only convert brittle-type punching failures into gradual and ductile shear failure, but also improved the ultimate punching shear loads and the deformation sustained at failure. The ultimate load increased by 48% as the fiber volume content increased from zero to 1%. In addition, the presence of steel fibers pulled away the failure surface from the edge of the column by about 2.62 to 2.96 times the slab depth and the shape of the punching shear failure region changed to more of a circular shape at higher values of fiber fraction. Moreover, as the compressive strength of concrete and column size increased, punching shear load increased. Punching

shear load increased by 57 % as the compressive strength increased from 35 to 65 MPa. Doubling the column size increased the punching shear by about 50 %.
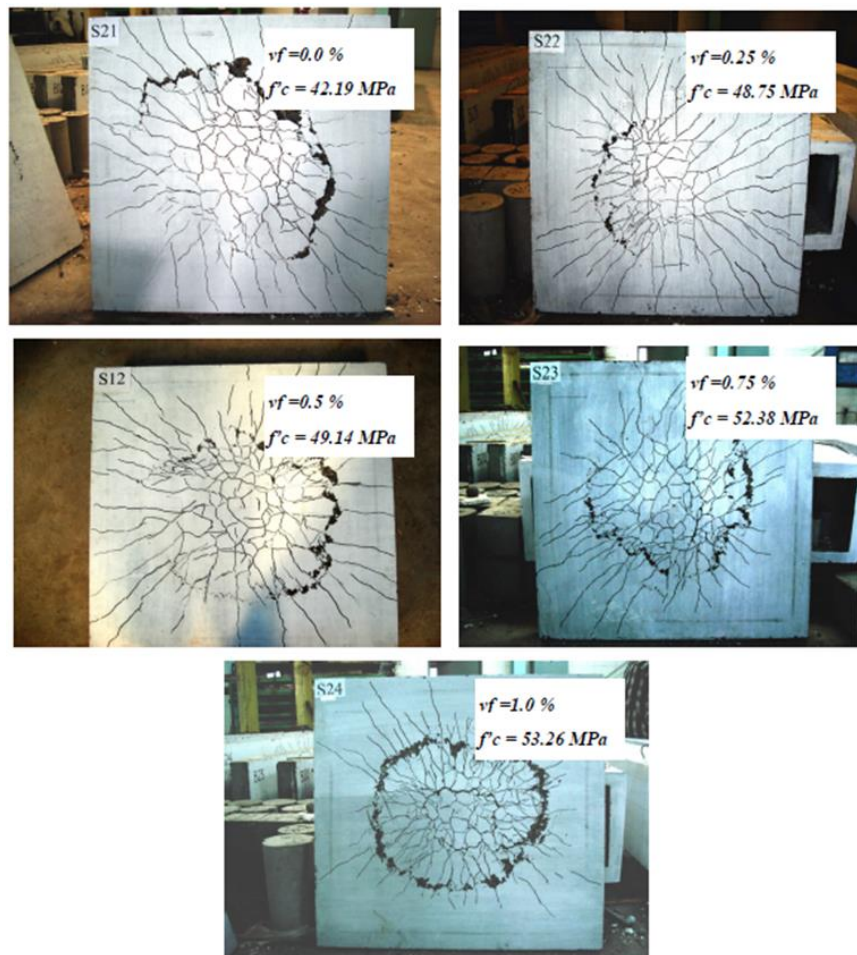

Figure 2.11 Failure modes of specimens (group Two and S12 from group One)

(A.Yaseen, 2006)

Recently, some studies have also been carried out using different types of fibers in the same mixture, called hybrid fiber reinforced concrete (HyFRC). Ramin (2014) performed an experimental program in order to evaluate the behavior of hybrid fiber reinforced concrete slabs. The experimental program contained of eight full scale two-way slabs with dimensions of 1900 x 1900 mm². Slabs were divided into two groups of thicknesses (200 and 250 mm). Steel fiber fraction was varied as 0, 0.68, 0.8 and 0.96% within each group. Synthetic fibers with 0.2 % by volume were added to all specimens except for reference specimens without any fibers. Flexural reinforcement ratio was 1.3% for all slabs.

The study revealed that the presence of fibers had more substantial effect on the stiffness and mode of failure of 200 mm-thick slabs than 250 mm-thick slabs, as seen in load-deformation curves shown in Figure 2.12 & Figure 2.13. Addition of fibers increased the ductility, stiffness, and energy-absorption capacities. Ultimate capacity of slabs with fiber content of 0.68, 0.8, and 0.96 % was increased by 15, 22, and 32%, respectively, compared to 200 mm thick reference slab. For the same amount of fibers, punching load capacity was increased by 20, 14, and 20% for 250 mm-thick slabs, respectively.
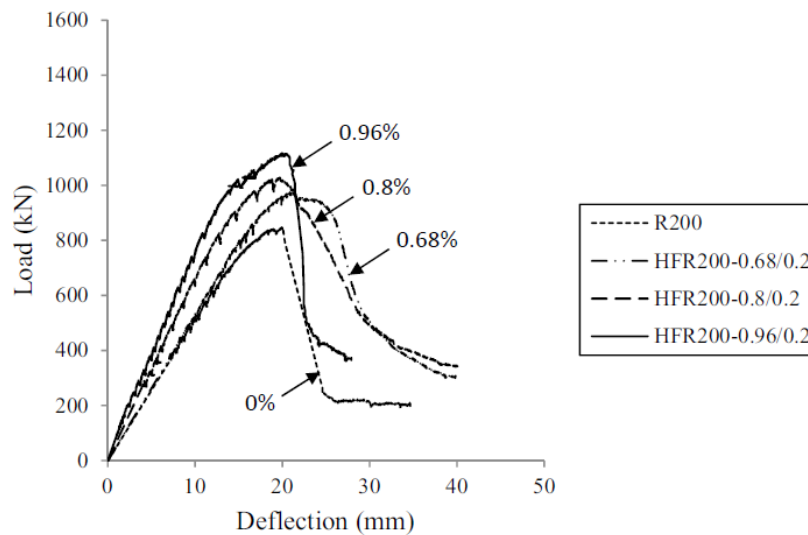

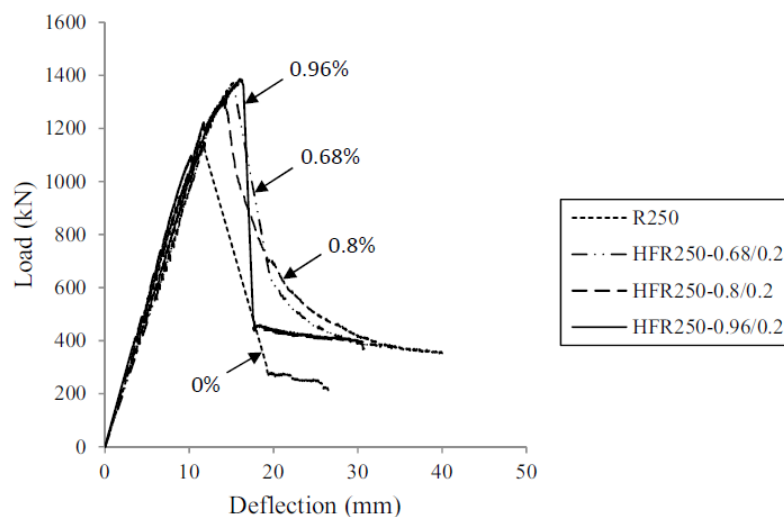Figure 2.12 Load–deflection characteristics of group 1

(Ramin, 2014)

Figure 2.13 Load–deflection characteristics of group 2

(Ramin, 2014)

CHAPTER 3

EXPERIMENTAL PROGRAM

An experimental program was carried out at Izmir Institute of Technology (IYTE) in order to investigate the punching behavior of hybrid fiber reinforced concrete (HyFRC) panels with and without ordinary steel reinforcement. The experimental program involved of designing, preparing, casting, testing, and assessment of the punching behaviors of 13 slabs. In addition, this chapter will discuss the test program in detail, including test specimens, material, as well as the test setup and instrumentation.

3.1 Test Specimens

In total, 13 slab specimens were cast. All specimens had dimensions of 1700 x 1700 x 50 mm (Figure 3.1). Ten of specimens were cast in five pairs. In every pair, one specimen was cast with steel fiber only and the other with steel fiber and PVA fiber. Four of the five pairs were cast without steel bar reinforcement, whereas one pair was cast with steel bar reinforcement. One specimen was cast with steel and PVA fibers, but 20% of fine aggregate was replaced with lightweight perlite. Two specimens were kept as reference, one of which was cast as plain concrete and one with ordinary steel bar reinforcement without any fibers.

Flexural reinforcement used in specimens were 5 mm diameter steel bars with a cross-sectional area of 19.63 mm^2. The reinforcements were in a welded wire mesh form. Same ratio of the reinforcement 0.462% was used in both directions with clear cover of 20 mm from the bottom of the slab. Spacing between the steel bars was 150 mm as shown in Figure 3.2

Two formworks were fabricated side by side in structural lab at Izmir Institute of Technology (IYTE) (Figure 3.3 a). Sixteen pieces of wood were nailed in the formworks and covered by steel pipes to create supporting holes that would be used to fix the specimens to the test setup (Figure 3.3 b). Also, four U-shaped reinforcement hooks were place at appropriate locations in order to ease lifting and transportation of specimens after casting.
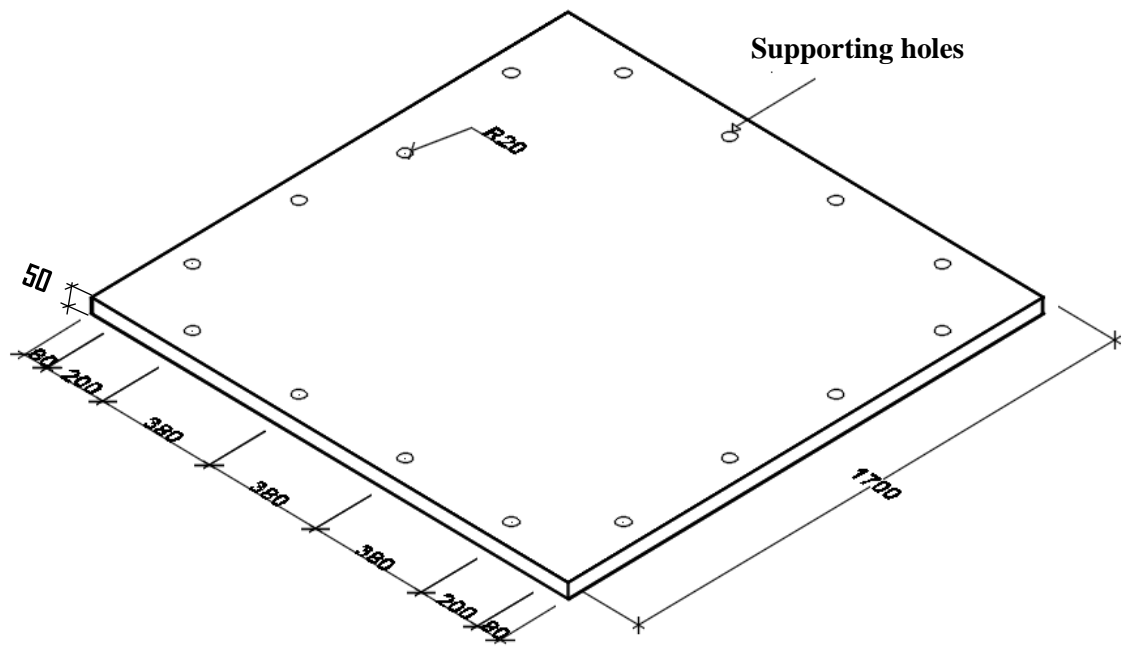
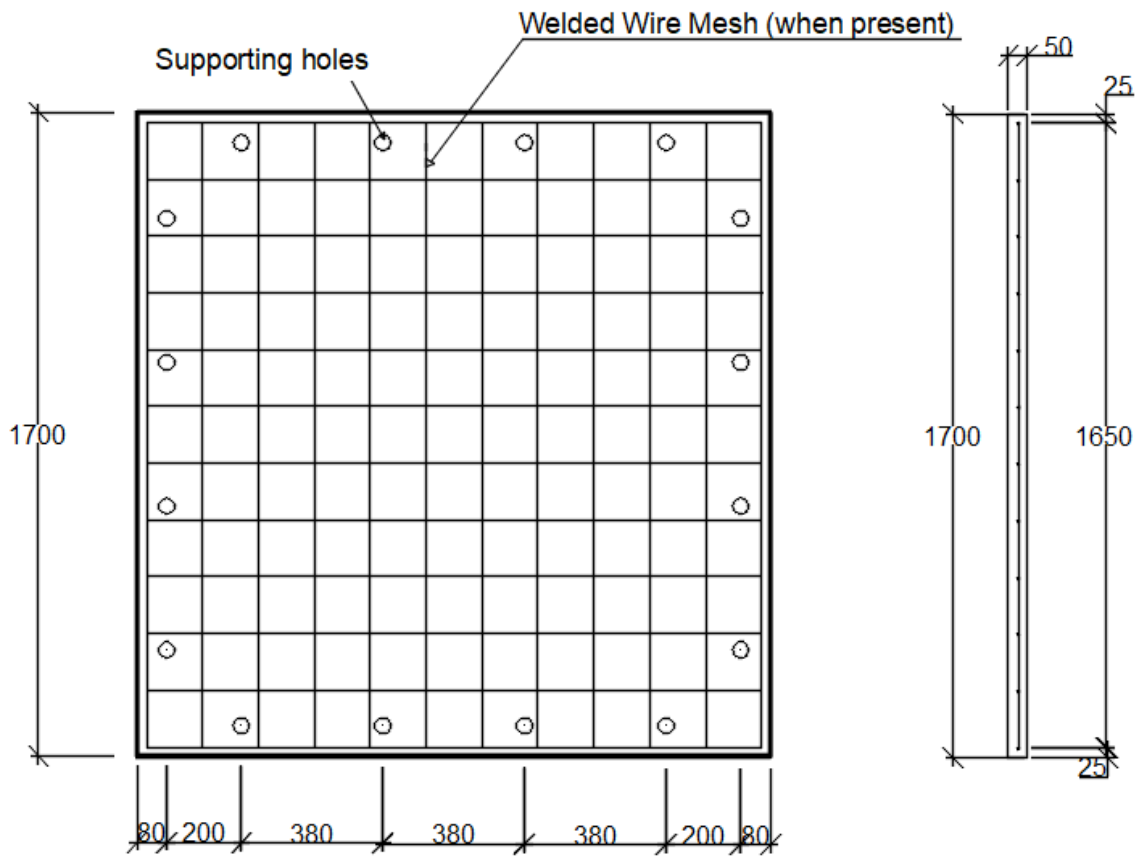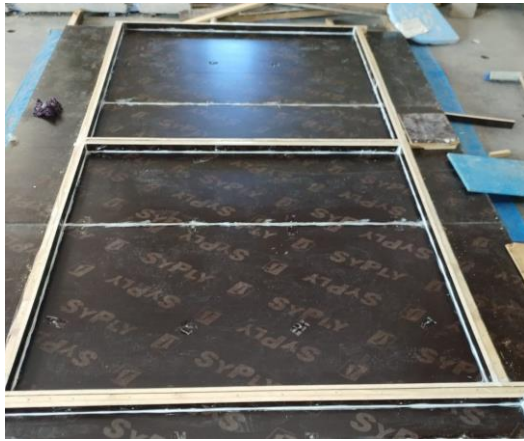Figure 3.1 Slab Specimen (all dimensions are in mm)

Figure 3.2 Slab Specimens with Conventional Reinforcement (all dimensions are in mm)

(a) Formworks	b) Pieces for supporting holes

Figure 3.3 Formworks

Concrete mixtures were prepared in materials laboratory and carried by wheelbarrows to the structural laboratory nearby. A rotating drum mixer with 200-liter capacity was used (Figure 3.4). The mixing process was performed step by step. First coarse and fine aggregate was mixed in the mixer with some of the water in order to gain a saturated surface dry condition. After then, cement and flay ash content were added, remaining water was poured into the mixer and well mixed. At the last stage, steel fibers and PVA fibers were gradually added to mixer to avoid balling of fibers (Figure 3.5). Concrete for each specimen was prepared in two parts since the mixer did not have sufficient capacity. First half of the concrete volume of mixture was prepared and poured into formwork, then the remaining half done in same manner (Figure 3.6 a). A handheld electric vibrator was used for compacting concrete (Figure 3.6 b). For each mixture, six cylinders (ϕ150 x 300 mm) were cast as well, in order to determine the mechanical properties of the concrete. Specimens were covered with burlap and plastic sheets for more than two weeks for curing (Figure 3.6 d) and kept in humid environment for approximately 90 days before testing.

Figure 3.4 Rotating drum mixer

(a)   (b)

Figure 3.5 (a) Adding steel Fiber into mixer (b) Adding PVA fiber into mixer

a) Pouring half mixture into formwork

b) Compaction by handheld electric vibrator

c) Finishing

d) Burlap and plastic for covering

Figure 3.6 Casting of Specimens

3.2 Material Properties

Portland cement (PC), CEM I 42.5 R in conformity with TS EN 197-1: 2012 was used. Specific gravity and Blaine fineness of the cement were (3.06 and 325 m^2/kg) relatively.

Class-F fly ash in conformity with ASTM C 618, which had specific gravity of 2.61 and Blaine fineness of 290 m^2/kg was used.

Coarse aggregate used, was crushed limestone with maximum aggregate size of 16 mm and river sand was used as fine aggregate. A proper combination of coarse and fine aggregate was provided, grading of which fits to the limitations of Turkish Standards. The

grading curves of coarse and combined aggregates are given in Figure 3.7 and Figure 3.8, respectively. 20% of the coarse aggregate and 80% of the combined aggregate were used in mix design.
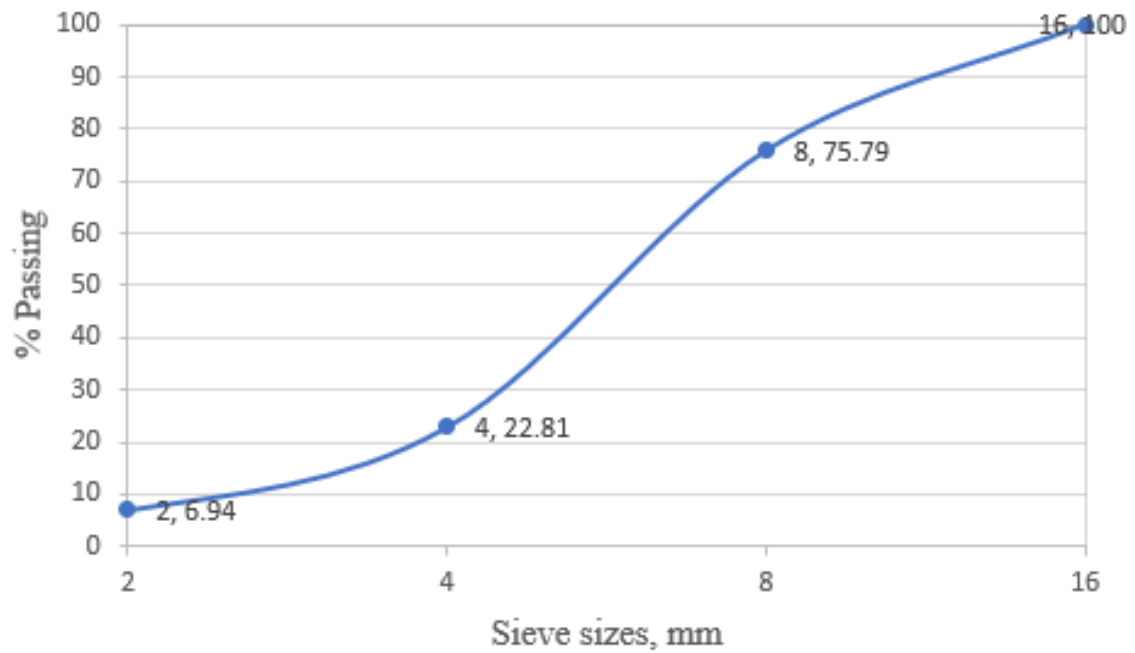

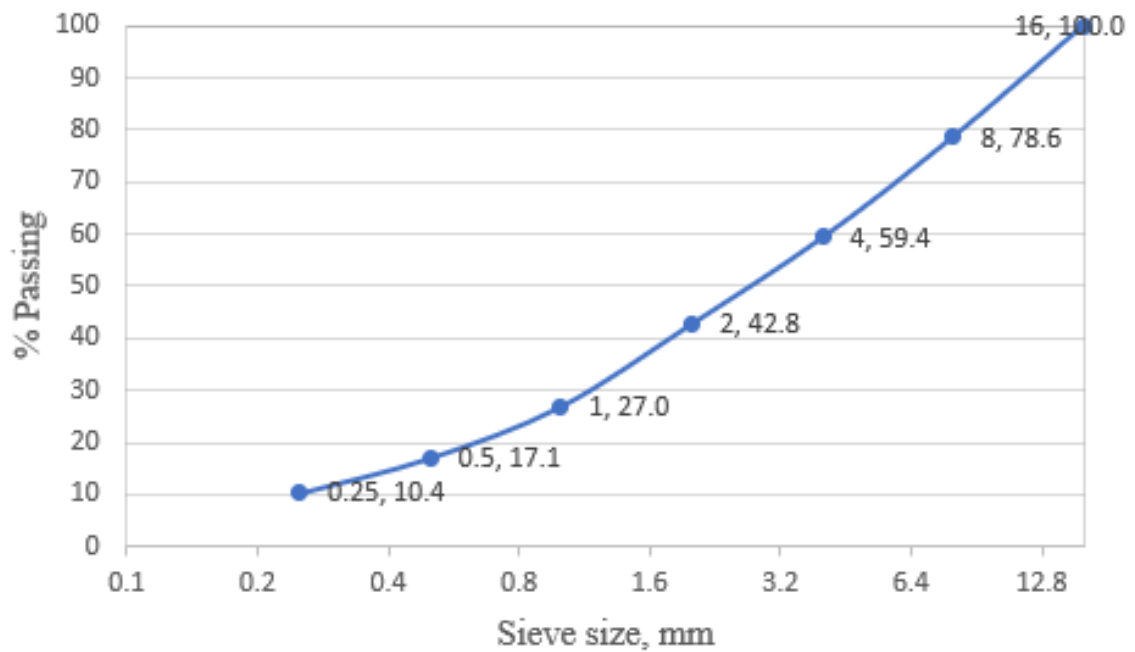Figure 3.7 Gradation curve of coarse aggregates

Figure 3.8 Gradation curve of combined aggregates

Expanded perlite aggregate was used in one specimen, which replaced 20% of the fine aggregate.

Polyvinyl Alcohol (PVA) fibers, Kuralon K-II RECS 15/8mm brand, were used in HyFRC mixture. Properties of PVA fibers are presented in Table 3.1.

Table 3.1 Mechanical properties of PVA fiber

Fiber Type	Length (mm)	Diameter (mm)	Specific Gravity	Nominal Strength (MPa)	Apparent Strength (MPa)	Strain (%)	Young Modulus (GPa)
PVA	8	40	1.3	1610	1092	6	42.8

Three type of hooked-end Bekaert brand Dramix® steel fibers were used in this study. The types used were 45/35 3D, 65/60 3D and 65/60 5D, properties of which presented in Table 3.2.

Table 3.2 Mechanical properties of steel fibers

Fiber Type	Aspect Ratio	Length (mm)	Diameter (mm)	Young's Modulus (MPa)	Tensile Strength (MPa)	Hook Geometry
Dramix ® 45/35 3D	45	35	0.75	210 000	1225	
Dramix ® 65/60 3D	65	60	0.90	210 000	1160	
Dramix ® 65/60 5D	65	60	0.90	210 000	2300	

To evaluate the compressive strength of concrete, cylinder samples were cast simultaneously with slab specimens, and using identical concrete mixtures. Cylinder specimens were 300 mm in length and 150 mm in diameter. Six cylinders for each slab specimen were provided, three of which were cast before adding fiber and the other three after adding fibers to the mixtures. The cylinders specimens were kept in water tank for approximately one month to cure, after then kept at same environment as the slab

specimens (Figure 3.9). The cylinder specimens were tested under a digital compressive machine as shown in Figure 3.10, at about the same time as the corresponding slab specimen, with a stroke rate of 0.6 N/mm2s. The compressive strength results are presented in Table 3.3 and Figure 3.11.

Figure 3.9 Cylinder Specimens

Figure 3.10 Digital compressive test machine

Table 3.3 Compressive strength test results

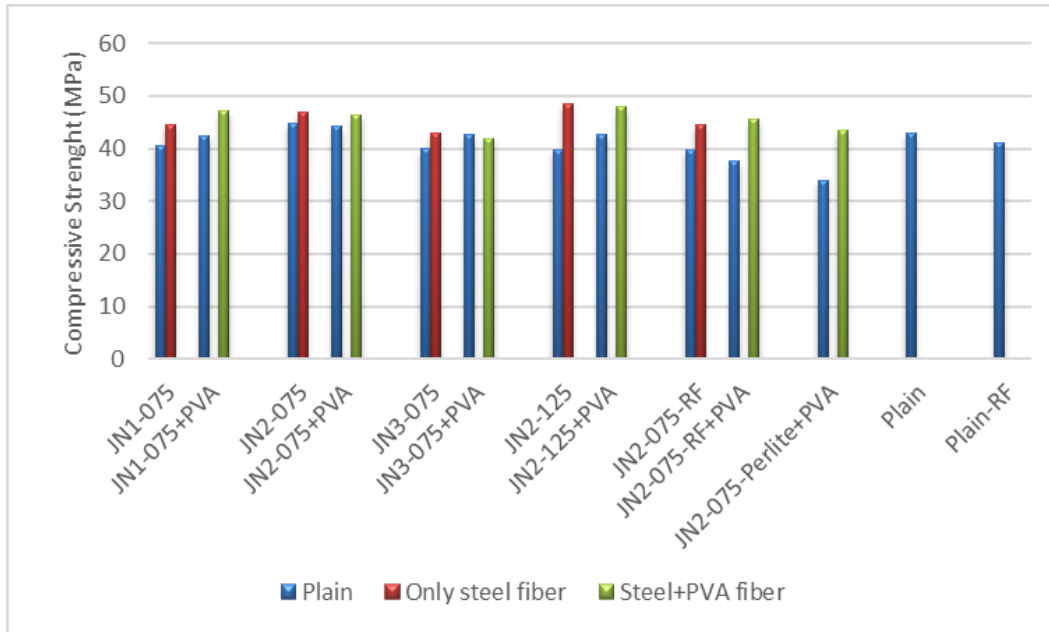| Mix	Compressive Strength Plain Concrete (without any fiber) (MPa)	Compressive Strength (with fibers) (MPa)
JN1-075	40.6	44.6
JN1-075+PVA	42.5	47.1
JN2-075	44.8	46.8
JN2-075+PVA	44.2	46.5
JN3-075	39.9	43.0
JN3-075+PVA	42.6	41.9
JN2-125	39.8	48.5
JN2-125+PVA	42.7	47.9
JN2-075-RF	39.8	44.4
JN2-075-RF+PVA	37.6	45.7
JN2-075-Perlite+PVA	34.0	43.4
JN-Plain	42.9	-
JN-Plain-RF	41.0	-

Figure 3.11 Compressive strength test results

Two typical reinforcing bars were tested under tension, which results in an average yield strength of f_y=700 MPa and ultimate strength of f_y=735 MPa. An average stress-strain curve obtained from the test is shown in Figure 3.12.
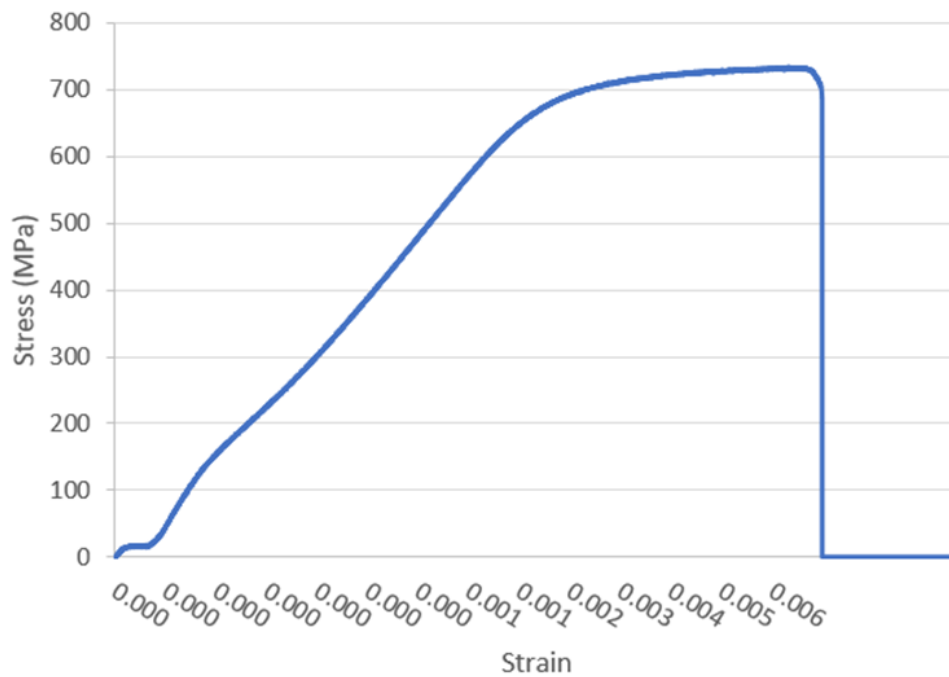

Figure 3.12 Average stress-strain curve for two typical reinforcing bars

3.3 Mix Design

Three types of mixture were used in this study as following.

- Plain concrete
- Steel Fiber Reinforced Concrete
- Hybrid Fiber Reinforced Concrete

The cement, water, aggregate, fly ash and PVA fibers proportion (when present) were same for all mixes. However, steel fiber content was varying. The parameters of mix design are presented in Table 3.4.

Table 3.4 Concrete Mixture

Cement	273 Kg/m^3
Flay ash	327 Kg/m^3
Water	240 Kg/m^3
Coarse aggregate	677 Kg/m^3
Fine aggregate	623 Kg/m^3
Steel fiber	58.5 & 97.5 Kg/m^3
PVA fiber	3.25 Kg/m^3

The specimens were named according to fiber type and volume content (Figure 3.13). The fiber volume content and names of specimens are given in Table 3.5.
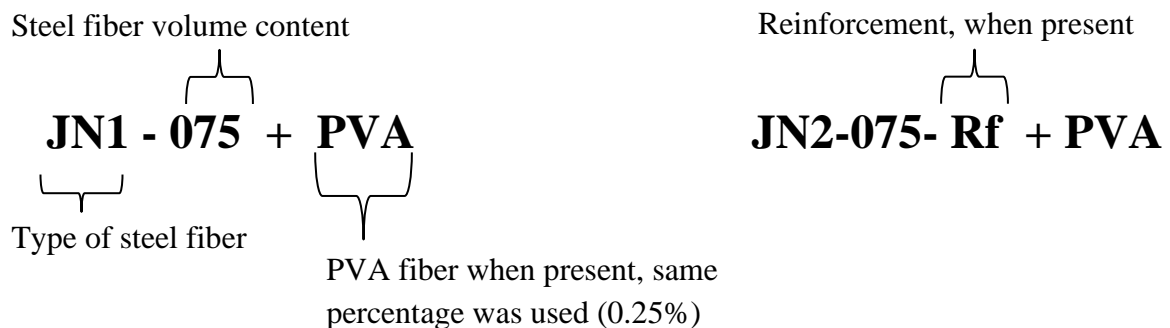
Steel fiber volume content

Reinforcement, when present

JN1 - 075 + PVA

JN2-075- Rf + PVA

Type of steel fiber

PVA fiber when present, same percentage was used (0.25%)

Figure 3.13 Naming of slab specimens

Table 3.5 Mixture proportions and specimen's names.

Mix	Fiber Type	Steel Fiber Volume content (%)	PVA Fiber Volume content (%)	Steel Reinforcement	Perlite Content
JN1-075	45/35 3D	0.75	-	-	-
JN1-075+PVA	45/35 3D	0.75	0.25	-	-
JN2-075	65/60 3D	0.75	-	-	-
JN2-075+PVA	65/60 3D	0.75	0.25	-	-
JN3-075	65/60 5D	0.75	-	-	-
JN3-075+PVA	65/60 5D	0.75	0.25	-	-
JN2-125	65/60 3D	1.25	-	-	-
JN2-125+PVA	65/60 3D	1.25	0.25	-	-
JN2-075-RF	65/60 3D	0.75	-	φ5/150 mm mesh	-
JN2-075-RF+PVA	65/60 3D	0.75	0.25	φ5/150 mm mesh	-
JN2-075-Perlite+PVA	65/60 3D	0.75	0.25	-	20% of fine aggregate
JN-Plain		-	-	-	-
JN-Plain-RF		-	-	φ5/150 mm mesh	-

3.4   Test Setup

A test setup was designed and fabricated in the structural lab (Figure 3.14 & Figure 3.15). Four steel I-beams were bolted on four footings which were mounted to the strong floor of the lab. The beams were 50 cm above the floor level in order to facilitate installation of displacement transducers. Specimens were simply supported on all four sides, in such a manner that they could not move in vertical direction, but they were free to rotate. High strength rods with 20 mm of diameter were used to connect the slab specimens to the beams through the holes left in the specimens when they were cast. Spherical washers were used at these support points to provide free rotation (Figure 3.16).
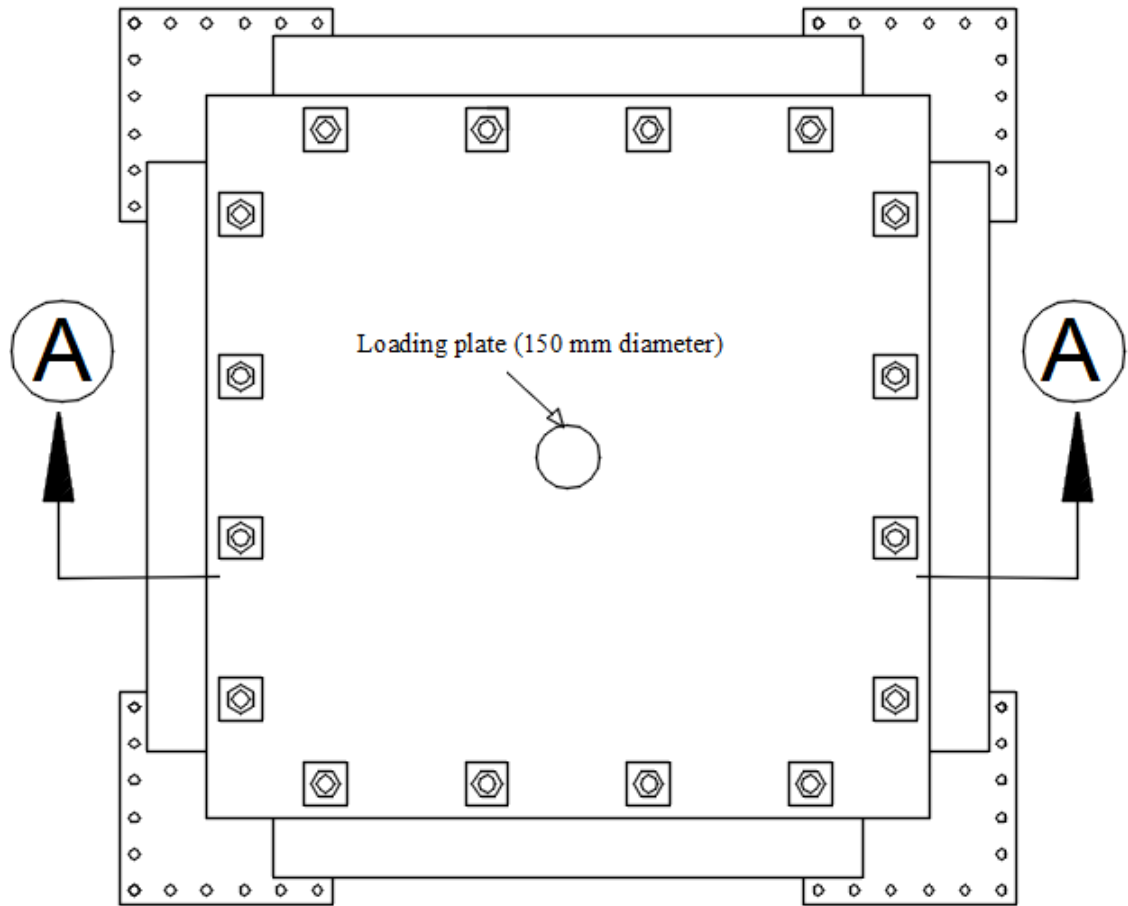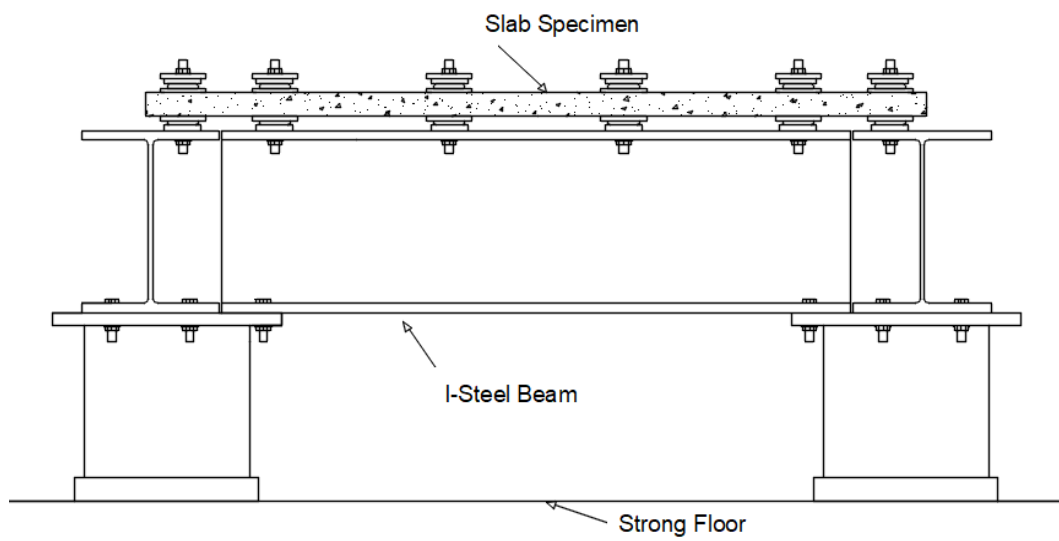
Figure 3.14 Test setup top view
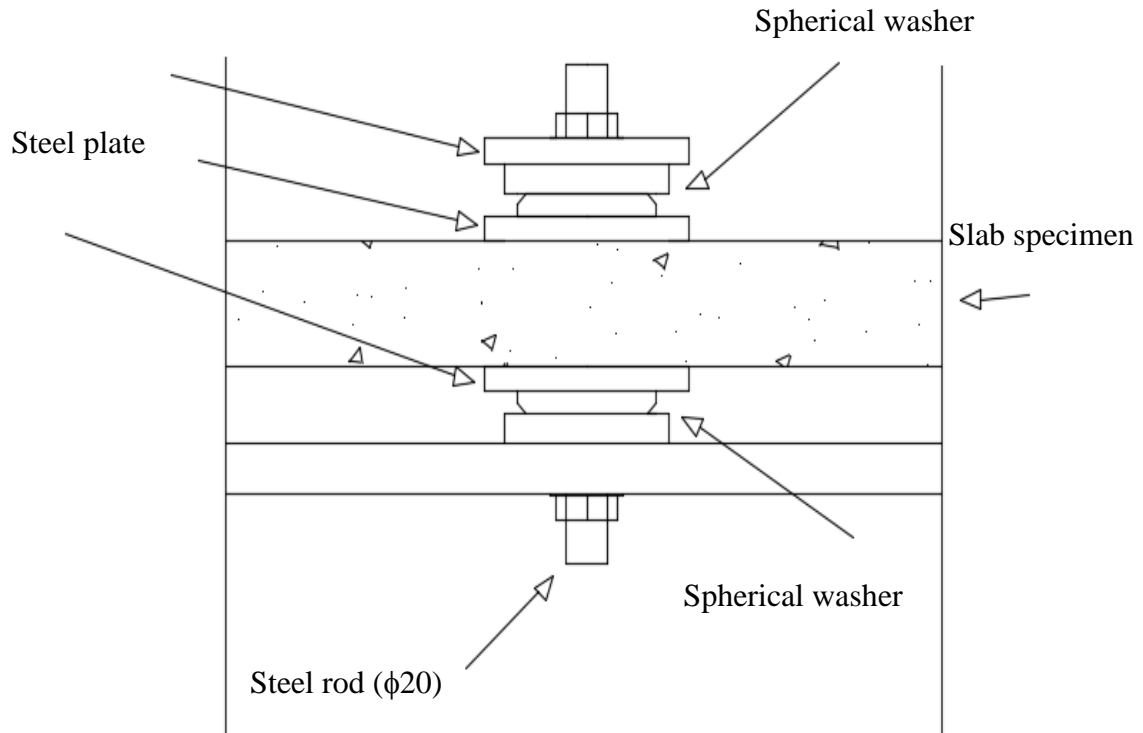

Figure 3.15 Test Setup section A-A

Figure 3.16 Detail of a support point on the setup

The tests were carried out using a 560-kN MTS actuator system. The load was applied at the center of specimen through a circular steel plate with diameter of 150 mm, at a displacement rate of 0.025 mm/min, as shown in (Figure 3.17 & Figure 3.18). Loading plate was connected to the loading head with a ball-and-socket joint so that any moment transfer at the loading point was prevented (Figure 3.19).
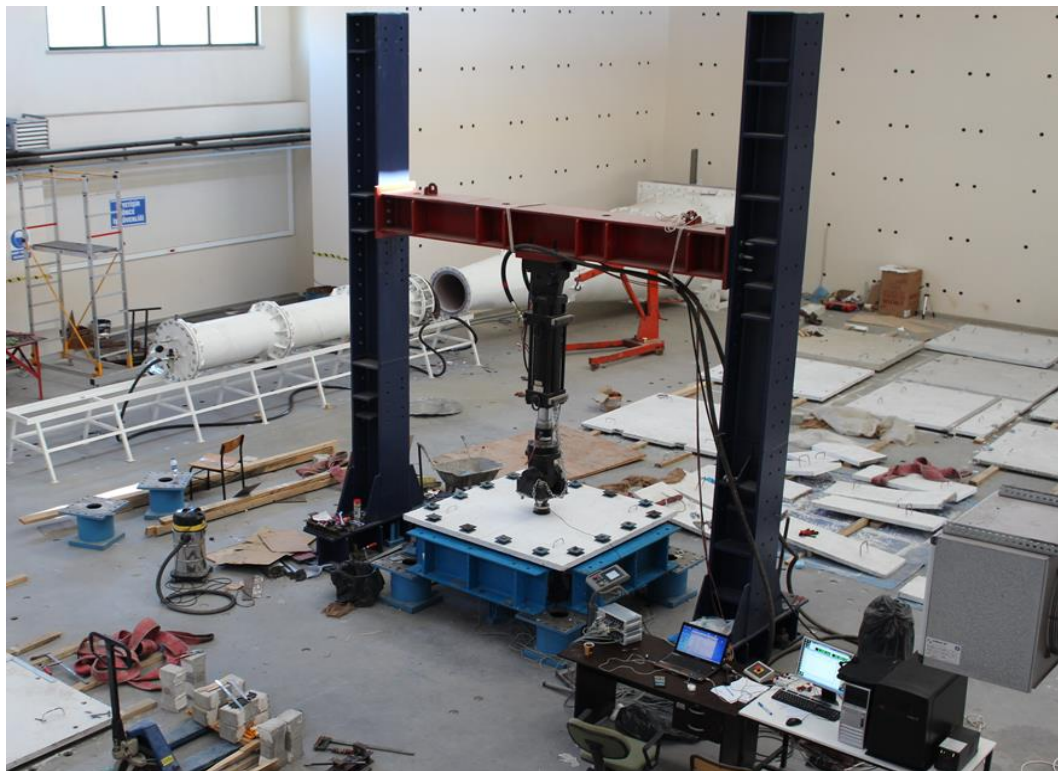
Figure 3.17 Test setup

Figure 3.18 Test setup

3.5 Instrumentation

The test specimens were instrumented by a load cell and displacement transducers (Resistive Linear Position Transducer, RLPT). A load cell with 50 kN capacity was placed under the actuator head at loading point to obtain accurate load readings (Figure 3.19).

15 RLPTs were used, locations of which are shown in Figure 3.20 . Steel rods were used to connect RLPTs to a hinge underneath the specimens in order to prevent any bending in the extension rods . Aluminum U-profiles, fixed on the bottom surface of the specimens by epoxy, were used to connect the hinges to the specimen's surface (Figure 3.21). A view of RLPTs is presented in Figure 3.22.

Data collected from 15 RLPTs and a load cell was collected by a data acquisition system at an 8 sample/second rate. Load and stroke data from the MTS system was also recorded (Figure 3.23). Photos were also taken throughout the test whenever a new crack formed.
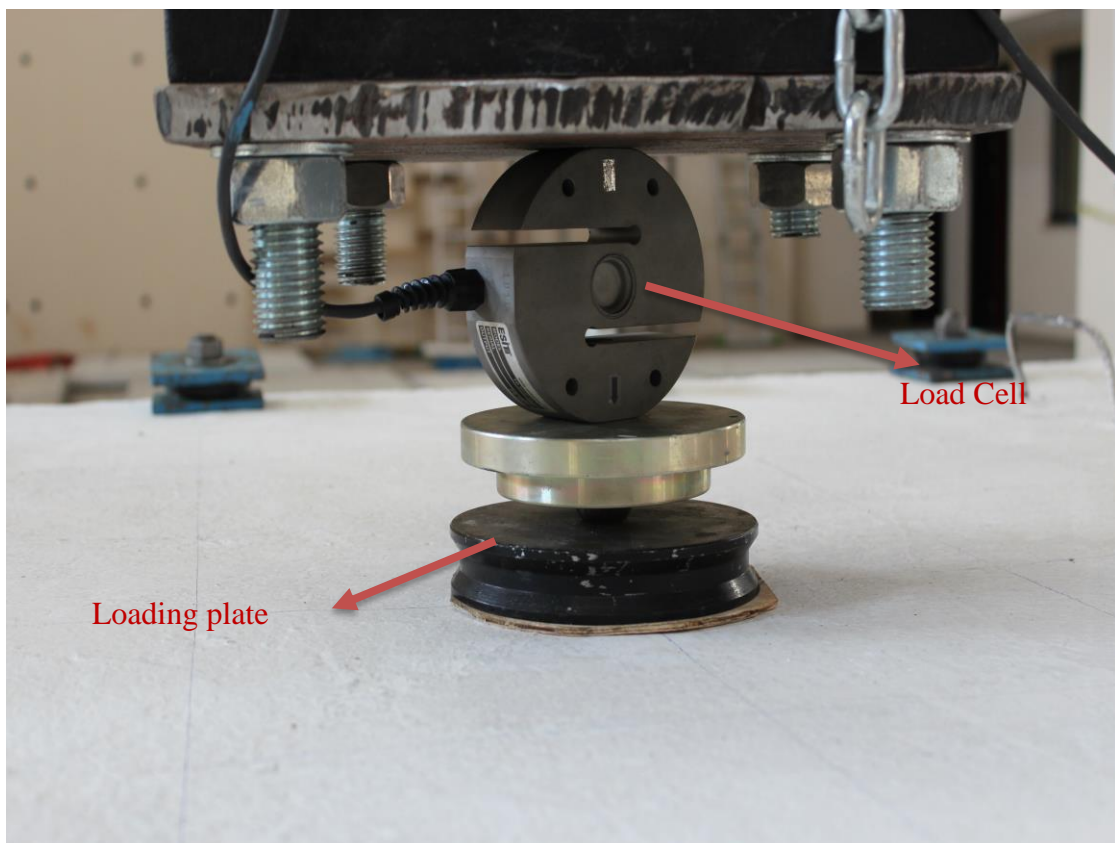

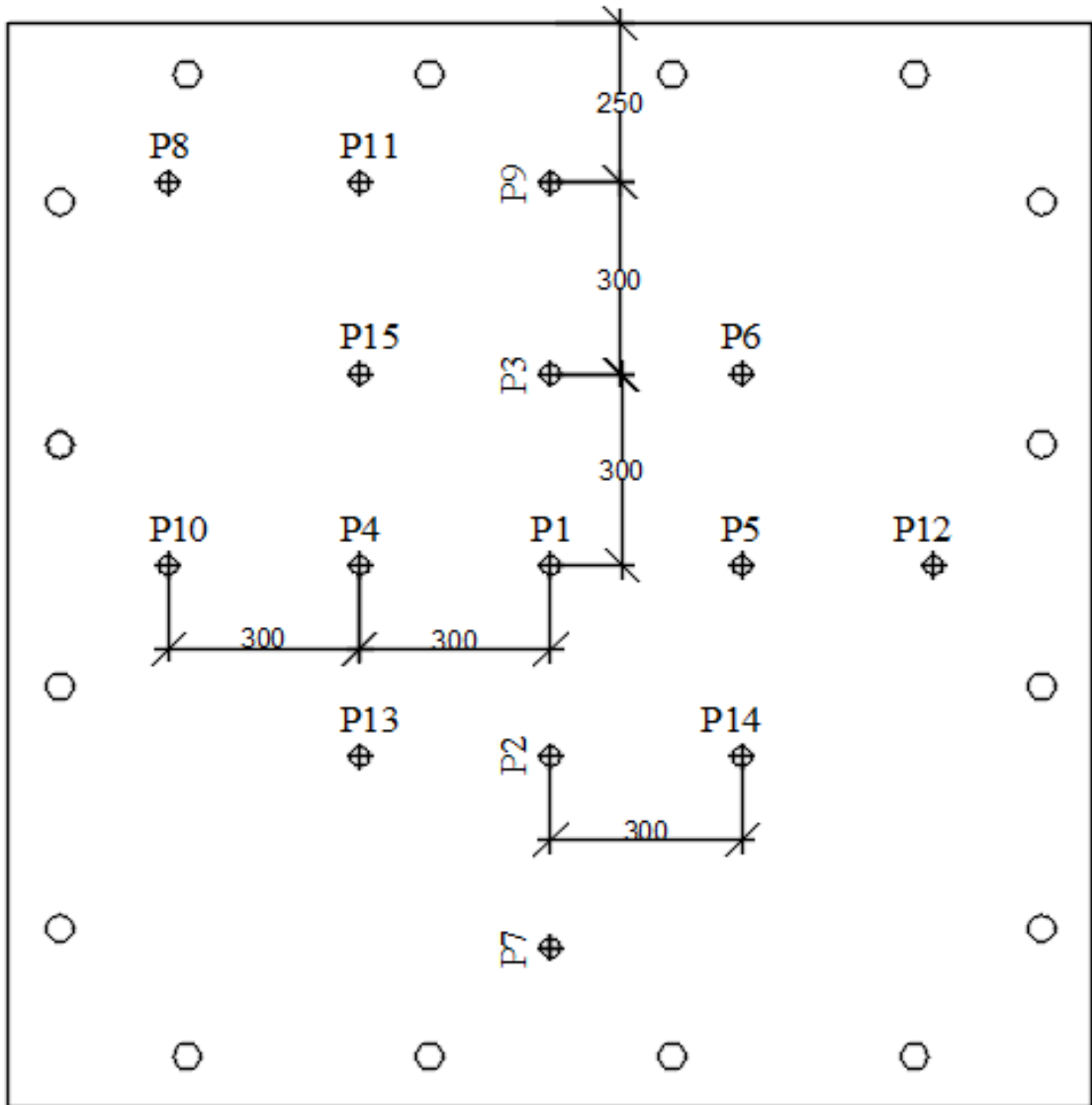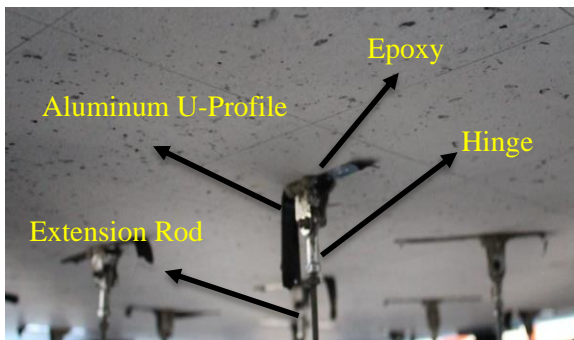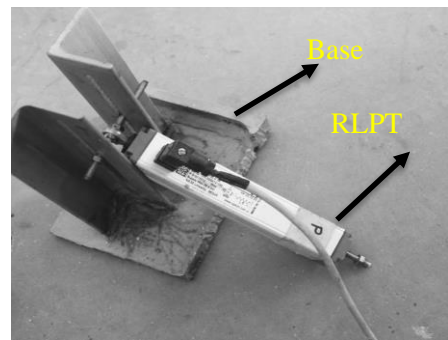Figure 3.19 Loading plate and cell

Figure 3.20 RLPTs Locations (All dimensions are in mm)

(a)

(b)

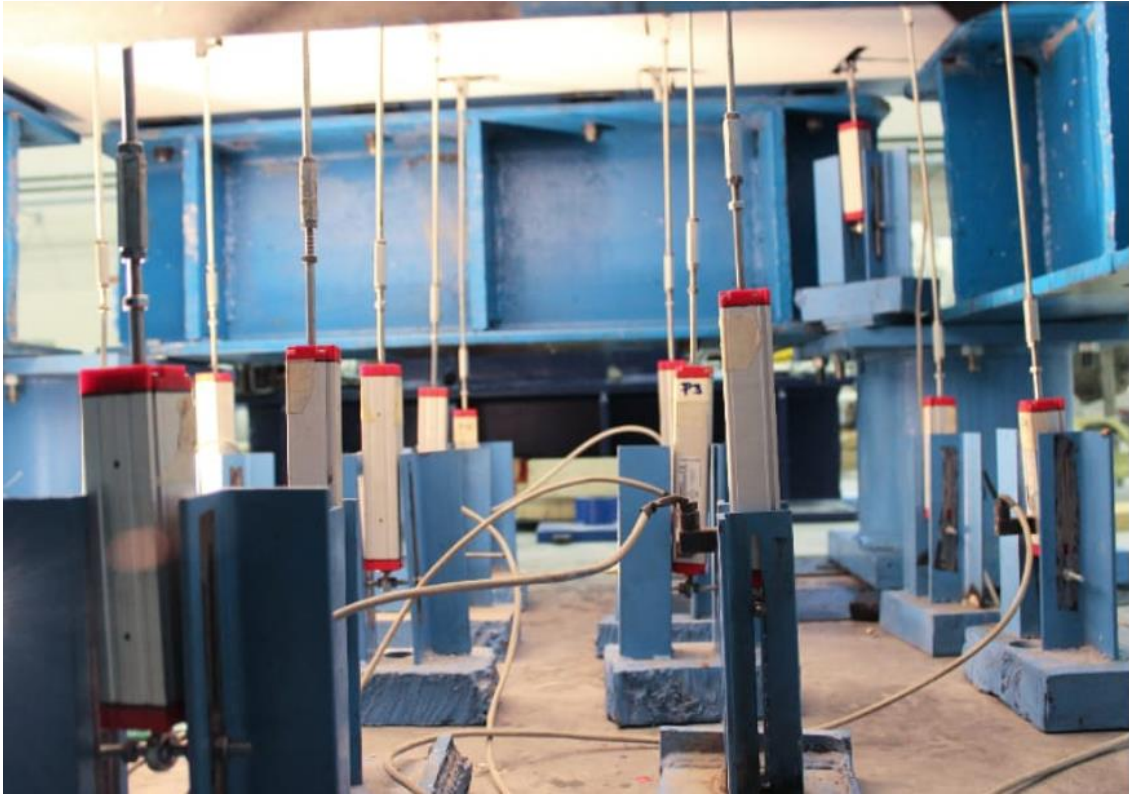Figure 3.21 (a) connection between specimen and hinge; (b) Connection between potentiometer and rod.
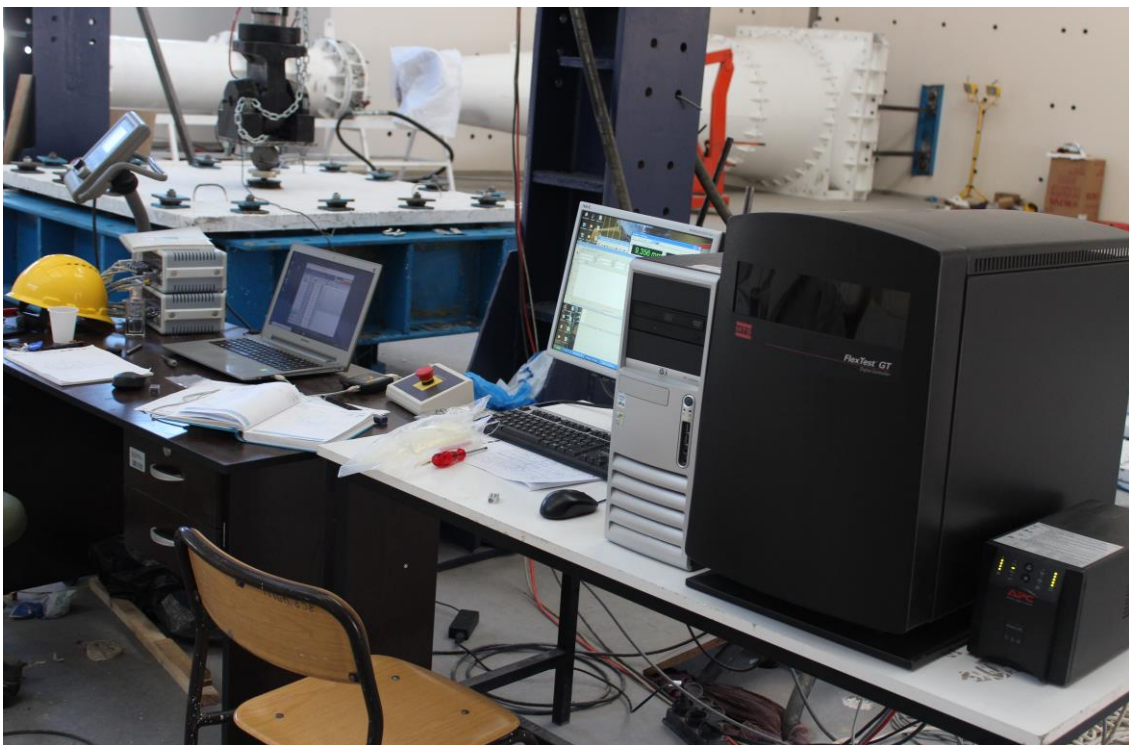
Figure 3.22 A view of RLPTs

Figure 3.23 Data acquisition system

CHAPTER 4

TEST RESULTS AND DISCUSSION

This chapter provides the data obtained during the testing of thin panel specimens. As mentioned before, the panel dimensions and PVA fiber volume ratio (whenever used) were identical for all specimens. The main variables were steel fiber types, steel fiber volume ratio and presence of steel bars. To assess the performance of tested specimens and determine the effects of the fiber and steel bar reinforcement on the punching shear strength, test results of thirteen panel specimens were compared with each other and results are discussed. In the following discussions, specimens with identical steel fiber content are grouped and results are presented and compared within the group in terms of effects of PVA addition, use of steel bars and use of perlite as fine aggregate. Then, specimens are cross compared to assess their behavior according to their fiber and reinforcement content in general. Moreover, energy absorption capacity was calculated as the area under the midpoint deflection curve at 80 % of the maximum load in post peak region.

4.1 Specimens JN1-075 and JN1-075+PVA

Load-midpoint deflection curve of JN1-075 and JN1-075+PVA is shown in Figure 4.1. As seen from the figure, at the initial state, JN1-075JN1-075 displayed stiffer behavior compared to JN1-075+PVA. In both panels, the applied load increased linearly with displacement. An immediate drop in the load was observed in JN1-075 after the first crack. As the crack formation stabilized, the load picked up again until after a midpoint deflection of approximately 36 mm, after which the load decreased gradually until failure. In specimen, JN1-075+PVA, the cracking load was sustained for a while, which later slightly dropped and continued to decrease gradually until failure. In both panels, punching failure was observed. The specimen without PVA showed more ductile punching failure compared to panel with PVA. However, the load capacity was slightly higher in panel with PVA until for a displacement around 87 mm. First crack observed in JN1-075 and JN1-075+PVA were approximately at 16.6 kN and 17 kN, respectively, which were almost the peak loads as well in both specimens. In specimen JN1-075,

absorption energy capacity was higher than the JN1-075+PVA and the increasement in absorption capacity was about 14.3 %.
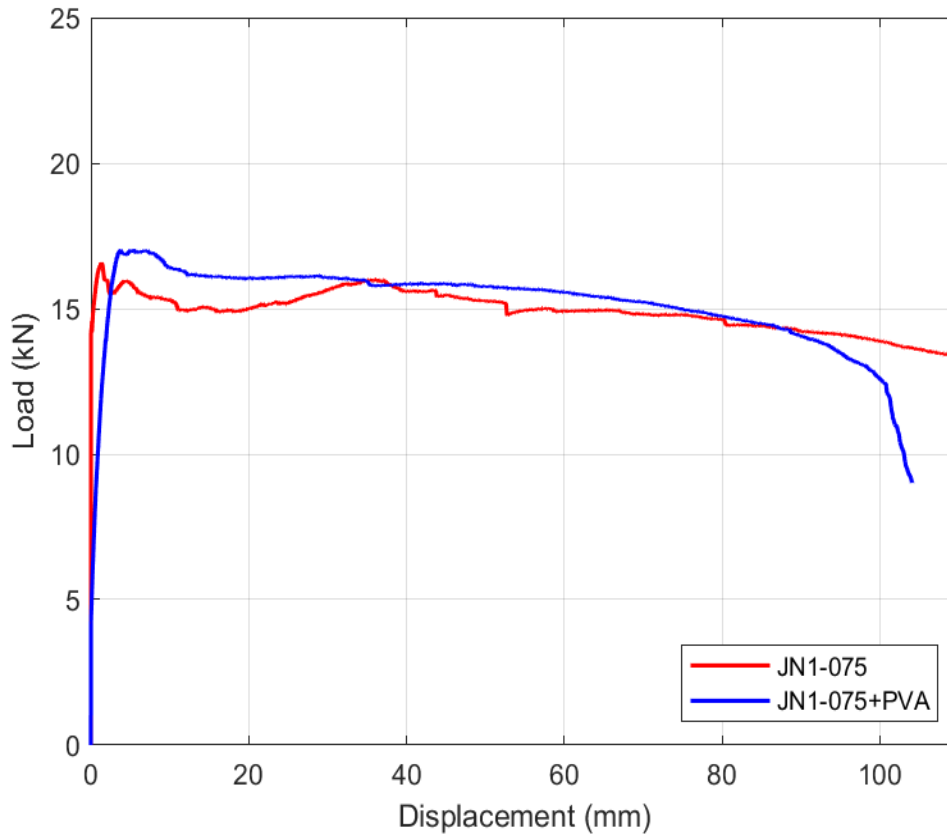

Figure 4.1 Load-midpoint deflection curve of panel JN1-075 and JN1-075 +PVA

Crack patterns for JN1-075 and JN1-075+PVA are presented from Figure 4.2 to Figure 4.5. In both panels, JN1-075 and JN1-075 +PVA, first cracks were observed on the bottom surface at the middle extending on diagonals toward the corners of the panels. As load was increased, in panel JN1-075 every diagonal crack divided into two at the middle of the cracks and passed near by the corner supports. However, in specimen JN1-075+PVA two of the diagonal cracks were similar with the one in panel JN1-075, and the other two, a parallel crack occurred with each crack from the center and passed near by the corner supports. In panel, JN1-075 two more cracks were observed between the diagonal cracks. In both panels, only one of the diagonal cracks were spread into small cracks . As the flexure cracks became wider, tangential cracks start to form on the top surface. In panel JN1-075 +PVA, the cracks were nearer to the steel plate than in the panel

JN1-075. The circular punching cracks occurred at the second peak load in panel JN1-075, whereas in panel JN1-075. +PVA, they occurred at a displacement around 16 mm. After the initiation of punching cracks, load started to decrease gradually in both panels. When the punching cone began to separate, decrease in load was faster in panel JN1-075+PVA than in panel JN1-075. Finally, both specimens failed by punching as clearly seen from the punching cone in Figure 4.2 to Figure 4.5.
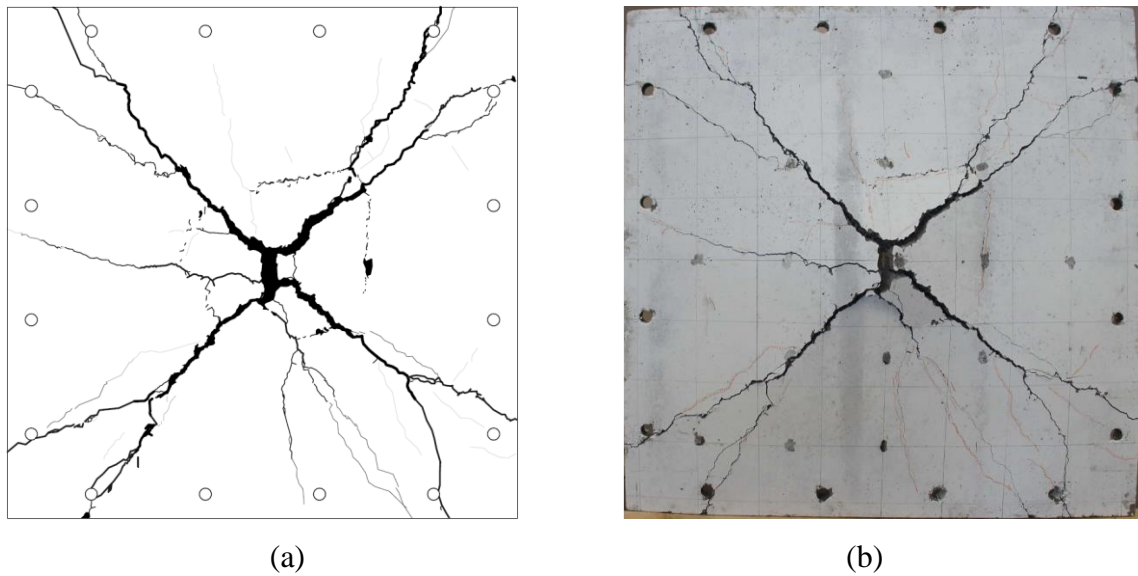

(a)   (b)

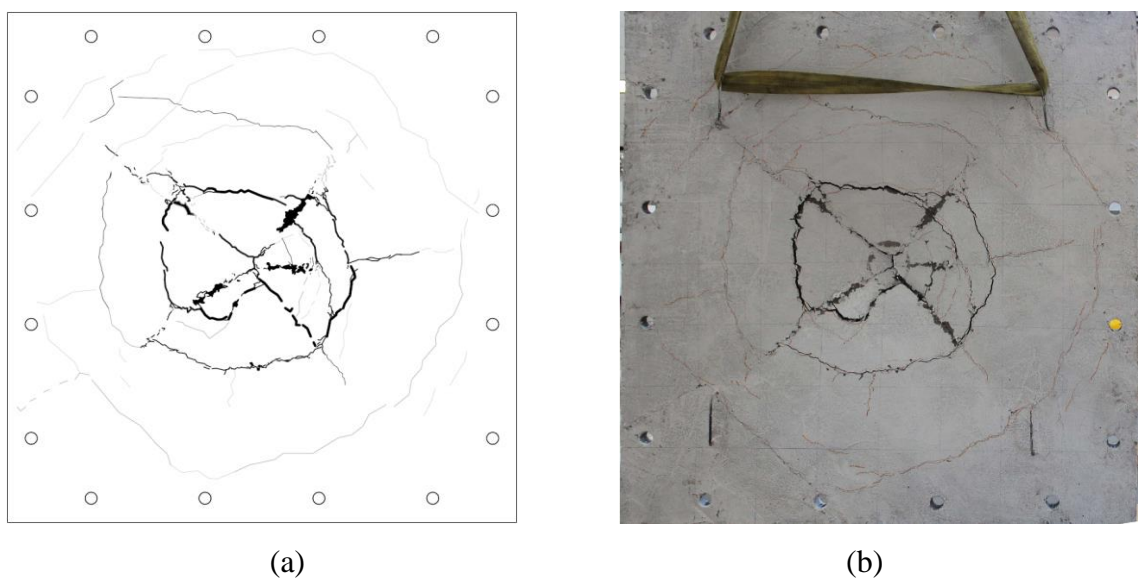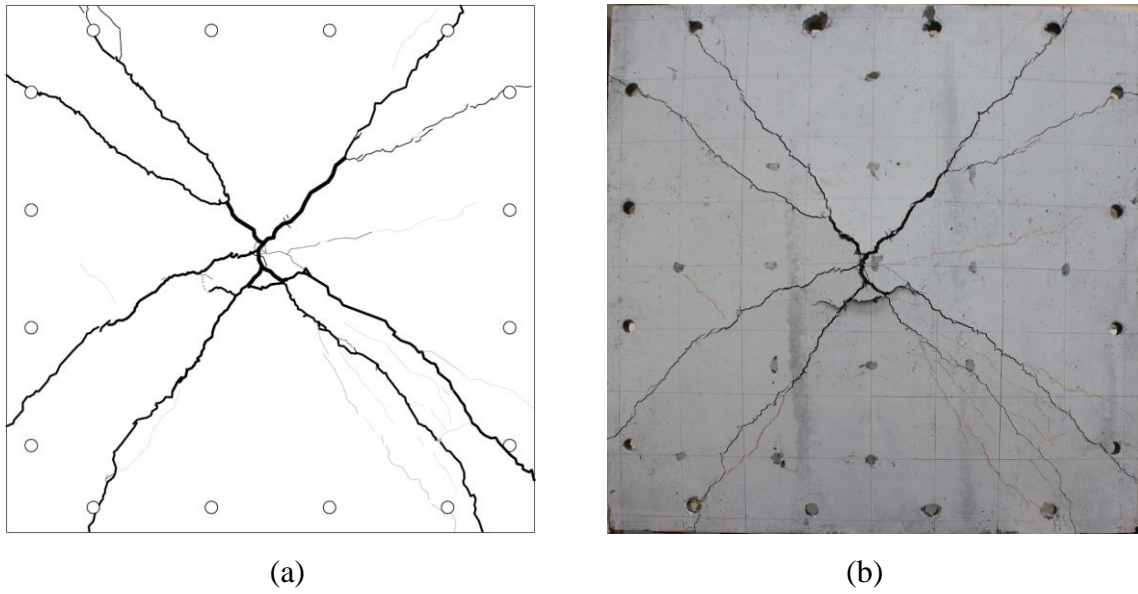Figure 4.2 Bottom surface crack patterns after testing for panel JN1-075

(a)   (b)

Figure 4.3 Top surface crack patterns after testing for panel JN1-075

(a)	(b)

Figure 4.4 Bottom surface crack patterns after testing for panel JN1-075 +PVA
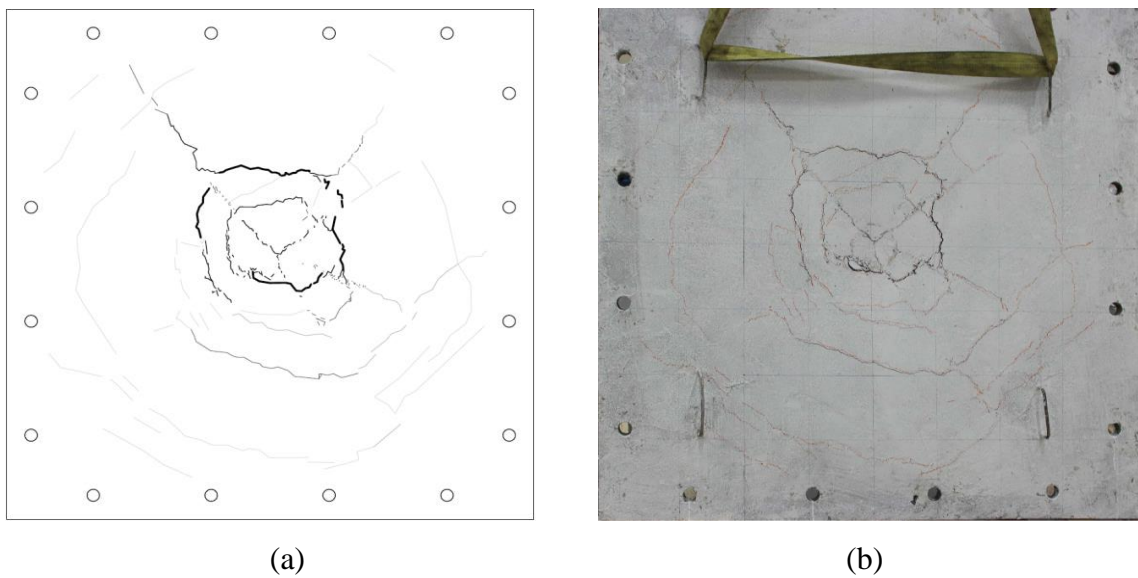

(a)	(b)

Figure 4.5 Top surface crack patterns after testing for panel JN1-075 +PVA

4.2 Specimens JN2-075, JN2-075+PVA and JN2-075-Perlite+PVA

Load-midpoint deflection curve of panels JN2-075, JN2-075+PVA and JN2-075_Perlite+PVA are presented in Figure 4.6. Up to first cracking, panels JN2-075 and JN2-075+PVA had almost same initial elastic behavior as applied load increased linearly with displacement. However, Panel JN2-075-Perlite+PVA displayed stiffer behavior.

Cracking load capacity was slightly higher in JN2-075+PVA compared to JN2-075. The panels JN2-075 and JN2-075_Perlite+PVA displayed more ductile behavior than the panel JN2-075+PVA. A gradual punching failure was observed in panels JN2-075 and JN2-075-Perlite+PVA. However, JN2-075+PVA failed in gradual flexural punching.
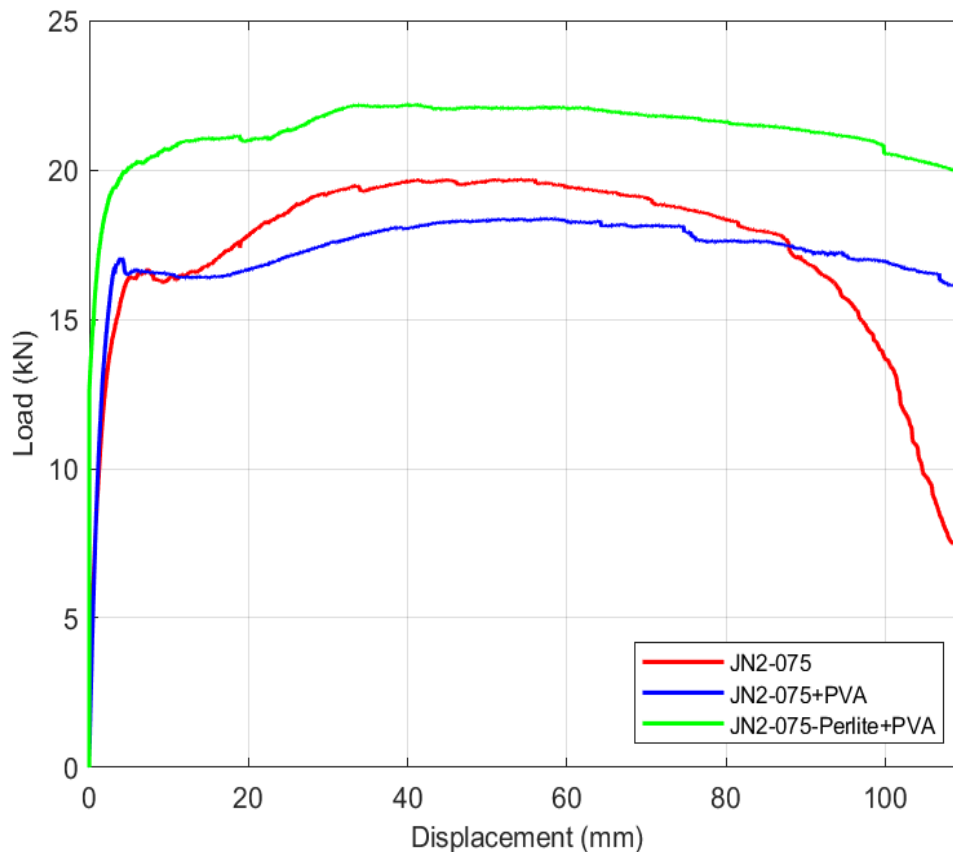

Figure 4.6 Load-midpoint deflection curve for panels JN2-075, JN2-075+PVA and JN2-075-Perlite+PVA

Crack patterns observed after tests are presented from Figure 4.7 to Figure 4.12. In specimen JN2-075+PVA, cracks on the bottom surface formed diagonal flexural yield lines and did not show extensive spreading. However, in specimen JN2-075 and JN2-075-Perlite+PVA, numerous small cracks propagated concentrating on the diagonals. The cracks in panel JN2-075+PVA were wider compared to panels JN2-075 and JN2-075_Perlite+PVA. As displacements increased, circumferential cracks on the top surface began around loading plate. In panel JN2-075 and JN2-075-Perlite+PVA, a punching cone was observed, which indicate a punching failure of the specimens. However, in

panel JN2-075, flexural cracks were wider and one of the diagonal cracks extended through the top surface and join the punching cone. So, it was not clear whether the panel failed in pure flexure or flexure-punching.
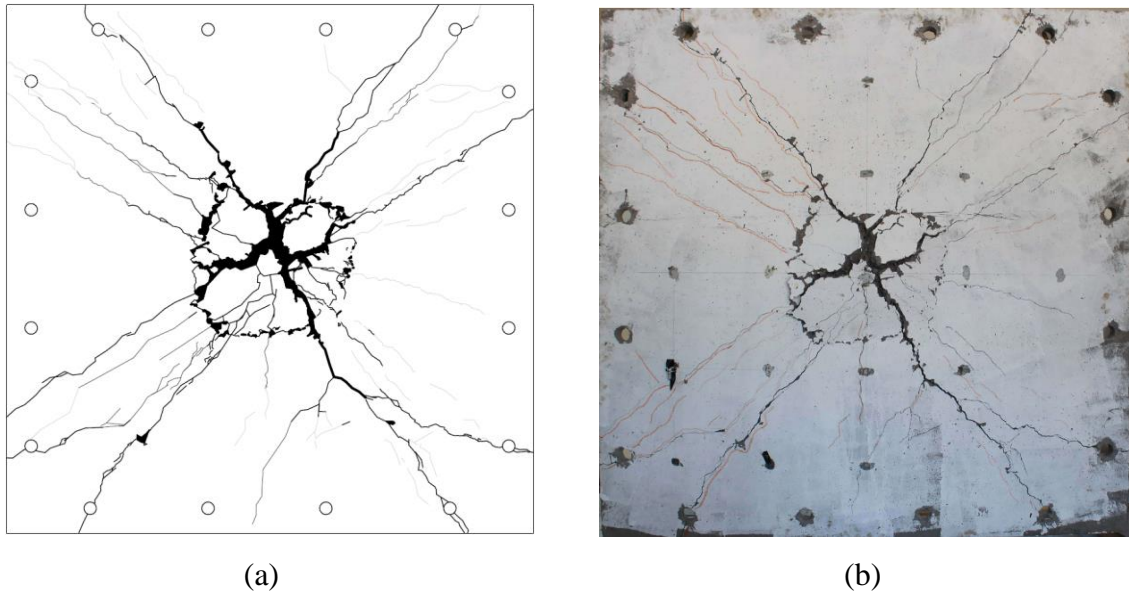

(a)   (b)

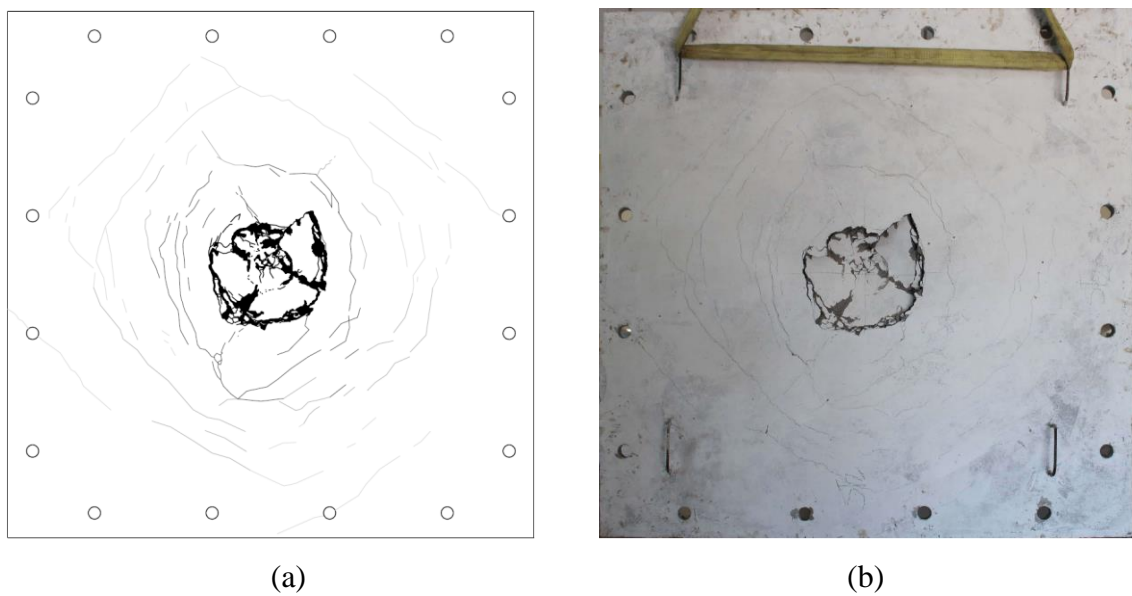Figure 4.7 Bottom surface crack patterns after testing for panel JN2-075

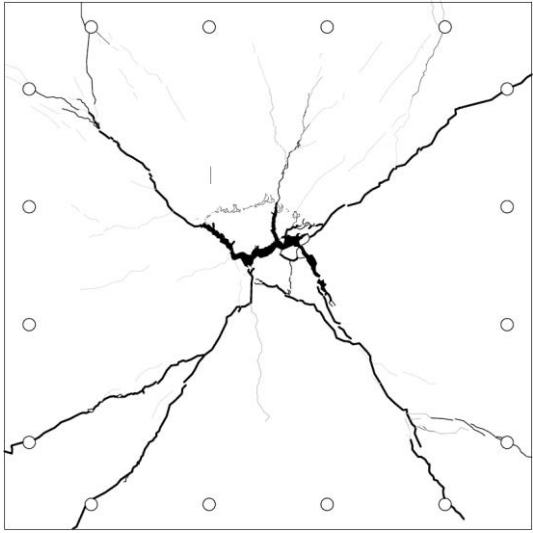(a)   (b)
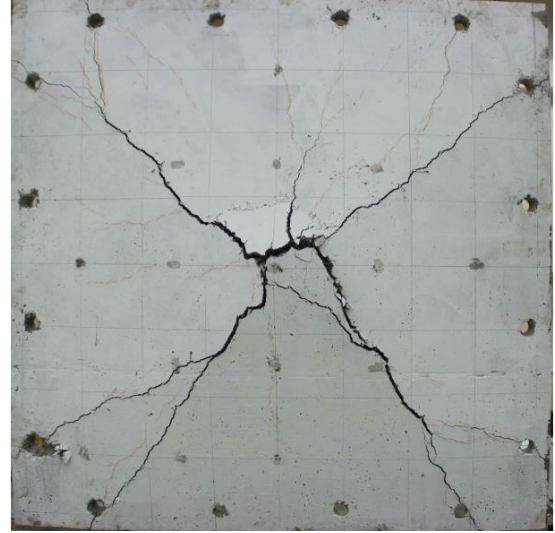
Figure 4.8 Top surface crack patterns after testing for panel JN2-075

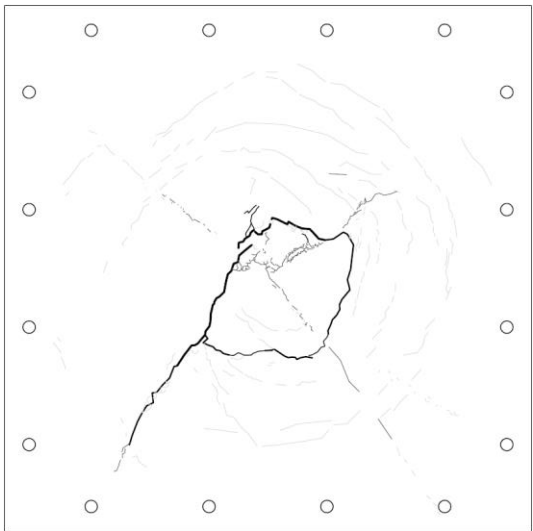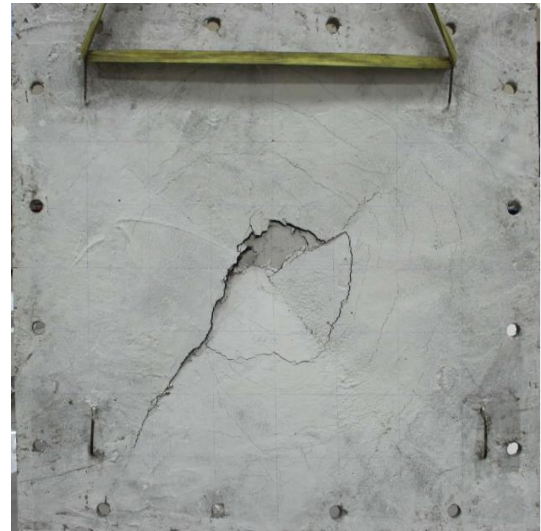<div align="center">(a)   (b)</div>

Figure 4.9 Bottom surface crack patterns after testing for panel JN2-075+PVA
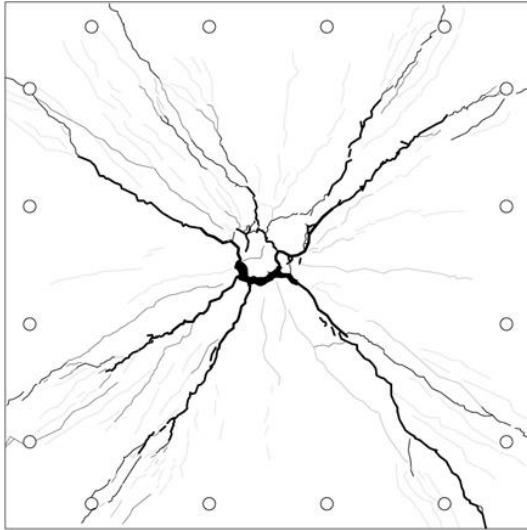

<div align="center">(a)   (b)</div>
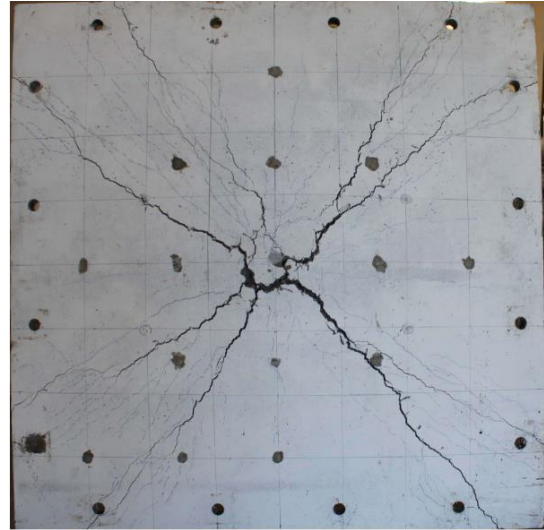
Figure 4.10 Top surface crack patterns after testing for panel JN2-075+PVA
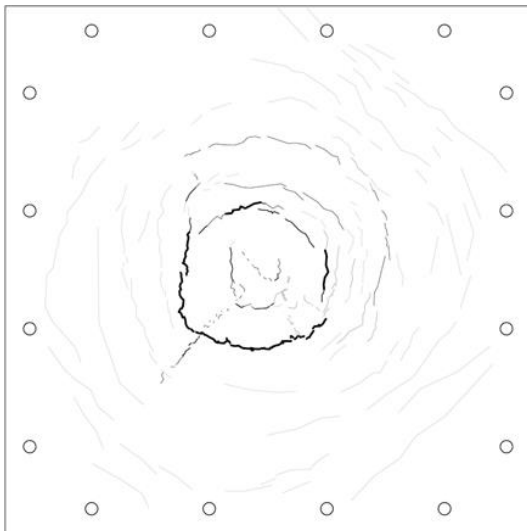
(a)   (b)

Figure 4.11 Bottom surface crack patterns after testing for panel JN2-075-Perlite+PVA

(a)   (b)

Figure 4.12 Top surface crack patterns after testing for panel JN2-075-Perlite+PVA

4.3 Specimens JN3-075and JN3-075+PVA

When panel JN3-075 was taken from the formwork, it experienced some damage. A crack, approximately 20 cm away from the center, developed parallel to panel's edge as a result of forcing the panel out of the formwork. Although this crack was not parallel to panel's expected cracking patterns and hence is not expected to have a serious effect, the results obtained from this test should be approached with caution.

As seen from the load–midpoint deflection curve in Figure 4.13, the applied load capacity was higher in panel JN3-075+PVA compared to panel JN3-075. First crack load appeared in panels JN3-075and JN3-075+PVA were around 15 kN and 19.1 kN at displacements of 2 mm and 4.8 mm relatively. The maximum load in panels JN3-075 and JN3-075+PVA were 17.7 kN and 21.7 kN at displacements of 23.7 mm and 28.5 mm, respectively. Specimen JN3-075 experienced punching failure while flexure failure was observed in specimen JN3-075+PVA.
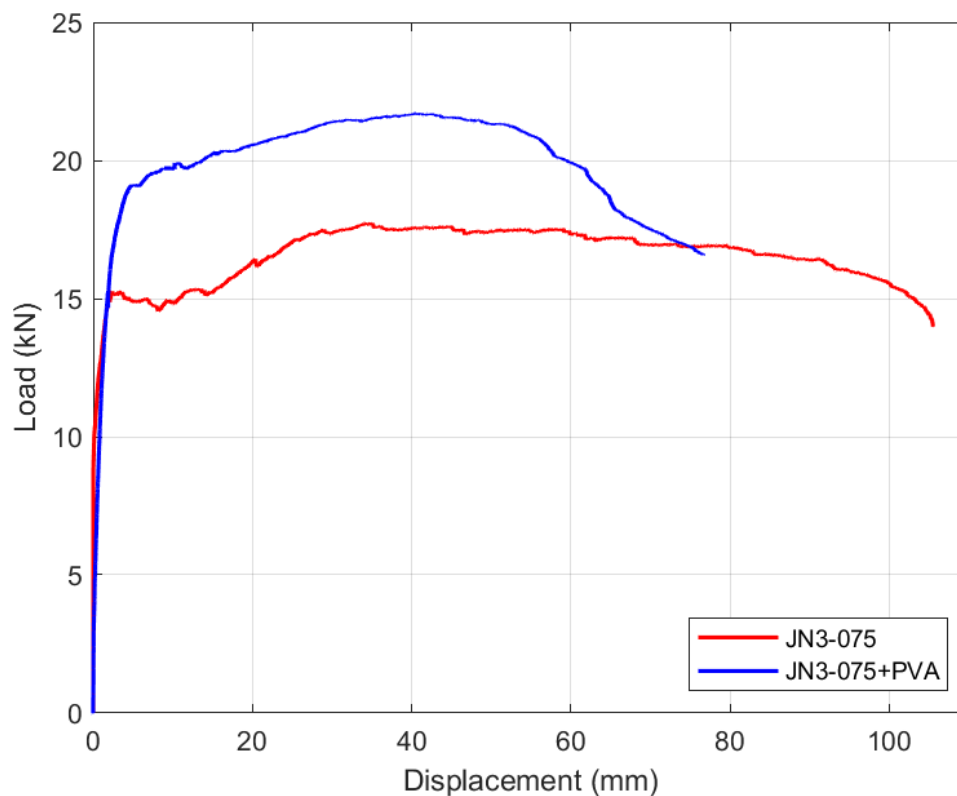

Figure 4.13 Load–midpoint deflection curve of panels JN3-075 and JN3-075+PVA

Cracks on the tension (bottom) surface of both panel JN3-075 and JN3-075+PVA started from mid-point and extended toward the corners. With increasing load, cracks in both panels spread widely, although still concentrated on diagonals. In specimen JN3-075, some cracks appeared at the center as well. In panel JN3-075, an extra crack was observed on the top surface, similar to the existing crack due to earlier damage. Width of the tangential cracks in panel JN3-075 were larger compared to specimen JN3-075+PVA. Punching cone in specimen JN3-075 indicating the punching failure. However, in JN3-075 +PVA no sign of the punching cone was observed, even one of the diagonal cracks extended through the top surface which shows flexural failure of the specimen. Cracks on bottom and top sides of the specimens JN3-075 and JN3-075+PVA are presented from Figure 4.14 to Figure 4.17.

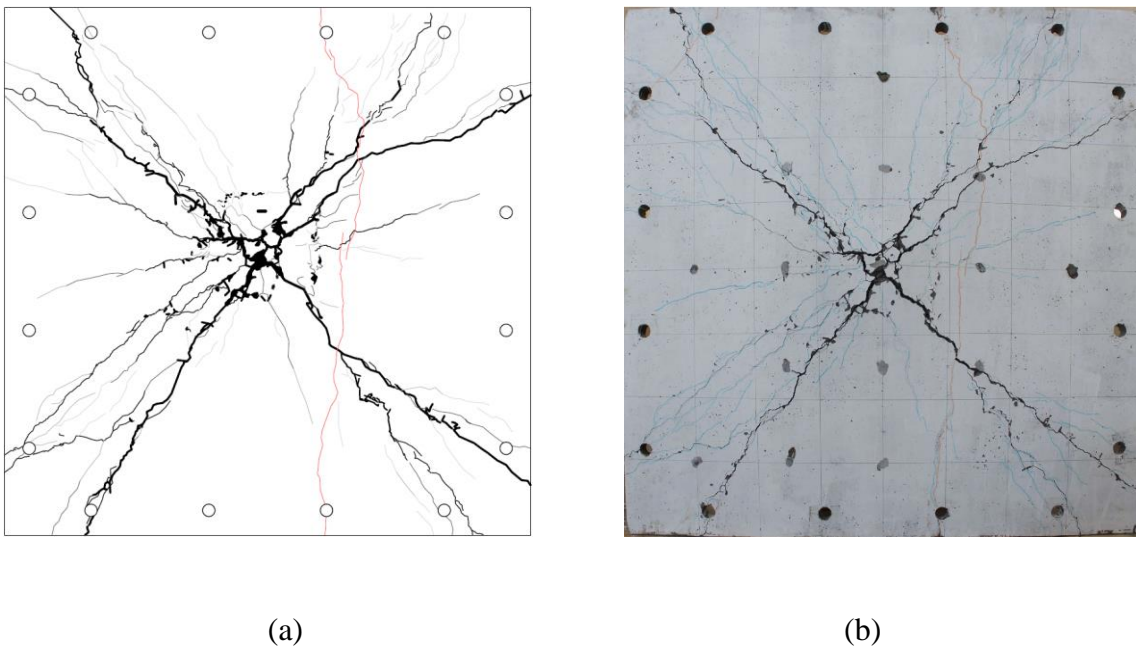(a)   (b)
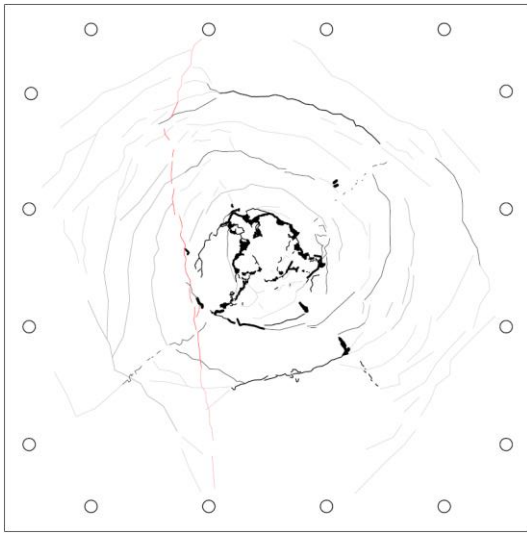
Figure 4.14 Bottom surface crack patterns after testing for panel JN3-075

(a)   (b)

Figure 4.15 Top surface crack patterns after testing for panel JN3-075

(a)   (b)
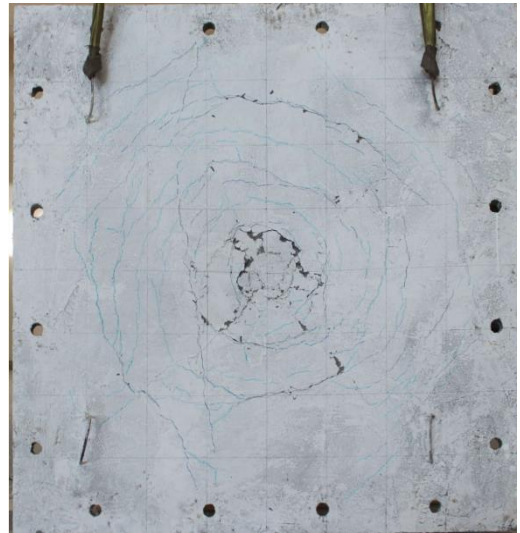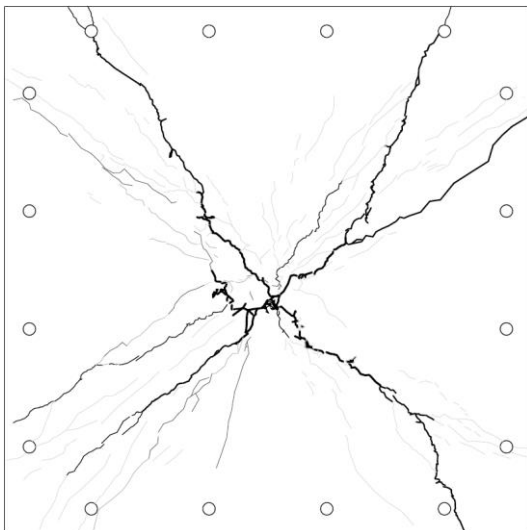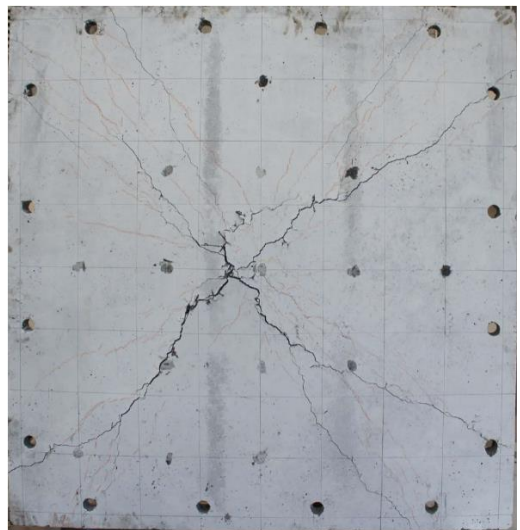
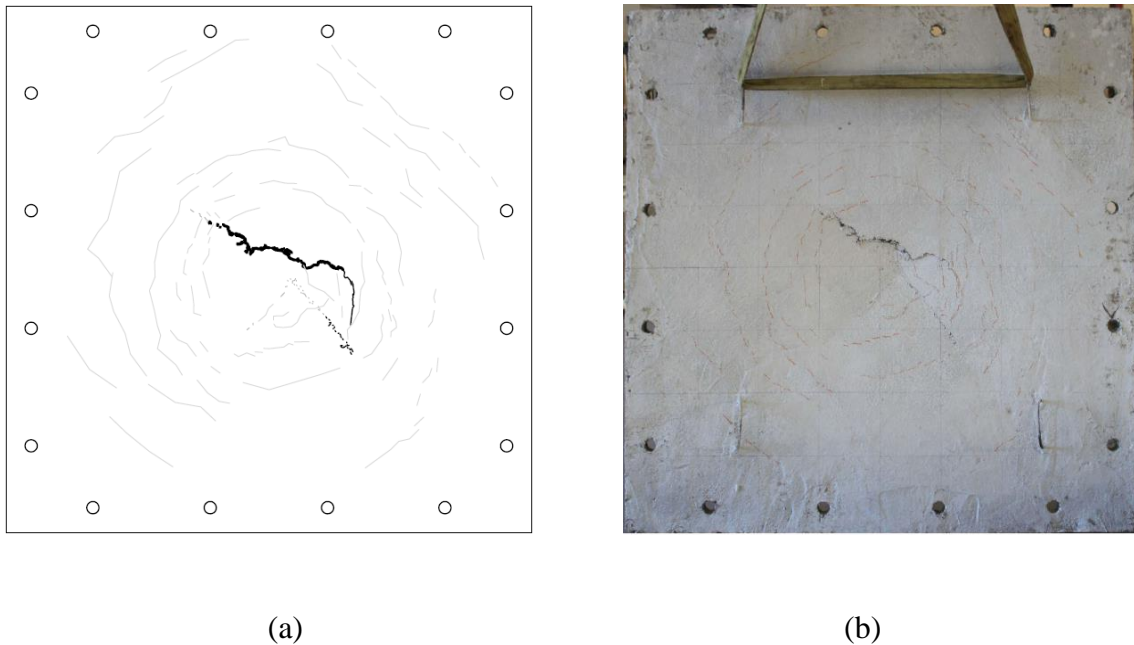Figure 4.16 Bottom surface crack patterns after testing for panel JN3-075+PVA

(a)   (b)

Figure 4.17 Top surface crack patterns after testing for panel JN3-075+PVA

4.4 Specimens JN2-1.25 and JN2-1.25+PVA

Load-midpoint deflection curves of JN2-125 and JN2-125+PVA are shown in Figure 4.18. Specimen JN2-125+PVA sustained a higher load deformation capacity compared to specimen JN2-125. Both specimens had similar load displacement behavior until about 15 kN, after which stiffness of panel JN2-125 began to decrease. Maximum load in panels JN2-125 and JN2-125+PVA were 22.1 kN and 27.5 kN at displacements of 32.7 and 43.8 mm, respectively. Energy absorption capacity was 35.9 % higher in specimen JN2-125+PVA than specimen JN2-125. Panel JN2-125 had a gradual punching failure, however panel JN2-1.25+PVA observed flexure-punching failure.

Crack on the tension surface of both panels JN2-125 and JN2-125+PVA formed from mid-point and extended toward the corners. As the applied load increased, cracks in both panels propagated around diagonal and some smaller cracks were observed perpendicular to edges. Punching cone in JN2-125 indicated a punching failure of the specimen. Tangential cracks on the top surface were very smaller outside of the punching cone in specimen JN2-125. A partial punching cone was observed in specimen JN2-125+PVA and the panel failed in flexure-punching. Cracks on both side of specimens JN2-125 and JN2-125+PVA are presented from Figure 4.19 to Figure 4.22.
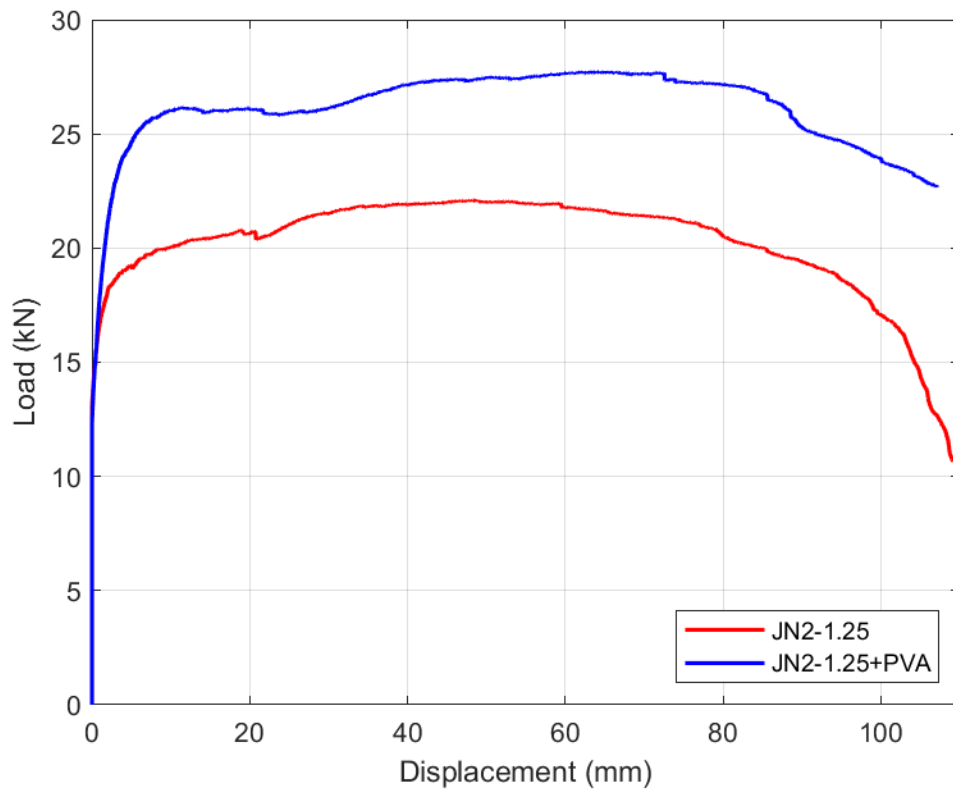
Figure 4.18 Load–midpoint deflection curve of panels JN2-125 and JN2-125+PVA

(a)   (b)

Figure 4.19 Bottom surface crack patterns after testing for panel JN2-125

(a)	(b)

Figure 4.20 Top surface crack patterns after testing for panel JN2-125
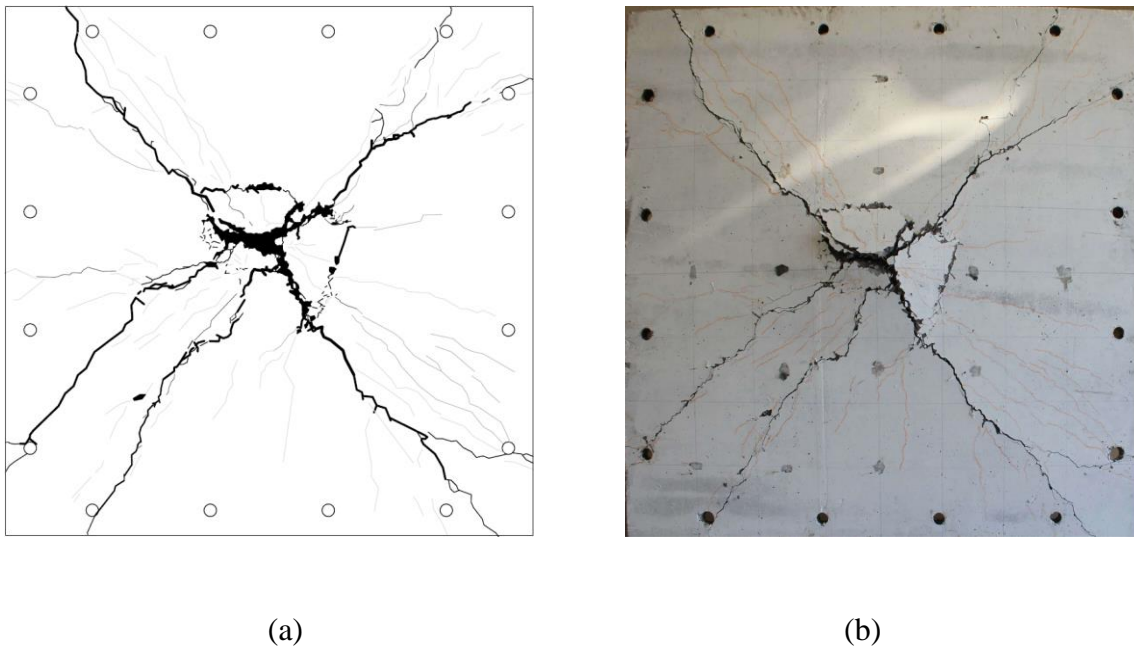

(a)	(b)

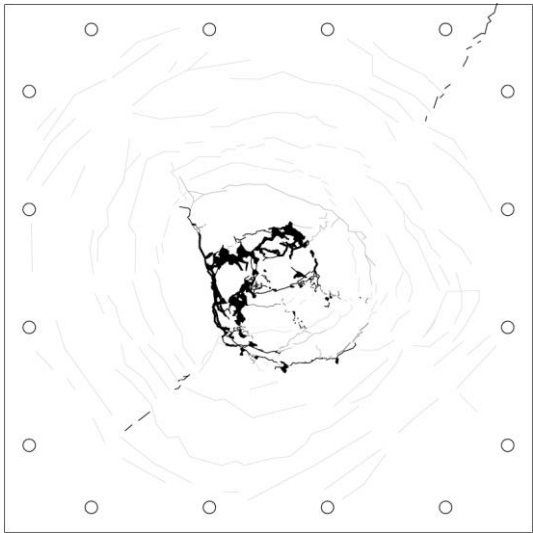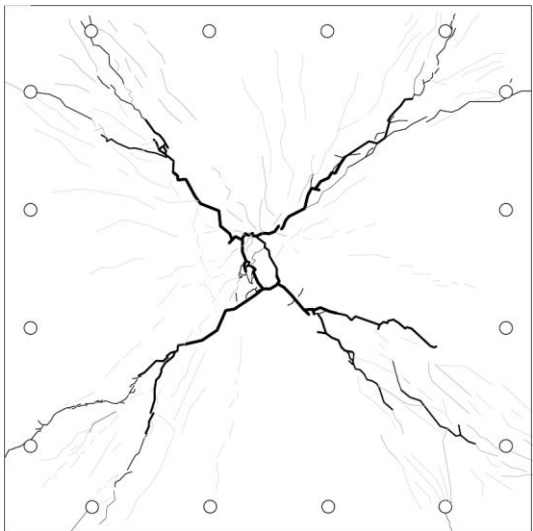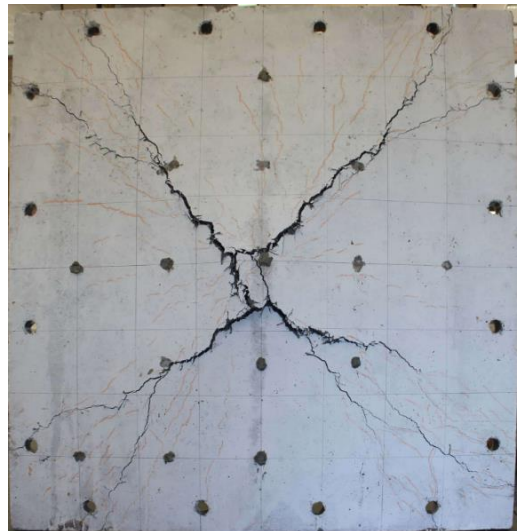Figure 4.21 Bottom surface crack patterns after testing for panel JN2-125+PVA

<div align="center">

(a)   (b)
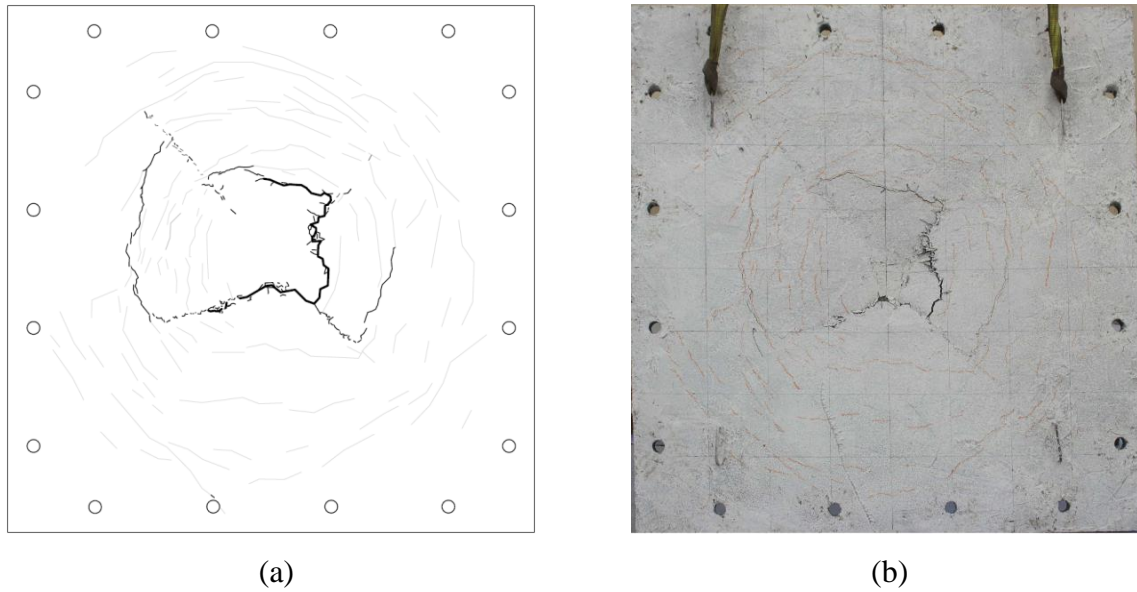
</div>

Figure 4.22 Top surface crack patterns after testing for panel JN2-125+PVA

4.5   Specimens with Conventional Reinforcement

Load-midpoint deflection curve of panels with conventional reinforcement are presented in Figure 4.23. Panels JN2-075-RF and JN2-075-RF+PVA had similar behavior up to cracking and their stiffnesses were higher in both panels compared to JN-Plain-RF panel. Stiffness significantly decreased after the first crack in all three panels. Lower stiffness was measured in JN-Plain-RF panel.   Addition of steel fibers increased the stiffness by 39 % compared to JN-Plain-RF. Using PVA fibers with steel fibers increased the stiffness by an additional 4%. Specimen with PVA displayed higher load deformation capacity and more ductile behavior compared to the one with steel fibers only and Plain-RF. Punching failure was observed in all three panels. Cracking and peak loads, corresponding displacements, and energy absorption capacities for all three panels are presented in Table 4.1. Steel fiber increased energy absorption capacity by 31% compared to JN-Plain-RF and addition of PVA fibers further increased energy absorption capacity by 155.3% compared to panel JN-Plain-RF.

Cracks on bottom and top sides of specimens JN-Plain-RF, JN2-075-RF and JN2-075-RF+PVA are presented from Figure 4.24 to Figure 4.29. Cracks on the bottom surface of all three panels began to form at mid-point and extended toward the edges. As the applied load increased, cracks in these panels spread around diagonals. Also, with

further increasing load, new cracks developed perpendicular to edges and widely propagated. Number of cracks were higher in panel JN2-075-RF+PVA compared to other panels in this group. With increasing load, circumferential cracks formed on the top surface for both JN2-075-RF and JN2-075-RF+PVA. Near the steel loading plate, the tangential crack became excessively wide. As the load reached to the maximum level, one of the steel reinforcing bars ruptured in the punching cone zone and a sudden drop was seen in load. The load started to rise up again until a second bar ruptured. Finally, the load capacity in JN2-075-RF and JN2-075-RF+PVA panels dropped sharply, and the steel plate started to punch through. However, in panel JN-Plain-RF, the punching cone suddenly spalled and loading plate punched through.

Table 4.1 Cracking and peak load with relative displacement and energy absorption capacity

Panel	First crack load (kN)	Displacement at first crack load (mm)	Peak load (kN)	Increase in peak load by percentage with respect to JN-Plain-RF	Displacement at peak load (mm)	Energy Absorption capacity (kN.mm x 10^3)
JN-Plain-RF	10.9	1.4	22.7		0.4	1.32
JN2-075-RF	15.1	1.6	33.1	45.8%	1.35	1.73
JN2-075-RF+PVA	18.2	2.6	41.4	82.4%	51.2	3.37
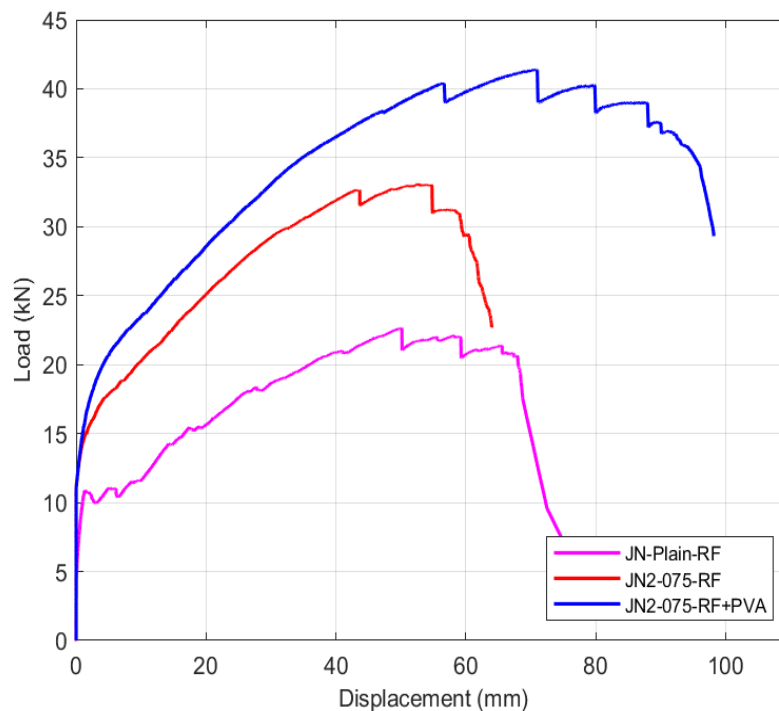
Figure 4.23 Load-midpoint deflection curve of panels with conventional reinforcement
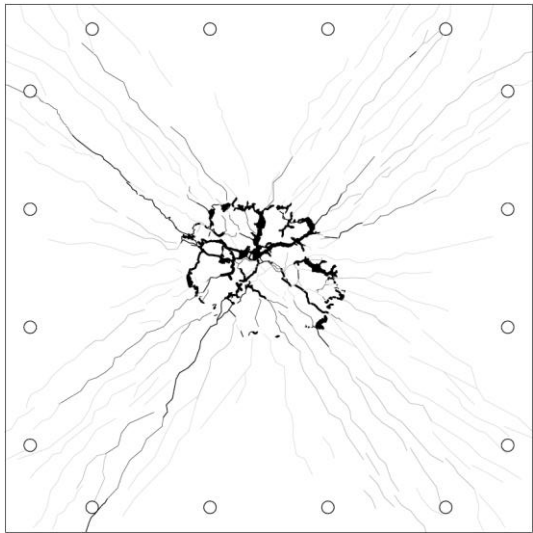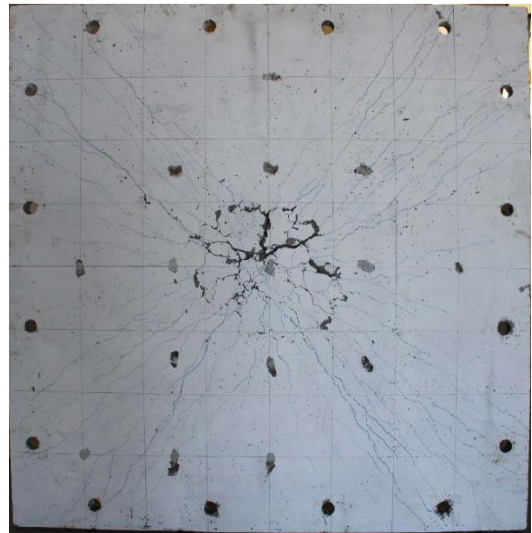
(a)   (b)

Figure 4.24 Bottom surface crack patterns after testing for panel JN2-075-RF
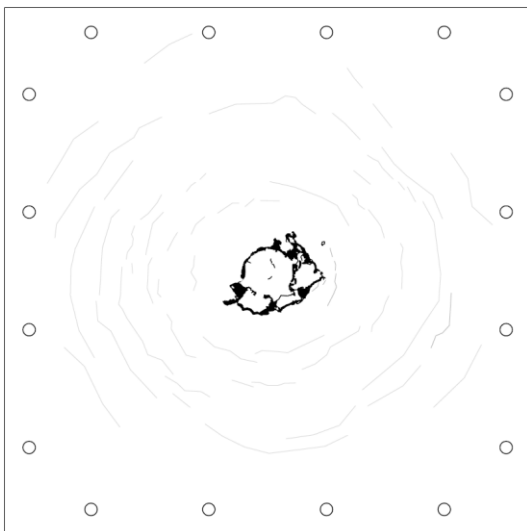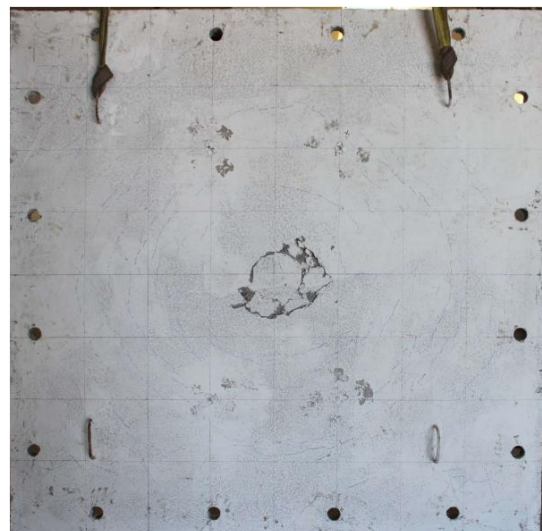
(a)   (b)

Figure 4.25 Top surface crack patterns after testing for panel JN2-075-RF
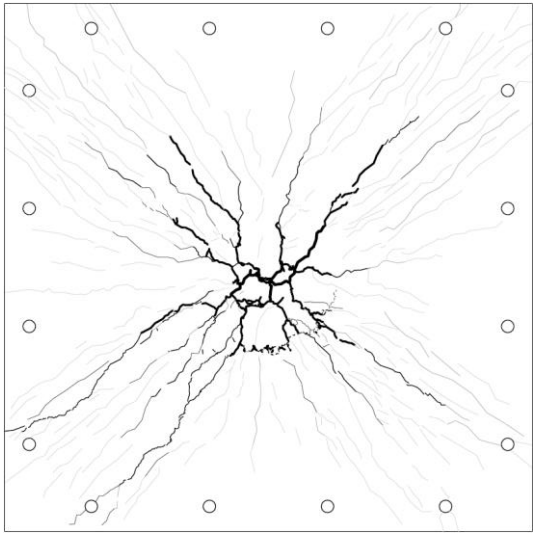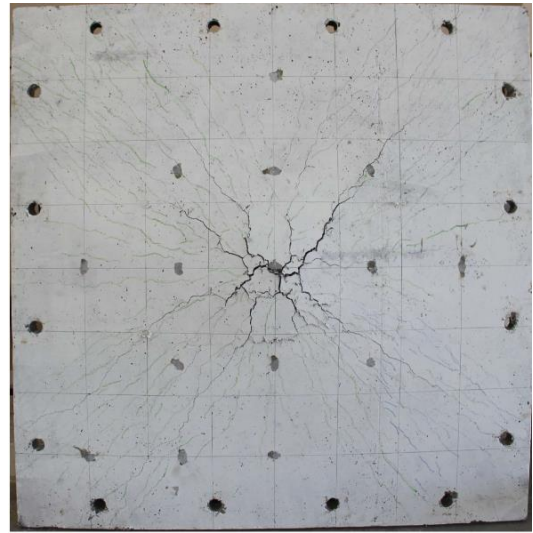
(a) (b)

Figure 4.26 Bottom surface crack patterns after testing for panel JN2-075-RF+PVA
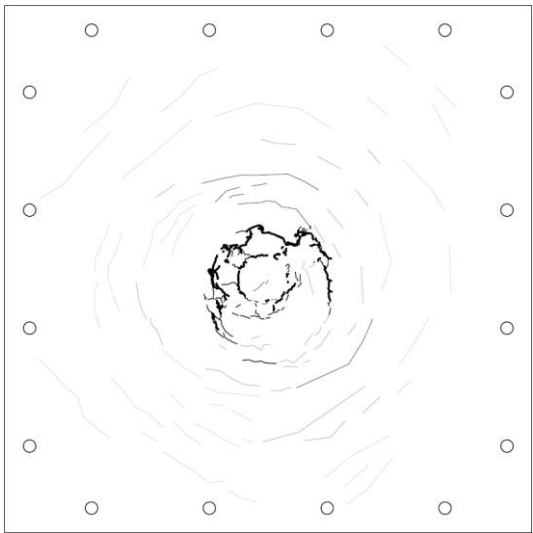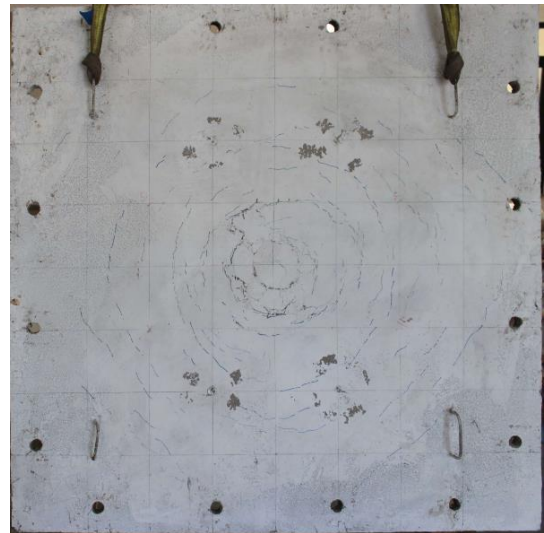
(a) (b)

Figure 4.27 Top surface crack patterns after testing for panel JN2-075-RF+PVA
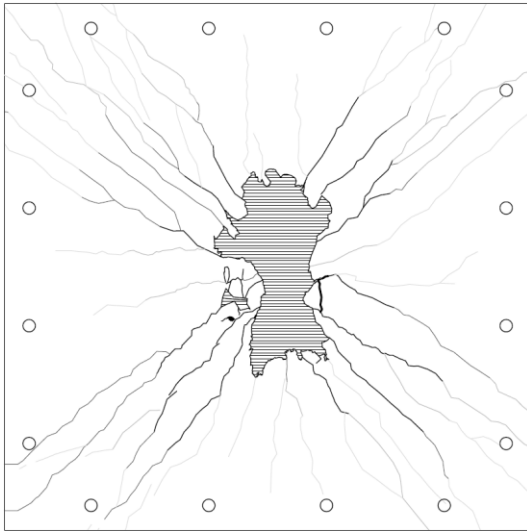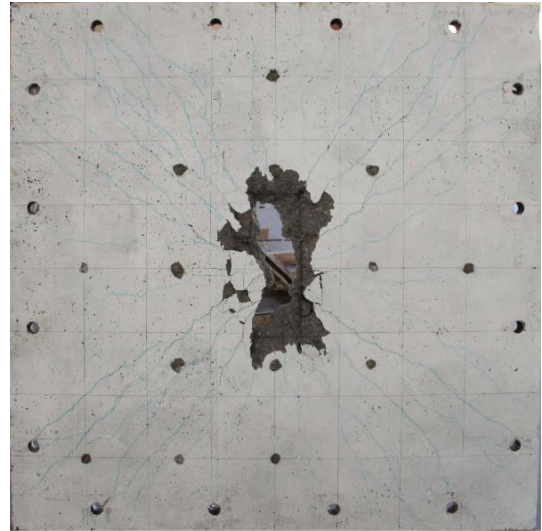
(a)   (b)

Figure 4.28 Bottom surface crack patterns after testing for panel JN-Plain-RF
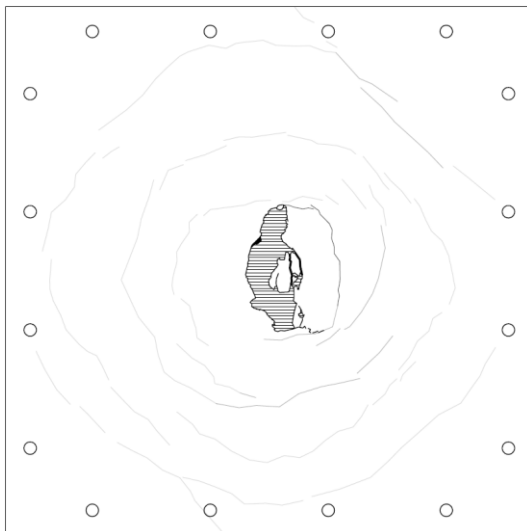
(a)   (b)

Figure 4.29 Top surface crack patterns after testing for panel JN-Plain-RF

4.6 Plain Concrete Specimens

Load-midpoint deflection curves of specimens JN-Plain and JN-Plain+RF are shown in Figure 4.30. Panel JN-Plain suddenly lost its capacity with the first crack and failed in brittle manner, in which the panel fell apart (Figure 4.31). However, panel JN-Plain+RF continued to carry load after cracking. After cracking panel JN-Plain abruptly lost its stiffness, but stiffness of the panel JN-Plain+RF was sustained, although significantly decreased. Cracking load in panels JN-Plain and JN-Plain+RF were 11.9 kN and 10.9 kN, respectively. Maximum load occurred in panel JN-Plane+RF was 22.6 kN. A brittle punching failure observed in panel JN-Plain+RF. However, the panel JN-Plain failed in brittle flexure.
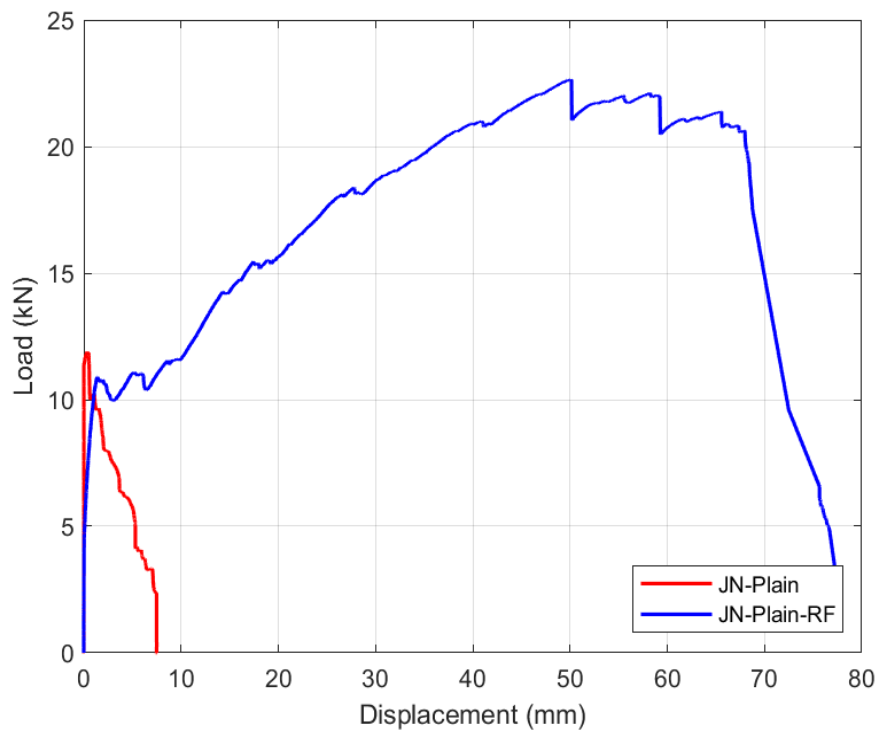


Figure 4.30 Load-midpoint deflection curves for panel JN-Plain+RF and JN-Plain

Crack on the tension surface of both panels JN-Plane and JN-Plane+RF began to form at mid-point and extended toward the edges on diagonals. Panel JN-Plane failed with diagonal cracking (Figure 4.31). However, in panel JN-Plane+RF cracks were widely spread on diagonals and failed in punching.

Figure 4.31 JN-plain panel after testing

4.7 Comparison of panel behaviors containing only steel fibers

Load-midpoint deflection curves for panels that had only steel fibers are presented in Figure 4.32. All specimens showed similar initial stiffness prior to crack except for JN2-075, which had a smaller stiffness compared to others. Although higher stiffness was observed in all panels up to cracking, significant decrease in stiffnesses were occurred in post crack region. Cracking and peak loads, corresponding displacements, and energy absorption capacities, as calculated by the area under the curves up to 80% of the peak load in the post-peak region, are presented in Table 4.2.

Addition of steel fibers significantly increased the load and displacement capacity of all specimens, regardless of the fiber type and ratio. All specimens with steel fibers had wide flexural diagonal cracking, followed by ultimate punching. In JN-Plain, failure was a result of brittle flexural cracking, which occurred at lower levels of load and therefore, did not allow a punching failure to develop. In specimens with steel fiber, steel fibers acted as a reinforcement and flexural stresses were able to be carried after cracking. Therefore, specimens were able to be loaded further until a punching failure start to develop.

When load-deflection behaviors of specimens were compared, it was clearly seen that fiber type and ratio played an important role. JN1-075, the specimen with shorter fibers (Dramix® 45/35-3D), sustained the lowest levels of load, where the load gradually dropped after reaching the peak at a low level of displacement. All other specimens showed a deflection hardening behavior, where the load continued to increase after the loss of stiffness where a yielding-like response started. Among the longer steel fibers with the same ratio, JN2-075 (with Dramix® 65/60-3D) was able to sustain higher level loads compared to JN3-075 (with Dramix® 65/60-5D). Although use of double hook end fibers was expected to result in a better response, the peak load sustained by JN3-075 was about 10% smaller than the one with single hook end fibers, JN2-075. However, it should be noted that JN3-075 was cracked when removed from formworks, which can be a reason of its lower response. On the other hand, JN3-075 was able to withstand higher displacements before ultimate failure. Overall other factors, steel fiber ratio seemed to be the most effective parameter. JN2-125, which has the same type of fibers (Dramix® 65/60-3D) with JN2-075 but with a higher ratio, sustained higher level of loads compared to all other specimens.

Steel fibers significantly enhanced the concrete panels ductility and energy absorption capacity. Among all, JN2-125 absorbed highest levels of energy. However, it is interesting to note that JN1-075 was the specimen that absorbed the second highest level of energy, while it was able to sustain the lowest level of load. This was due to the higher displacement capacity of this specimen compared to other specimens in this group. JN1-075 was able to sustain lower levels of load, probably due to the shortness of the fibers. However, this poorer performance of fibers resulted in a more flexure dominant behavior and the panel was able to deform under flexure to very high levels before punching occurred. This increased the panel's energy absorption capacity. Other specimens with stronger fibers sustained higher levels of load since fibers were able to sustain higher levels of stresses at flexural cracks, but this resulted in earlier development of punching failure since those specimens were stronger under flexure. Therefore, JN1-075 was able to absorb even more energy compared to specimens with longer fibers. On the other hand, steel fiber ratio was dominant in terms of energy absorption capacity too, as it absorbed the highest level of energy.

Table 4.2 Cracking and peak load with relative displacement and energy absorption
capacity

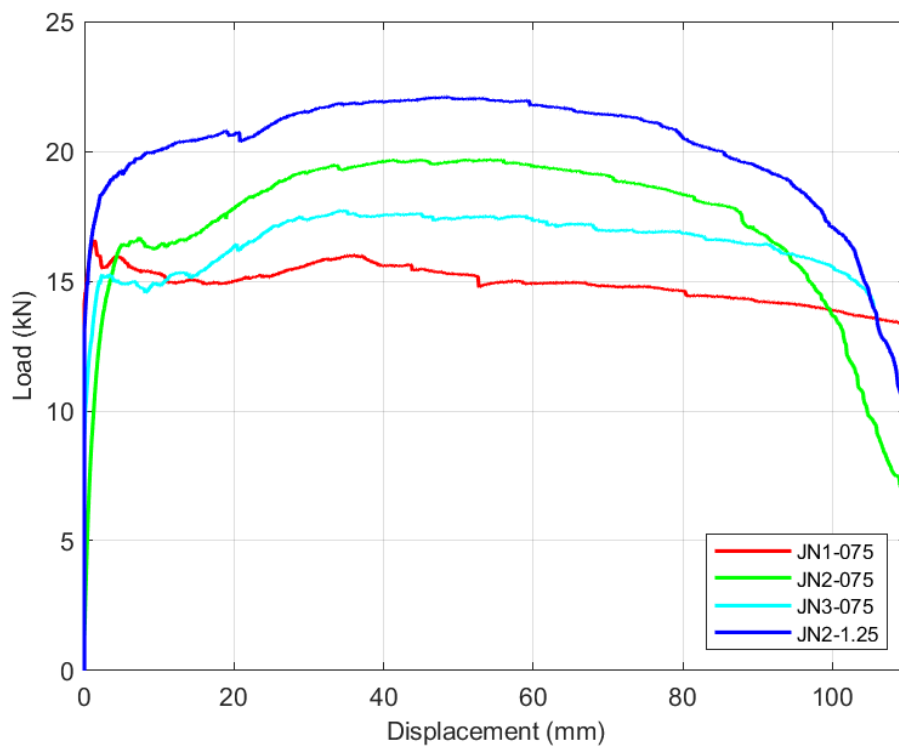| Panel	First crack load (kN)	Displacement at first crack load (mm)	Peak load (kN)	Increase in peak load by percentage with respect to JN-Plain	Displacement at peak load (mm)	Energy absorption capacity (kN.mm x 10^3)
JN-Plain	11.9	0.4	11.9		0.4	0.0505
JN1-075	16.6	1.35	16.6	39.5%	1.35	1.80
JN2-075	16.5	5.1	19.7	65.5%	51.2	1.74
JN3-075	15.0	2.0	17.7	48.7%	35.0	1.75
JN2-125	18.4	2.2	22.1	85.7%	48.8	2.06

Figure 4.32 Load-midpoint deflection curve of panels with only steel fibers

4.8 Comparison of panel behaviors containing PVA fibers

Load-midpoint deflection curves for panels having hybrid (steel and PVA) fibers
are presented in Figure 4.33. Initial elastic stiffness of panels JN1-075+PVA, JN2-
075+PVA and JN3-075+PVA were almost identical and lower than other specimens JN2-

075-Perlite+PVA and JN2-125+PVA. Beyond the first crack, stiffness was reduced significantly in all these panels. Similar to the case with panels with only steel fibers, all panels except for JN1-075+PVA showed a slight deflection hardening behavior after reaching a yield-like deflection, whereas for JN1-075+PVA load sustained gradually dropped after this point. Cracking and peak loads with corresponding displacement and energy absorption capacities are presented in Table 4.3. For these panels, PVA fiber volume content was kept unchanged among specimens. Therefore, main variables were types of steel fibers and steel fiber content ratio. General trend between the specimens were similar to the case with only steel fibers. Therefore, it can be said that steel fibers were dominant in the behavior. Among the specimens, JN1-075+PVA, the one with shorter steel fibers, sustained lowest level of loads. JN2-125+PVA sustained highest level of loads, indicating that the steel fiber ratio was the most effective factor for hybrid fiber specimens as well. Unlike the case with only steel fibers, JN3-075+PVA (with Dramix® 65/60-5D) sustained higher levels of load compared to JN2-075+PVA (with Dramix® 65/60-3D). It has to be noted that for the case with steel fibers only, JN3-075 suffered a damage prior to testing, which can be a reason of its lower performance compared to JN2-075. Such a previous damage was not present in the case with PVA fibers, so it can be said that 5-D double hook end fibers were able to show their advantage in this test. On the other hand, presence of PVA fibers could have had an effect, increasing the performance of 5-D fibers. Unfortunately, it was not possible to come to a definite conclusion since repeating the testing of JN3-075 was not possible within the time frame of this study.

Group of specimens with PVA fibers had an extra specimen JN2-075+PVA of which 20% fine aggregate was replaced by light weight perlite. This panel with perlite had a peak load 21% higher than JN2-075+PVA. For these panels, light weight perlite seemed to enhance the performance of fibers, probably affecting the bonding of steel fibers, and enhancing their slippage characteristics. On the other hand, since this panel did not have a steel fiber only counterpart, it was not possible to see the effect of PVA fibers in particular.

Table 4.3 Cracking and peak load with relative displacement and energy absorption
capacity

| Panel	First crack load (kN)	Displacement at first crack load (mm)	Peak load (kN)	Increase in peak load by percentage with respect to JN-Plain	Displacement at peak load (mm)	Energy absorption capacity (kN.mm x 10^3)
JN-Plain	11.9	0.4	11.9		0.4	0.0505
JN1-075+PVA	17.0	3.8	17.0	42.9 %	3.8	1.47
JN2-075+PVA	16.8	3.2	18.4	54.6 %	58.3	1.90
JN3-075+PVA	19.1	4.8	21.7	82.4 %	40.6	1.47
JN2-075-Perlite+PVA	19.4	3.2	22.2	86.6 %	40.2	2.44
JN2-1.25+PVA	24.1	4.0	27.8	133.6 %	63.5	2.8
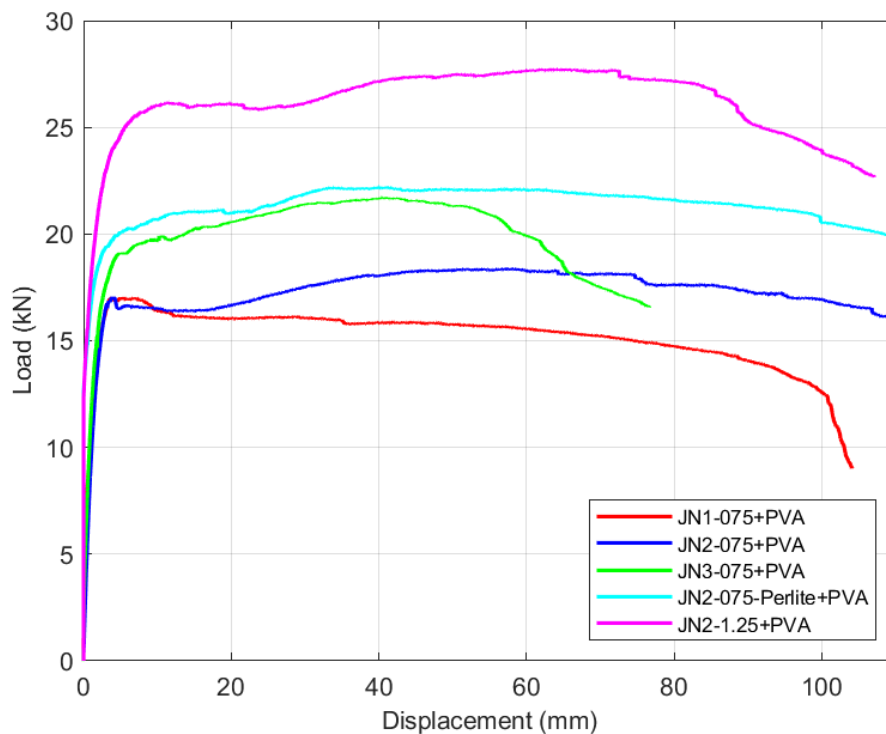
Figure 4.33 Load-midpoint deflection curve of panel with steel fibers plus PVA

Only two panels, JN1-075+PVA and JN2-075_Perlite+PVA suffered a punching failure. Other specimens failed either in flexure-punching or flexure. In general, panels without PVA displayed a more ductile load-displacement behavior compared to panels with PVA.

In all panels, first, fine flexural cracks occurred on the bottom surface. These cracks were developed from the mid-point under the loading plate and extended radially along the diagonals towards the edges. The cracks in panels with the smallest aspect ratio of steel fibers were fewer in number and larger in width. As the aspect ratio and steel fibers content increased and single hook end 3D fibers were replaced with double hook end 5D fibers, number of cracks were increased and width of cracks were decreased, but still they were concentrated on diagonals. As a comparison, in the panel with conventional reinforcement, number of cracks were higher, and their width was smaller in all three panel. Additional cracks were developed alongside central axes and widely propagated on flexure surface in these panels. As the load and displacement increased, cracks started to appear on the top surface in a tangential direction around the loading plate in all panels. In panels with only steel fiber and panel with conventional reinforcement , these circumferential cracks turned excessively wide. The load carrying capacity in panels with only steel fibers dropped gradually as the loading plate started to punch through, whereas in panel with conventional reinforcement it dropped abruptly in a brittle manner. In panels with PVA, only specimens JN1-075+PVA and JN2-075-Perlite+PVA failed in punching and remaining panels failed either in flexure-punching or flexure, since larger flexural cracks formed on the positive moment region.

4.9   Deflection profiles

As mentioned before, fifteen displacement transducers (RLPT) were used at different locations in order to measure vertical deflections, as shown in Figure 3.20. Here, normalized central line deflection profiles and deflection contours of each specimen at the point of failure are presented from Figure 4.34 to Figure 4.44. In general, higher deformations were observed in panels without PVA compared to the ones with PVA, except for JN2-075-RF+PVA. The deformation levels were decreased as steel fiber type was changed from Dramix® 45/35-3D to Dramix® 65/60-3D and from Dramix® 65/60-3D to Dramix® 65/60-5D. By adding conventional flexural steel reinforcement, further reduction was observed in deformation levels. Normalized centerline deflection profiles at failure were obtained by dividing the measured displacements on a line parallel to one edge and passing through the center to the maximum midpoint displacement. From these profiles and deflection contours, it can be seen that in hybrid fiber reinforced panels with

PVA, deformations were more spread on panels' area rather than concentrating on the midpoint at the punching cone zone. Due to better stress transfer from loading point around the punching cone, these panels were able to deform on a wider area, which contributed their ultimate deflection capacity as well. This is more visible in specimens with conventional reinforcement as seen in Figure 4.44. In JN-Plain-RF, deformations were concentrated around the midpoint, whereas addition of steel fibers in JN2-075-RF and further addition of PVA in JN2-075-RF+PVA resulted in an increased spreading of deformation over the entire panel.
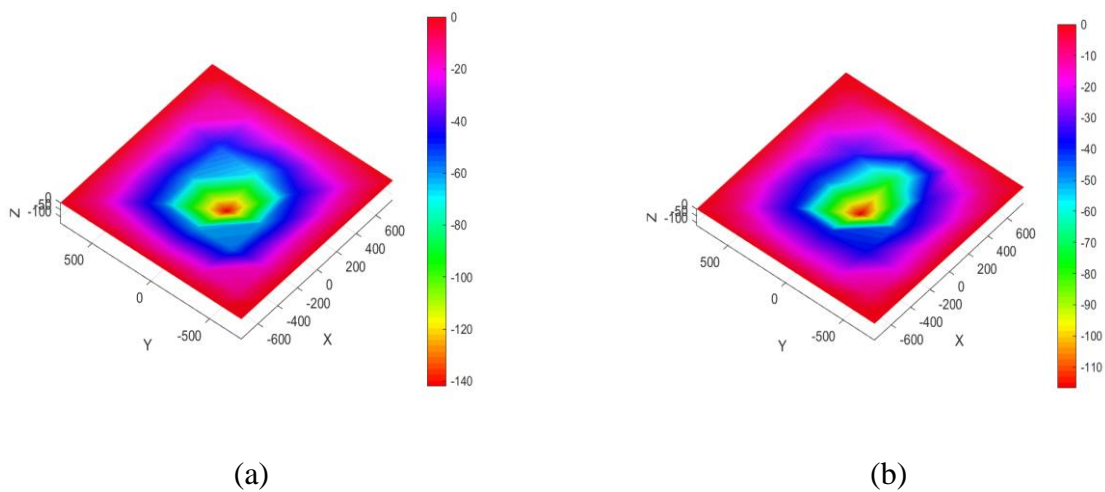

(a)   (b)

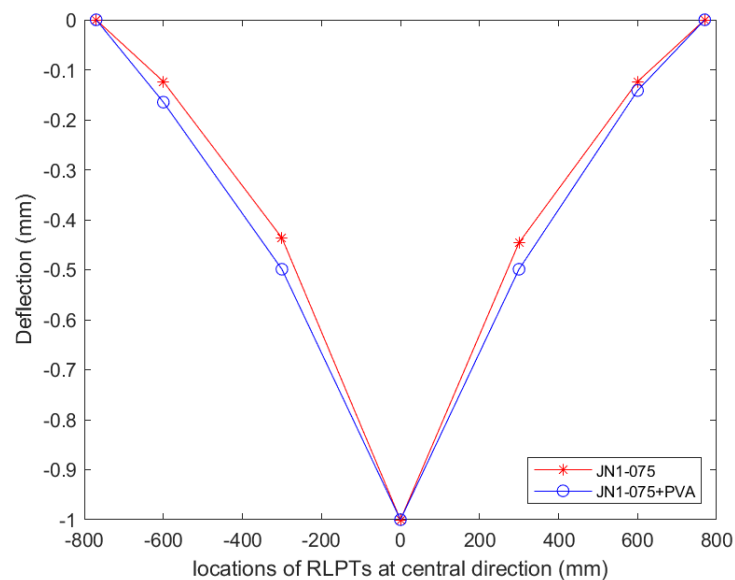Figure 4.34 Deflection contour of panels at failure; (a) JN1-075; (b) JN1-075+PVA
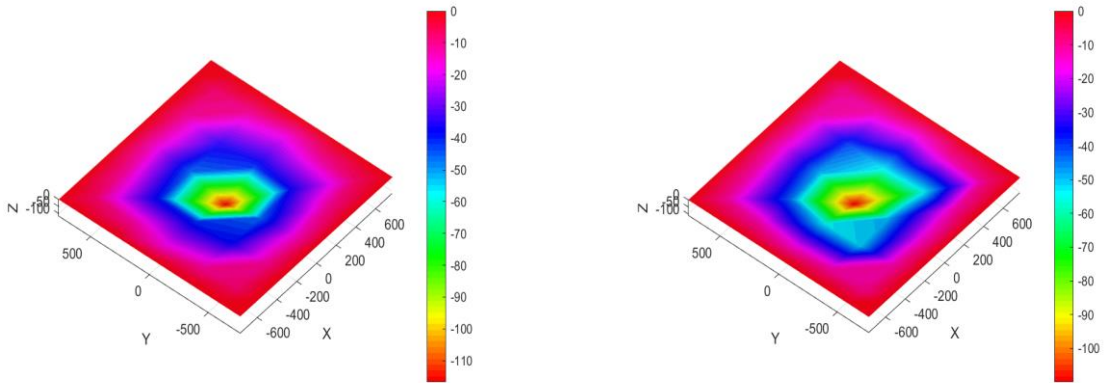

Figure 4.35 Normalized centerline deflection of panels JN1-075 and JN1-075+PVA

(a)

(b)

(c)

Figure 4.36 Deflection contour of panels at failure; (a) JN2-075; (b) JN2-075+PVA; (c)
JN2-075 -Perlite+PVA

Figure 4.37 Normalized centerline deflection of panels JN2-075, JN2-075+PVA and
JN2-075-Perlite+PVA

(a)   (b)

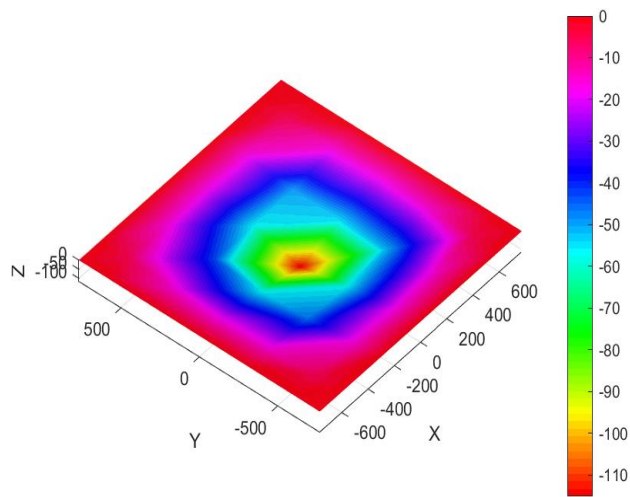Figure 4.38 Deflection contour of panels at failure; (a) JN3-075; (b) JN3-075+PVA

Figure 4.39 Normalized centerline deflection of panels JN3-075 and JN3-075+PVA

(a)

(b)

Figure 4.40 Deflection contour of panels at failure; (a) JN2-125; (b) JN2-125+PVA

Figure 4.41 Normalized centerline deflection of panels JN2-125, JN2-125+PVA

(a)   (b)

Figure 4.42 Deflection contour of panels at failure; (a) JN2-075-RF; (b) JN2-075-
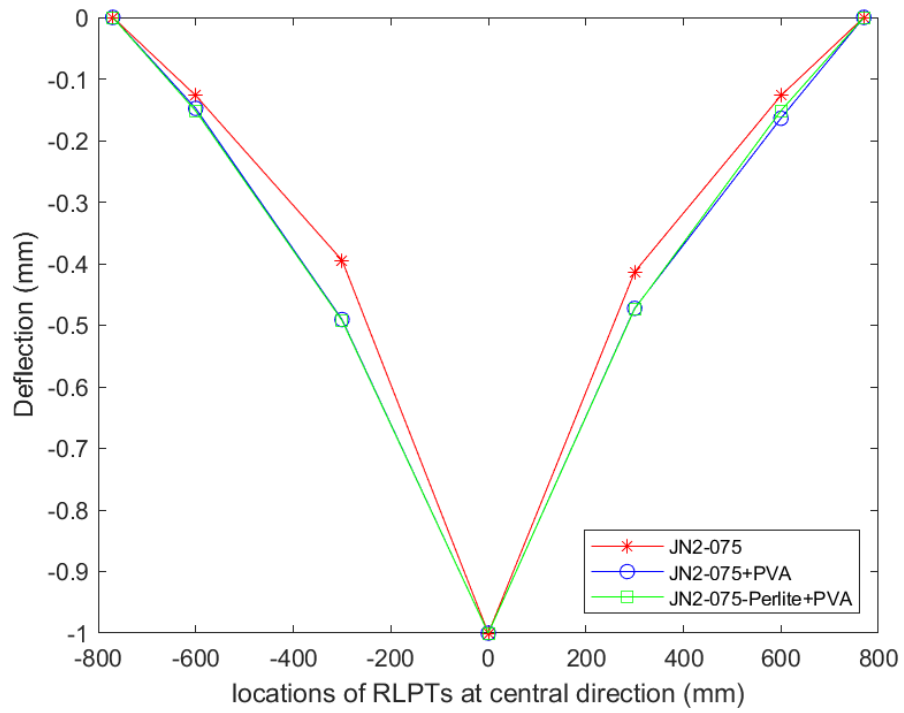RF+PVA

(a)   (b)
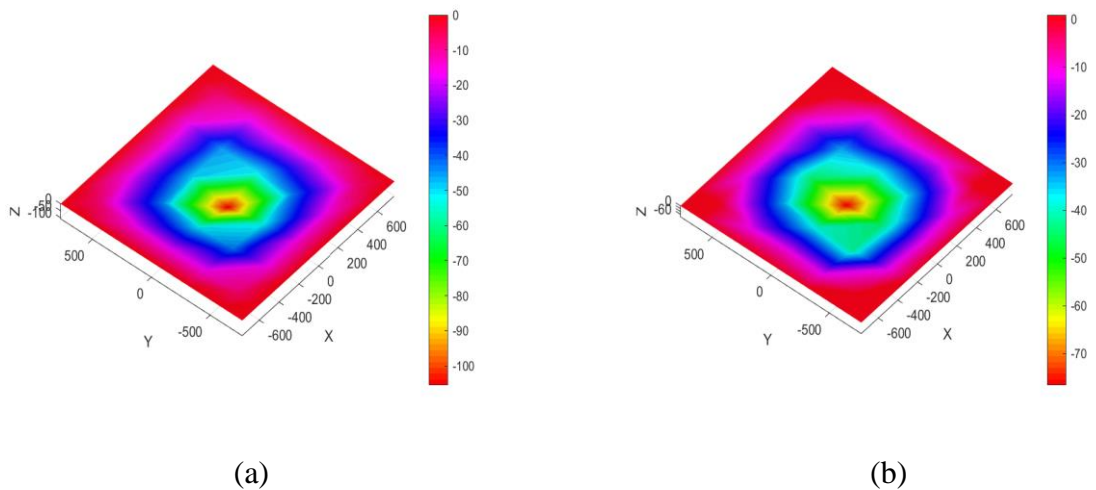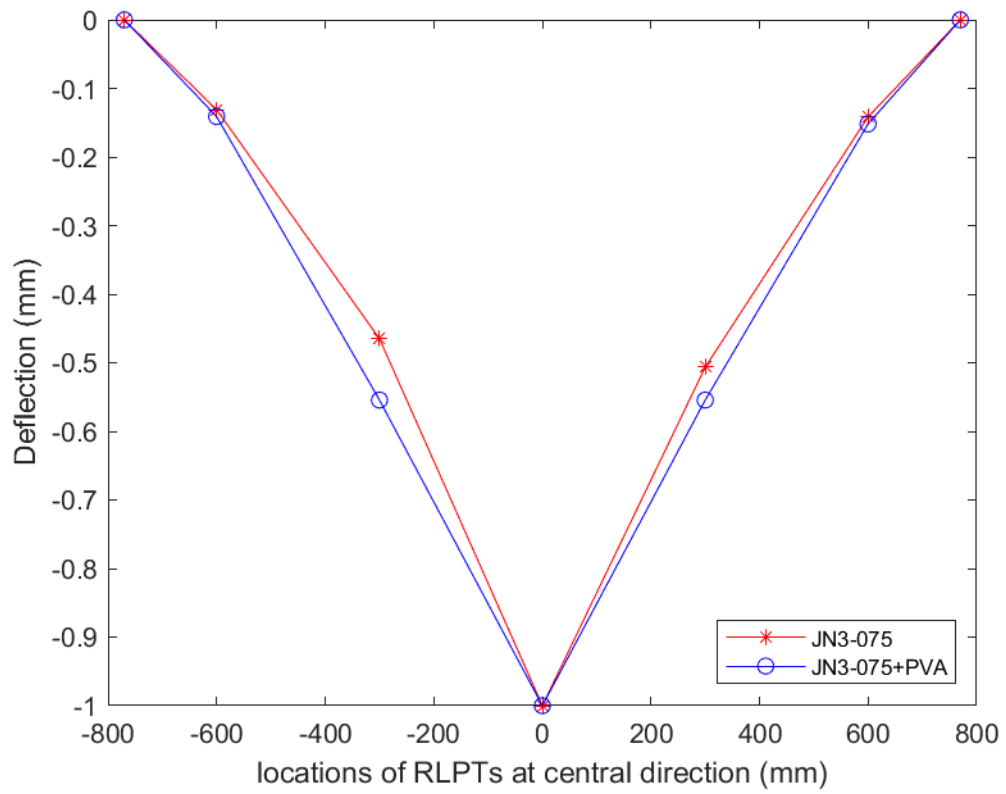
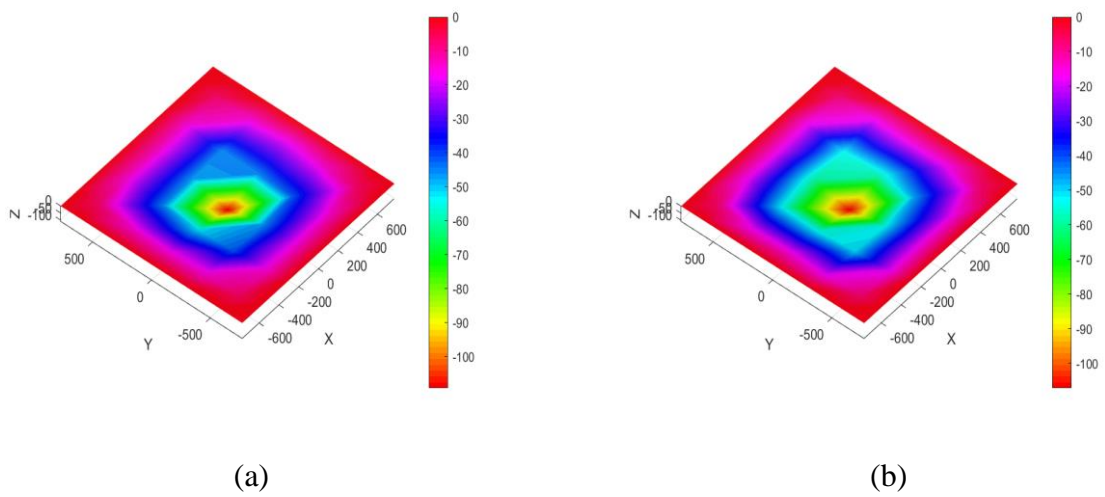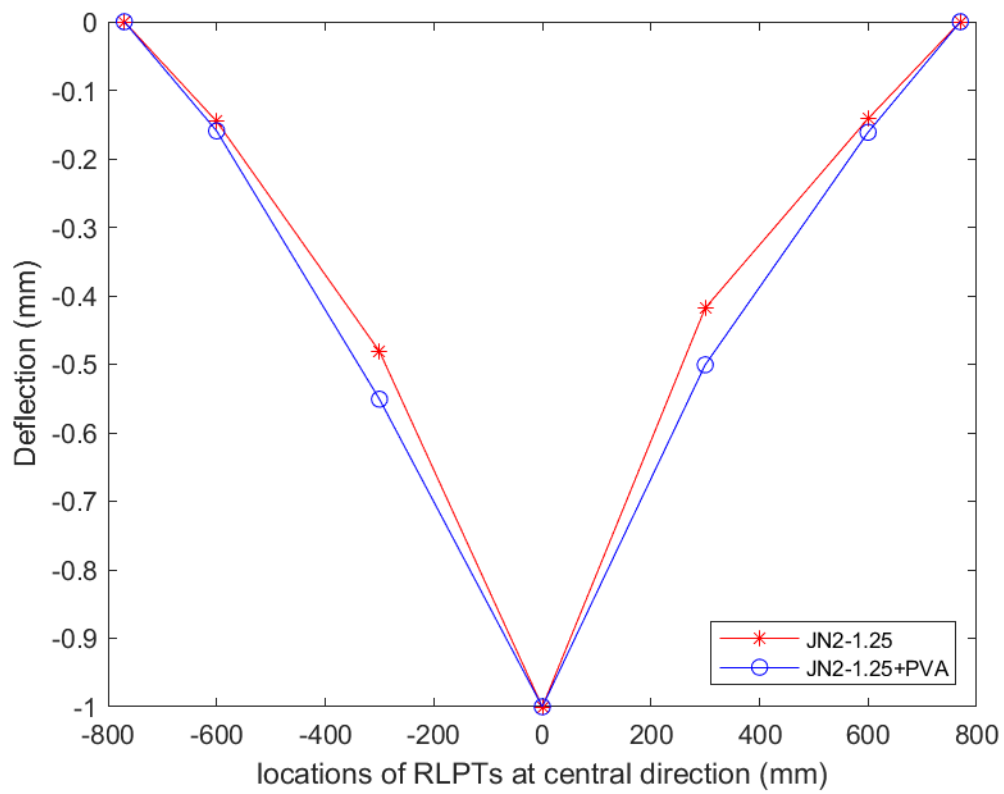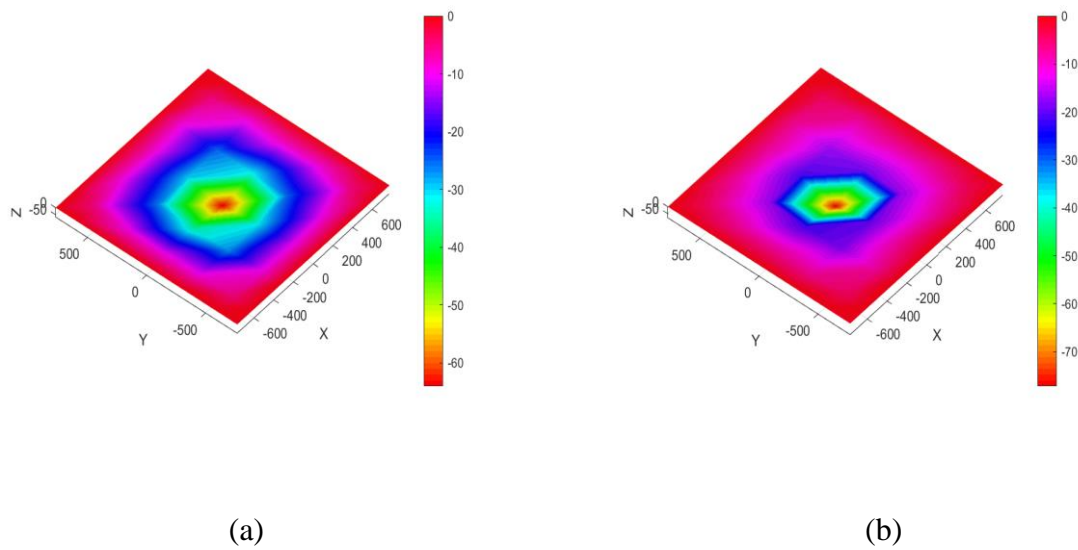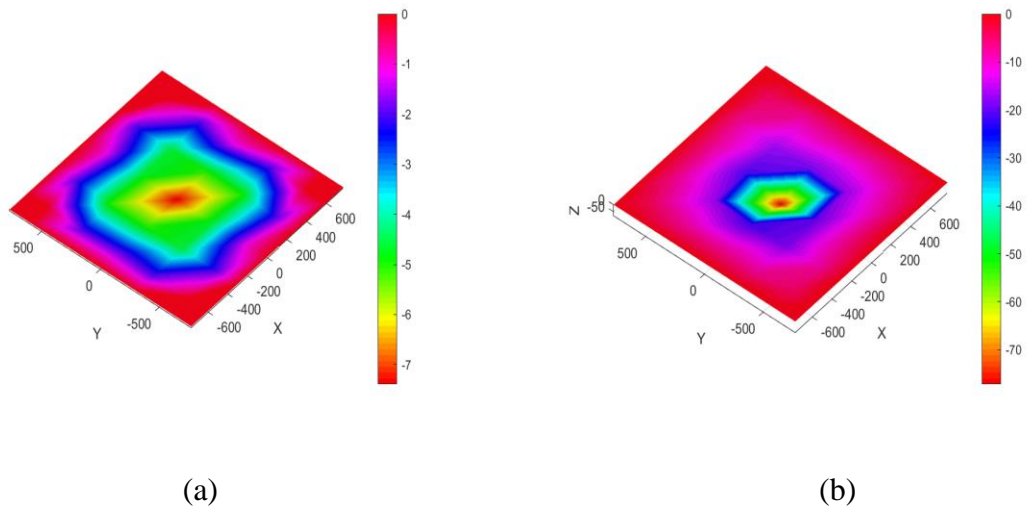Figure 4.43 Deflection contour of panels at failure; (a) JN-Plain; (b) JN-Plain-RF
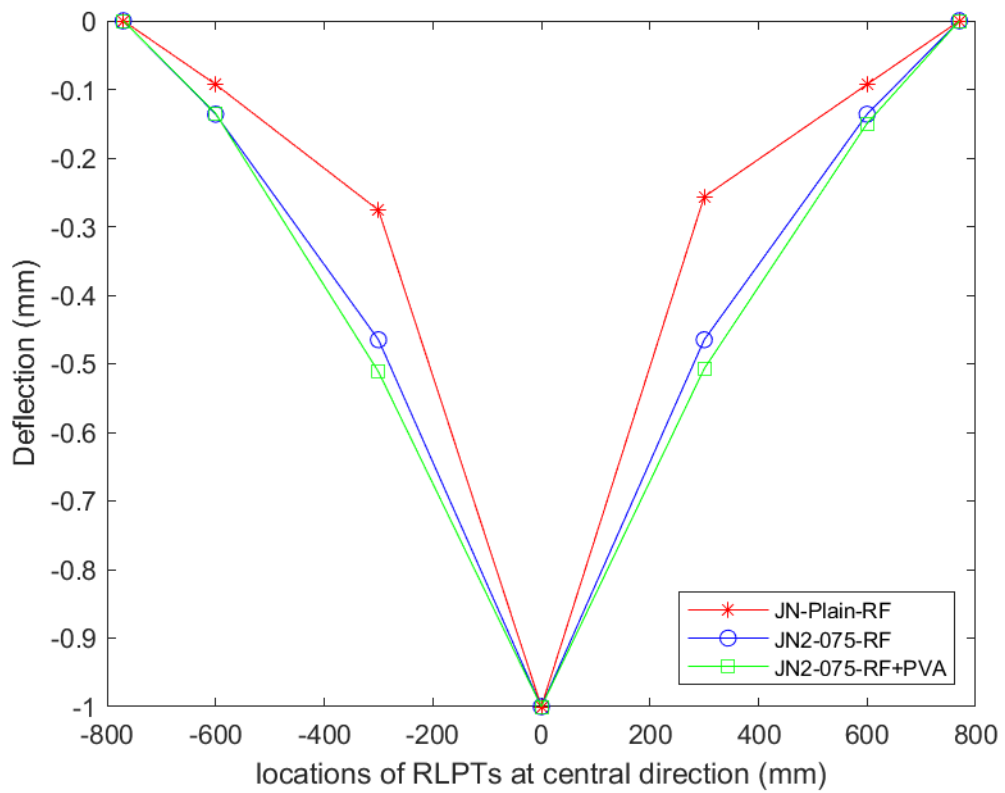

Figure 4.44 Normalized centerline deflection of panels JN-Plain-RF, JN2-075-RF and
    JN2-075-RF+PVA

CHAPTER 5

CONCLUSION

The study presented here aimed to investigate the punching behavior of hybrid fiber reinforced concrete in thin panels. 13 simply supported square panels were tested under a point load applied at their midpoint. The study was concentrated on considering the effects of different fiber types, fiber lengths and fiber volume ratios, as well as fiber hybridization by using steel and PVA fibers in the same mix. Effects of using traditional reinforcement with fibers was also investigated. Three types of steel fiber and PVA fibers were used with same ratio except for type Dramix® 65/60 for which a higher ratio was also considered. The behavior was assessed in terms of load-deflection behavior, ductility, stiffness, energy-absorption capacities, and cracking patterns. In the light of experimental results obtained, following conclusions could be drawn.

- All specimens that contained only steel fibers failed under punching, where a punching cone was developed and separated from the specimen under the loading point. In hybrid fiber reinforced specimens with steel and PVA fibers, either a flexural failure or a punching failure followed by significant flexural deformations. However, for panels JN1-075+PVA and JN2-075-Perlite+PVA, punching failure was more dominant. Meanwhile, all specimens with conventional steel reinforcement failed in punching. Steel fibers introduced significant levels of ductility to all members. On the other hand, fiber hybridization further increased specimens' load capacity and moved the behavior to a more ductile flexural behavior. Evidenced by the member deformation characteristics, specimens with PVA had more widespread deformations on entire specimen rather than concentrated deformation around the punching zone.

- In general, specimens with only steel fibers displayed a more ductile behavior compared to hybrid fiber reinforced specimens with steel and PVA fibers. Although fiber hybridization increased the load capacity for most of the specimens, it decreased their maximum displacement capacities. Specimens with PVA fibers had a more flexure dominant behavior. Thus, flexural cracks were able to open wider, which probably

decreased the middle punching cone's deformation capacity in these specimens.

- In general, addition PVA fibers considerably increased the load displacement capacity of the panels compared to the ones with only steel fibers. Effect of fiber hybridization was minimal for panel with 35 mm single end hook steel fiber. In panels with 60 mm single end hook steel fiber of 0.75 % ratio, addition of PVA had an adverse effect on the maximum load capacity. However, with the same fiber length and ratio, load carrying capacity increased significantly when 20% of fine aggregate was replaced by light weight perlite.

- The crack widths were higher in width and less in number in specimens with the shortest steel fibers. As the steel length and ratio increased and single hook end steel fibers were changed to double hook end steel fibers, crack widths decreased while number of cracks increased. This condition was more pronounced in panels with conventional reinforcement.

In general, it can be concluded that fiber reinforced concrete has a very significant effect on thin panel's punching load and displacement capacity. Hybridization of two different types of fiber, steel and PVA fibers, brings advantages in terms of punching load capacity, deformation characteristics and failure mode. However, it has to be noted that these advantages are not always present, or they may be rather slight improvements in certain cases that may not worth the extra cost. Steel fiber type (length, end hook types, aspect ratio) and ratio is dominant on panels' behavior.

REFERENCES

A.Yaseen, Abdulhameed. "Punching Shear Strength of Steel Fiber High Strength Reinforced Concrete Slabs." *Master thesis, College of Engineering, University of Salahaddin, Erbil, Iraq,* (2006): 111.

Destrée, Xavier, and Jürgen Mandl. "Steel Fibre Only Reinforced Concrete in Free Suspended Elevated Slabs: Case Studies, Design Assisted by Testing Route, Comparison to the Latest Sfrc Standard Documents." *Tailor Made Concrete Structures* (2008): 437-43.

Fürst, A., and P Marti. "Robert Maillart's Design Approach for Flat." *Journal of Structural Engineering* 123, no. 8 (1997): 1102-10.

Gasparini, D. A., and M.ASCE. "Contributions of C. A. P. Turner to Development of Reinforced Concrete Flat Slabs 1905–1909." *Journal of Structural Engineering* 1243-1252 (1905-1909).

Gouveia, Nuno D., Duarte M. V. Faria, and António Pinho Ramos. "Assessment of Sfrc Flat Slab Punching Behaviour – Part I: Monotonic Vertical Loading." *Magazine of Concrete Research* 71, no. 11 (2019): 587-98. https://doi.org/10.1680/jmacr.17.00343.

Gouveia, Nuno D., Massimo Lapi, Maurizio Orlando, Duarte M. V. Faria, and António M. P. Ramos. "Experimental and Theoretical Evaluation of Punching Strength of Steel Fiber Reinforced Concrete Slabs." *Structural Concrete* 19, no. 1 (2018): 217-29. https://doi.org/10.1002/suco.201700136.

Harajli, M. H., D. Maalouf, and H. Khatib. "Effect of Fibers on the Punching Shear Strength of Slab-Column Connections." *Cement & Concrete Composites* 17, no. 2 (1995): 161-70.

Hedebratt, Jerry, and Johan Silfwerbrand. "Full-Scale Test of a Pile Supported Steel Fibre Concrete Slab." *Materials and Structures* 47, no. 4 (2014): 647-66. https://doi.org/10.1617/s11527-013-0086-5.

Maya, L. F., M. Fernández Ruiz, A. Muttoni, and S. J. Foster. "Punching Shear Strength of Steel Fibre Reinforced Concrete Slabs." *Engineering Structures* 40 (2012): 83-94. https://doi.org/10.1016/j.engstruct.2012.02.009.

Menétrey, Ph. "Synthesis of Punching Failure in Reinforced Concrete." *Cem Concr Compos.* 24, no. 6 (2002): 497–507.

Michels, Julien, Danièle Waldmann, Stefan Maas, and Arno Zürbes. "Steel Fibers as Only Reinforcement for Flat Slab Construction – Experimental Investigation and Design." *Construction and Building Materials* 26, no. 1 (2012): 145-55. https://doi.org/10.1016/j.conbuildmat.2011.06.004.

Muttoni, Aurelio. "Punching Shear Strength of Reinforced Concrete Slabs without Transverse Reinforcement." *ACI Struct J* 105(4) (2008): 440–50.

Narayanan, R., and I. Y. S. Darwish. "Punching Shear Tests on Steel-Fibre-Reinforced Micro-Concrete Slabs." *ICE Publishing* 39 no. 138 (1987): 42-50.

Ramin, Pourreza. "Investigating the Effects of Hybrid Fibres on the Structural Behaviour of Two-Way Slabs." Master thesis, Memorial University of Newfoundland, 2014.

Saatcı, Selçuk, Süleyman Yaşayanlar, Yonca Yaşayanlar, and Baturay Batarlar. "Çelik Fiber Katkısının Farklı Boyuna Donatı Oranına Sahip Betonarme Döşemelerin Zımbalama Davranışı Üzerinde Etkileri." *Gazi Üniversitesi Mühendislik-Mimarlık Fakültesi Dergisi* 2018, no. 18-2 (2018). https://doi.org/10.17341/gazimmfd.460507.

Singh, Harvinder. "Steel Fibers as the Only Reinforcement in Concrete Slabs: Flexural Response and Design Chart." *Structural Engineering International* 25, no. 4 (2015): 432-41. https://doi.org/10.2749/101686615x14355644771090.

Tan, Kiang-Hwee, and P. Paramasivam. "Punching Shear Strength of Steel Fiber Reinforced Concrete Slabs." *Journal of Materials in Civil Engineering* 6, no. 2 (1994): 240-53.

Tan, Kiang Hwee, and Akshay Venkateshwaran. "Punching Shear in Steel Fiber-Reinforced Concrete Slabs with or without Traditional Reinforcement." *ACI Structural Journal* 116, no. 3 (2019). https://doi.org/10.14359/51713291.